Fission product transport during pipebreaks in a PBMR confinement

Preparer : **Mathhew Sanyasi**

Student Number : **22048308**

Supervisor : **Frederik Reitsma**

Date : **May 2011**

Dissertation submitted in partial fulfilment of the requirements for the degree of Master of Engineering in Nuclear Engineering at the Potchefstroom Campus of the North-West University

ABSTRACT

The Pebble Bed Modular Reactor (PBMR) (Pty) Ltd Company intends to develop a demonstration power plant to be operated by the South African state owned utility Eskom. This demonstration plant will be a high temperature gas cooled reactor (HTGR) that will be graphite moderated and helium cooled.

In the event of a pipe break within the helium pressure boundary (HPB) of a PBMR module, the circulating helium coolant is released into the confinement building and if the resulting pressures are large enough, is vented through high efficiency particulate air (HEPA) filters into the environment. In support of the design and safety analysis of the plant, pipe break scenarios are analysed to provide insight on the expected consequences of such an event.

This study focused on quantifying the retention capability of the confinement building for graphite dust and fission products that follow pipe breaks in a modular HTGR. The high pressure and temperature gases that are released during the accident may result in intolerable pressures within the confinement therefore the structural integrity of the building was investigated by analysis. Iodine is a major contributor to the source term that could be released to the environment, the HEPA filter filtration efficiency of I_2 is lower than that compared to aerosols while almost negligible for organic iodides thus the chemical form of iodine reaching the filters was analysed. Two separate cases were investigated, the first considered a single 65 mm double-ended guillotine break (DEGB) of the reactor outlet pipe near the inlet to the steam generator, while the second case considered a simultaneous 65 mm DEGB of the steam generator outlet pipe.

The integral accident analysis code ASTEC (Accident Source Term Evaluation Code) was used to simulate these scenarios. ASTEC has been developed jointly by the French institute IRSN (Institut de Radioprotection et de Sûreté Nucléaire) and the German institute GRS (Gesellschaft Für Anlagen-Und Reaktorsicherheit Mbh) since 1994. It was developed for investigating scenarios of a hypothetical severe light water reactor (LWR) accident, from initiating event to possible radionuclide release outside the reactor containment. For this study, only the CPA and IODE modules were used from the ASTEC package since these modules compute the thermalhydraulic, aerosol and fission product, and iodine behaviour in the containment respectively.

Analyses of the results have shown that the design pressure limit is exceeded for at most three compartments during the transients. It was also found that organic iodide production is possible during the initial release phase only as the compartmental temperatures are higher during this phase than during the delayed release phase. The higher temperatures increase reaction kinetics in favour of organic iodide production.

An analysis of the results obtained from the metal fission products of the delayed release showed that ASTEC could not tolerate the small masses of fission products that were injected into the system, with the mass balance of the system not converging. This deficiency is attributed to the fact that ASTEC was developed specifically for LWR accident scenarios. LWR accident scenarios typically involve significant fission product release into the containment with the possibility of a core melt. This is in contrast to a PBMR accident scenario since the silicon carbide layer of the fuel kernel retains the

majority of the fissions products with only little escaping into the reactor building. The analysis of the delayed release is an important aspect for the PBMR safety analysis therefore it is suggested for future work that a more suitable code which can tolerate small quantities of fission products be used.

Key words: PBMR; thermalhydraulic; iodine; chemistry; fission product; pipebreak; ASTEC; source term.

DECLARATION

I, the undersigned, hereby declare that the work contained in this project is my own original work.

_____

Mathhew Sanyasi

Date: 14 February 2011

Randburg

CONTENTS

ABBREVIATIONS 9

LIST OF SYMBOLS 10

1. INTRODUCTION 11

1.1 BACKGROUND 11
1.2 MOTIVATION FOR THIS STUDY 13
1.3 PROBLEM STATEMENT 14
1.4 KNOWLEDGE GAP TO BE FILLED 14
1.5 RESEARCH AIMS AND OBJECTIVES 15
1.5.1 GENERAL AIMS 15
1.5.2 SPECIFIC OBJECTIVES 15

2. ASTEC V2.0 SEVERE ACCIDENT ANALYSIS CODE 16

2.1 OVERVIEW 16
2.2 ASTEC MODULES 17
2.3 CPA (CONTAINMENT PART OF ASTEC) MODULE 18
2.3.1 Thermalhydraulic formulation of CPA 18
2.3.2 Aerosol and fission product (AFP) formulation of CPA 19
2.3.2.1 Aerosol modelling 20
2.3.2.1.1 Agglomeration 20
2.3.2.1.2 Deposition 22
2.4 IODE (IODINE CHEMISTRY) MODULE 24
2.4.1 Gas phase reactions 24
2.4.2 Liquid phase reactions 24
2.5 VERIFICATION AND VALIDATION 25

3. CALCULATION MODEL 26

3.1 DEMONSTRATION MODULE 26
3.2 CONFINEMENT MODEL 27
3.2.1 Junctions 29
3.2.2 Concrete data 29
3.3 THERMALHYDRAULIC SOURCE 30
3.3.1 Helium source 30
3.3.2 Steam source 31
3.3.3 Delayed release driving force 31
3.4 GRAPHITE DUST SOURCE 33
3.4.1 Dust size distribution 33
3.4.2 Dust injection 33
3.5 FISSION PRODUCTS 34
3.5.1 Initial release 34
3.5.1.1 Gaseous fission products 34
3.5.1.2 Fission products sorbed onto dust 36
3.5.2 Delayed release 37
3.5.2.1 Size distribution 37
3.5.2.1.1 Best estimate size 37
3.5.2.1.2 Conservative size estimate 38
3.5.2.2 Release rates 39
3.6 MODEL ASSUMPTIONS 40

4. RESULTS AND DISCUSSION 41

4.1 HELIUM PIPE BREAK ANALYSIS 41
4.1.1 Thermalhydraulic results 41

4.1.1.1 Pressure 41
4.1.1.2 Temperature 42
4.1.1.3 Junction flowrates 44
4.1.2 Graphite dust and fission product results 45
4.1.2.1 Graphite dust 45
4.1.2.2 Fission products 49
4.1.2.2.1 Initial release of metallic fission products 49
4.1.2.2.2 Initial release of fission products sorbed onto dust 52
4.1.2.2.3 Delayed release of fission products 56
4.1.3 Iodine chemistry results 58
4.2 HELIUM AND STEAM PIPE BREAK ANALYSIS 61
4.2.1 Thermalhydraulic results 61
4.2.1.1 Pressure 61
4.2.1.2 Temperature 62
4.2.1.3 Junction flowrates 64
4.2.1.4 Steam mass and liquid volume 65
4.2.2 Graphite dust and fission product results 67
4.2.2.1 Graphite dust 67
4.2.2.2 Fission products 70
4.2.2.2.1 Initial release of metallic fission products 70
4.2.2.2.2 Initial release of fission products sorbed onto dust 74
4.2.2.2.3 Delayed release of fission products 77
4.2.3 Iodine chemistry results 80

5. CONCLUSION 83

6. REFERENCES 85

7. APPENDIX A 87

7.1.1 List of Partners for the SARNET programme 87

8. APPENDIX B 89

9. APPENDIX C 97

9.1 ASTEC MAIN INPUT FILE 97

FIGURES

Figure 1: Illustration of the modular nature of ASTEC [15]. 18
Figure 2: Flowsheet of the PBMR 200MW$_{th}$ Cycle. 26
Figure 3: Compartmental layout of the PBMR module. 28
Figure 4: Symbols used to represent the inter-compartmental junctions. 29
Figure 5: Helium mass flowrate and cumulative mass profile. 30
Figure 6: Helium temperature and pressure profile. 31
Figure 7: Steam mass flowrate and cumulative mass profile. 32
Figure 8: Steam temperature and pressure profile. 32
Figure 9: Graphite dust particle size distribution used as input for the models. 33
Figure 10: Cumulative graphite dust injection used for the models. 34
Figure 11: Gaseous ^{110m}Ag and ^{137}Cs releases. 35
Figure 12: Gaseous ^{131}I and ^{90}Sr releases. 35
Figure 13: ^{137}Cs and ^{90}Sr sorbed onto dust. 36
Figure 14: ^{110m}Ag sorbed onto dust. 36
Figure 15: Dependence of deposition velocity on particle diameter [8]. 38
Figure 16: Delayed releases for ^{111}Ag, ^{90}Sr and ^{131}I. 39
Figure 17: Delayed releases for ^{137}Cs. 39
Figure 18: Pressure response of compartments in Module 2. 42
Figure 19: Temperature profile of compartments in Module 2 (200 seconds). 43
Figure 20: Temperature profile of compartments in Module 2 (18000 seconds). 43
Figure 21: Junction mass flowrates at 10 seconds. 44
Figure 22: Junction mass flowrates at 700 seconds. 45
Figure 23: Graphite dust mass within the confinement (700 seconds). 46
Figure 24: Graphite dust mass within the confinement (18000 seconds). 46
Figure 25: Graphite dust mass deposited in the filter and released into the environment. 47
Figure 26: Graphite dust distribution on hosts (18000 seconds). 48
Figure 27: Graphite dust mass balance. 48
Figure 28: Initial release of ^{110m}Ag. 49
Figure 29: Initial release of ^{137}Cs. 50
Figure 30: Initial release of ^{90}Sr. 50
Figure 31: Mass balance on the initial release of ^{110m}Ag. 51
Figure 32: Mass balance on the initial release of ^{137}Cs. 51
Figure 33: Mass balance on the initial release of ^{90}Sr. 52
Figure 34: Initial release of ^{110m}Ag sorbed onto dust. 53
Figure 35: Initial release of ^{137}Cs sorbed onto dust. 53
Figure 36: Initial release of ^{90}Sr sorbed onto dust. 54
Figure 37: Mass balance of ^{110m}Ag sorbed onto dust. 54
Figure 38: Mass balance of ^{137}Cs sorbed onto dust. 55
Figure 39: Mass balance of ^{90}Sr sorbed onto dust. 55
Figure 40: Mass balance on delayed release of ^{111}Ag. 56
Figure 41: Mass balance on delayed release of ^{137}Cs. 57
Figure 42: Mass balance on delayed release of ^{90}Sr. 57
Figure 43: Molecular iodine mass distribution. 59
Figure 44: Methyl iodide mass distribution. 59
Figure 45: Iodine mass balance. 60
Figure 46: Pressure response of compartments in Module 2. 62
Figure 47: Temperature profile of compartments in Module 2 (200 seconds). 63
Figure 48: Temperature profile of compartments in Module 2 (18000 seconds). 63
Figure 49: Junction mass flowrates at 10 seconds. 64
Figure 50: Junction mass flowrates at 700 seconds. 65
Figure 51: Total steam mass and liquid volume in the confinement. 66

Figure 52: Graphite dust mass within the confinement. 68
Figure 53: Graphite dust mass deposited in the filter and released into the environment. 68
Figure 54: Graphite dust distribution on hosts (18000 seconds). 69
Figure 55: Graphite dust mass balance. 69
Figure 56: Initial release of metallic ^{110m}Ag. 70
Figure 57: Initial release of metallic ^{137}Cs. 71
Figure 58: Initial release of metallic ^{90}Sr. 71
Figure 59: Mass balance on the initial release of metallic ^{110m}Ag. 72
Figure 60: Mass balance on the initial release of metallic ^{137}Cs. 72
Figure 61: Mass balance on the initial release of metallic ^{90}Sr. 73
Figure 62: Initial release of ^{110m}Ag sorbed onto dust. 74
Figure 63: Initial release of ^{137}Cs sorbed onto dust. 75
Figure 64: Initial release of ^{90}Sr sorbed onto dust. 75
Figure 65: Mass balance of ^{110m}Ag sorbed onto dust. 76
Figure 66: Mass balance of ^{137}Cs sorbed onto dust. 76
Figure 67: Mass balance of ^{90}Sr sorbed onto dust. 77
Figure 68: Mass balance on delayed release of ^{111}Ag. 78
Figure 69: Mass balance on delayed release of ^{137}Cs. 78
Figure 70: Mass balance on delayed release of ^{90}Sr. 79
Figure 71: Molecular iodine mass distribution. 81
Figure 72: Methyl iodide mass distribution. 81
Figure 73: Iodine species found in the aqueous phase. 82
Figure 74: Iodine mass balance. 82

TABLES

Table 1: Concrete material properties used 29
Table 2: Physical properties of Cs, Sr and Ag 37
Table 3: Compartmental characteristics for Module 1 89
Table 4: Compartmental characteristics for Module 2 91
Table 5: Junction characteristics for module 1 93
Table 6: Junction characteristics for module 2 95

ABBREVIATIONS

This list contains the abbreviations used in this document.

Abbreviation or Acronym	Definition
AFP	Aerosol and Fission Product part of CPA
ASTEC	Accident Source Term Evaluation Code
AVR	Arbeitsgemeinschaft Versuchsreaktor
CFD	Computational Fluid Dynamics
COCOSYS	Containment Code System
CPA	Containment Part of ASTEC
DEGB	Double Ended Guillotine Break
DFT	De-aerator Feed Tank
DPP200	Demonstration Power Plant 200 MW_{th}
EC FwP	European Commission Framework Programme
EVITA	European Validation of the Integral code ASTEC
GRS	Gesellschaft Für Anlagen- und Reaktorsicherheit mbH
GSD	Geometric Standard Deviation
HEPA	High Efficiency Particulate Air
HPB	Helium Pressure Boundary
HPS	Helium Purification System
HTGR	High Temperature Gas-Cooled Reactor
HTR	High Temperature Reactor
HTR-PM	High Temperature Reactor Pebble Bed Module
IRSN	Institut de Radioprotection et de Sûreté Nucléaire
LWR	Light Water Reactor
NEA	Nuclear Energy Agency
NNR	National Nuclear Regulator of South Africa
PBMR	Pebble Bed Modular Reactor
SARNET	Severe Accident Research Network of Excellence
SG	Steam Generator
THY	Thermalhydraulic part of CPA
TRISO	Triple Coated Isotropic Particle

LIST OF SYMBOLS

This list contains the symbols used in this document.

Symbol	Definition	Unit
A_{Wd}	Wall surface area	m^2
$C(Kn)$	Slip correction	-
D	Particle diameter	m
D_p	Particle diameter	m
d	Particle effective diameter	m
F_{SI}	Particle slip factor	-
F_{Th}	Thermal accommodation factor	-
g	Gravitational acceleration	m^2/s
G_{Wd}	Steam mass flow on the wall	kg/s
k	Boltzmann constant	J/K
l	Mean relocation distance	m
m	Particle mass	kg
M_{ncG}	Average molecular weight of the non condensable gases	kg/kmol
M_W	Molecular weight of water	kg/kmol
$p_{D,Atm}$	Partial steam pressure in the atmosphere	Pa
$p_{D,Wd}$	Partial saturation pressure on the wall	Pa
p_{Tot}	Total pressure	Pa
q_T	Dissipation rate of turbulent energy	m^2/s^3
R	Universal gas constant	kJ/kmolK
T_{Atm}	Atmosphere temperature	K
T_G	Gas temperature	K
v	Mean thermal speed	m/s
v_{Dif}	Deposition velocity for diffusion	m/s
v_G	Kinematic gas viscosity	m^2/s
v_{Sed}	Sedimentation velocity	m/s
γ	Agglomeration shape factor	-
δ_{Dif}	Thickness of the diffusion boundary layer	m
η_G	Dynamic gas viscosity	kg/ms
λ	Average mean free path length of the gas molecules	m
λ_G/λ_p	Ratio of the heat conductivity of the gas to that of the particle	-
ρ_G	Gas density	kg/m^3
ρ_p	Density of the particle material	kg/m^3
$\overline{r}_D$	Average steam density in the diffusiophoretic boundary layer	kg/m^3
χ	Dynamic shape factor	-
∇T	Temperature gradient in the boundary layer of the surface	K/m

1. INTRODUCTION

1.1 BACKGROUND

The energy demand within South Africa is growing rapidly and it is planned that the generating capacity to meet this demand will be obtained from a diversified mix of coal-fired, nuclear and renewable energy technologies. The lack of current generating capacity to meet the demand has resulted in severe blackouts across the country with the economic loss estimated at 50 billion Rand in 2008 [1]. The majority of South Africa's electricity is generated by traditional coal-fired power plants situated deep inland near coal mines within the countries eastern half due to the constant need for supply of coal directly to the power station. Some of these older power stations will reach their end of life after 2025, therefore South Africa will need to prepare for additional demand that will be required after 2025.

In a bid to alleviate some of the growing energy demand a nuclear energy generating sector was established within South Africa by the Pebble Bed Modular Reactor (PBMR) (Pty) Ltd Company. The company intends to develop a demonstration power plant to be operated by the South African state owned utility Eskom. This demonstration plant will be a high temperature gas cooled reactor (HTGR) that will be graphite moderated and helium cooled. The reactor will be fuelled with spherical elements, which contain the coated uranium dioxide fuel particle traditionally known as the triple coated isotropic (TRISO) particle. The TRISO fuel concept has been successfully demonstrated with the operation of the German experimental *Arbeitsgemeinschaft Versuchsreaktor* (AVR) reactor. Operation of the AVR commenced in 1967 and the reactor was shut down in 1988, over this period many fuel concepts were tested with the TRISO fuel in significant use over the years 1984 to 1987.

The accidents at Three Mile Island and Chernobyl have greatly increased the safety measures of all nuclear installations. Unlike the conventional light water reactor (LWR) designs, the HTGR is designed with inherent safety features. A core melt scenario that is possible with a LWR design is virtually impossible for the small, modular HTGR since the core can dissipate heat by natural mechanisms of conduction, convection and radiation in the event of a loss of forced cooling and, limits the fuel temperatures to below maximum allowed values. This is possible because of the high thermal inertia of the core and the low core power density. For reactivity excursions the system is capable of automatic shut down due to resonance absorption. These safety features require no human intervention, cannot be bypassed or rendered ineffective and have become popularly known as passive or inherent safety features.

Indeed the primary market targeted for the operation of the PBMR has been the electricity generating market however, the ability to produce high temperature heat provides an incentive for process heat application. The heat generated from the PBMR can be supplied to in-situ oil sands recovery, steam-

methane reforming which is an upstream process for ammonia and methanol production, and hydrogen production from the high temperature decomposition of water is also possible. In arid areas it is possible to provide fresh water through the desalination of seawater. The awareness of the impact of carbon dioxide emission on global climate change promoted the international community to reduce greenhouse gas emissions and apply stringent laws for emission control. Nuclear energy in particular will offer the attractive incentive of minimal greenhouse gas emission, and its process heat can be applied to processes that currently incinerate fossil fuel for operation.

The vision for small and modular units allows for the possibility of construction near points of demand as both local and international utilities experience brief, sharp demands during seasonal changes with load follow on characteristics of larger power stations much slower. A short construction time allows ease for electricity supply planning and the economic competitiveness of the electricity generated will be comparable to present major electricity generating systems [2]. For cycle efficiency the PBMR will have a higher thermodynamic efficiency as compared to traditional LWR power stations, this is primarily due to the high gas temperatures produced with the PBMR.

The HTGR has yet to become commercially available technology, however the Chinese have planned the construction of their two unit demonstration module of 250 MW_{th} each, after the gratifying demonstration of their research reactor, the HTR-10. The research reactor was designed and operated in Beijing by the Institute of Nuclear and New Energy Technology (INET) of the Tsinghua University. INET have also reported that their demonstration module, named the high temperature reactor pebble bed module (HTR-PM) is planned to be completed and operational by 2013 [3]. This demonstration plant is of the indirect cycle design that uses a steam generator to drive steam to a turbine for electricity production; the plant will be licensed and operated by the Huaneng Shandong Shidao Bay Nuclear Power Company. The project goals of INET are to demonstrate the economic competitiveness of HTGR technology and to provide evidence that minimal accident management procedures will be required thus demonstrating the passive safety characteristics of HTGRs.

1.2 MOTIVATION FOR THIS STUDY

In the event of a pipe break within the helium pressure boundary (HPB) of a PBMR module, the circulating helium coolant is released into the confinement building and if the resulting pressures are large enough, is vented through high efficiency particulate air (HEPA) filters into the environment. These filters are capable of removing particulate matter, either graphite or metallic dust, but cannot filter airborne fission products[1]. This is termed the initial release while the delayed release is a much more concentrated release that follows.

The delayed release results from the heat-up of the core due to the loss of forced cooling following the pipe break. The above normal operation fuel temperatures promote an increase in the diffusion rate of fission products out of the protection of the fuel elements and into the reactor unit. This may result in the transport of these fission products into the confinement (reactor building).

In support of the design and safety analysis of the plant, pipe break scenarios are analysed in great detail to provide insight on the expected consequences of such an event. In most instances these analyses are performed using sophisticated computer codes which have been extensively validated for its application.

The South African National Nuclear Regulator (NNR) states in their basic licensing requirements document [4] that a concept of multiple, independent physical barriers to the uncontrolled release of radioactive material to the environment be shown. For the PBMR design of the HTGR, these barriers are made up of firstly, the TRISO fuel particle which is proven to retain fission products as demonstrated by the successful operation of the German AVR test reactor [5] and in numerous irradiation and heating experiments, the second barrier for fission product retention is the reactor unit and piping system of the primary system which can act as deposition and condensation sites for fission products that have been released from the fuel, while the third barrier is the surrounding confinement building. The NNR explicitly states [4]:

‘The demonstration of the adequacy of these barriers is an important part of the safety analysis’

The fundamental safety functions of, reactivity control, heat removal and, confinement of radioactivity are required to be demonstrated for all nuclear installations. As stated above the NNR imposes strict requirements on the retention performance of the plant during an accident scenario, it therefore becomes imperative to investigate the retention capability and structural integrity of the confinement. The retention capability will influence the radiological doses to the workers and public, which must remain within the regulatory limit, while structural integrity demonstrates safety and investment protection. This therefore highlights the need for a retention and thermalhydraulic analysis of the plant during accidents. The absence of this study will jeopardise the licensing process of the nuclear installation with respect to the regulatory requirements.

[1] Although a fission product and activation product are strictly different, this report will refer to both collectively as fission products unless otherwise stated.

1.3 PROBLEM STATEMENT

This study will focus on quantifying the retention capability of the confinement building for graphite dust and fission products that follow a pipe break in the primary system of a modular HTGR. The high pressure and temperature helium that is released during the accident may result in intolerable pressures within the confinement therefore the structural integrity of the building will be investigated by analysis. Iodine is a major contributor to the source term that could be released to the environment, the HEPA filter filtration efficiency of I_2 is lower than that compared to aerosols while almost negligible for organic iodides [7] therefore the chemical form of iodine reaching the filters will be analysed.

The size distribution of the fission products that may be present in aerosol form (notably the metal fission products) will be investigated thorough a literature survey and compared to the size that results in the lowest deposition rate. The size distribution of aerosols that results in the lowest deposition rate (gravitational and diffusive settling) is discussed in the Nuclear Energy Agency (NEA) report on nuclear aerosols [8].

A scenario that includes a pipe break within the secondary system of the steam generator will result in the release of steam into the confinement. This situation offers the unique complication of having a wet atmosphere during the accident, which is not present during a pipe break in the HPB alone. The presence of steam (which can condense into water) will influence the chemical form of iodine during the transient therefore it is imperative to consider this situation for a safety assessment. It should also be borne in mind that a simultaneous helium and steam line break will result in higher confinement pressures than a helium pipe break alone.

In summary, a retention and structural integrity analysis will be performed for the initial and delayed releases for both a dry environment (no steam line break) and a wet environment (simultaneous steam line break).

1.4 KNOWLEDGE GAP TO BE FILLED

A further motivation for this study is the fact that a confinement analysis has not been performed at the PBMR Company involving the iodine chemistry and the simultaneous break of a helium and steam line resulting in a wet atmosphere. Therefore this study will be a first attempt at the PBMR Company to quantify the retention capability, iodine chemistry and structural integrity during a simultaneous helium and steam pipe break.

This study will increase the technical knowledge of the PBMR Company regarding the retention capability and iodine chemistry in both a dry and wet environment during accident conditions, thus increasing confidence in the safety of their design.

1.5 RESEARCH AIMS AND OBJECTIVES

1.5.1 GENERAL AIMS

- To simulate the transport of fission products within the confinement building of a modular HTGR during a pipe break accident and thereby quantifying the retention capability of the confinement.
- To investigate the pressure response within the confinement due to the pipebreaks and determining whether this will be tolerable by the confinement structure.

1.5.2 SPECIFIC OBJECTIVES

1. Create a model for the modular confinement building of the PBMR indirect cycle DPP200 using the ASTEC code.
2. Simulate a single 65 mm double-ended guillotine break (DEGB) of the reactor outlet pipe at the steam generator inlet only and quantify the retention within the building of fission products and dust released from the break while also determining if the structural integrity is maintained after the depressurisation through the break. During the transient the iodine chemistry within the confinement will also be investigated with ASTEC.
3. The delayed release due to the heat up of the core will also be investigated as retention within the building. A size distribution for the metal fission products based on the best estimate and worst case will be analysed for retention.
4. Steps 2 and 3 will be repeated for the situation with a simultaneous 65 mm DEGB of the steam generator outlet pipe.

2. ASTEC V2.0 SEVERE ACCIDENT ANALYSIS CODE

2.1 OVERVIEW

The integral code ASTEC (Accident Source Term Evaluation Code) [6] has been developed jointly by the French institute IRSN (Institut de Radioprotection et de Sûreté Nucléaire) and the German institute GRS (Gesellschaft Für Anlagen- Und Reaktorsicherheit Mbh) since 1994. ASTEC simulates the scenario of a hypothetical severe light water reactor (LWR) accident, from initiating event to possible radionuclide release outside the reactor containment. The ASTEC code forms part of the Severe Accident Research Network (SARNET) programme, which is a 51-member organisation. For information on the extensive use of ASTEC this membership list is given in Appendix A. The code is distributed free amongst the partnering SARNET members and it is available to non-partners at a fee.

The ASTEC modules have been successfully validated for LWR application in a number of internationally collaborated initiatives such as the EVITA (2000-2003) [9] and the SARNET (2004-2008) [10] programmes. The first programme, EVITA, was conducted by 19 organisations across Europe, their validation exercises were successfully completed on experiments and plant applications such as the German KONVOI, Russian VVER, Westinghouse PWR 1000 and the EPR, these plant applications were analysed by code benchmarking. The SARNET programme was hosted by 51 organisations comprised of safety authorities, technical support organisations, industries, utilities and universities; their focus was on further experimental validation of ASTEC against phenomena of interest and was successfully completed in 2008. Both validation initiatives fell under the European Commission Framework Programmes (EC FwP) (4th, 5th and 6th) with a mandate to develop and maintain ASTEC as the integral code of reference in Europe. Currently SARNET-2 which forms part of the 7th EC FwP is underway.

The GRS involvement with the ASTEC project is solely on the development of the CPA (Containment Part of ASTEC) module, which is the containment analysis tool of the ASTEC suite. GRS proprietarily develops the dedicated containment code called COCOSYS [29], which is based largely on mechanistic modelling treating all phenomena in an elaborate coupled manner. Due to the collaboration between IRSN and GRS on the development of ASTEC, CPA of ASTEC has inherited many of the models available in COCOSYS but in a simplified fashion which will allow ASTEC to perform integral calculations in more reasonable times. It has been reported by the Nuclear Energy Agency [8] that the CPA module of ASTEC is almost identical to the COCOSYS code, although some phenomena are treated in a simplified manner.

2.2 ASTEC MODULES

ASTEC is an integral code; this means that it is comprised of many modules (that could be run in a stand-alone mode) capable of simulating severe accidents in LWR systems. This includes operation of the reactor from steady state, initiating the accident scenario, and simulating all responses of the system, including a possible core melt, the resulting corium interaction with the containment, transport of radionuclides and aerosols in the containment and the simulation of engineered safety systems such as thermal recombiners and spray systems used for mitigation.

The main modules of ASTEC are described below.

- CESAR for thermalhydraulics in the reactor coolant system;
- DIVA for core degradation up to vessel lower head failure;
- ELSA for fission product release from fuel rods;
- SOPHAEROS for fission product vapour and aerosol transport in the reactor coolant system;
- RUPUICUV for direct containment heating (DCH);
- CORIUM for heat transfer between containment atmosphere and corium entrained out of the cavity by direct containment heating;
- WEX for molten-corium concrete interaction in the cavity;
- CPA for thermalhydraulics, aerosol and fission product behaviour inside the containment;
- IODE for iodine behaviour in the containment;
- ISODOP for calculation of activity and decay heat in the reactor zones;
- SYSINT for management of engineered safety systems.

The modular nature of ASTEC is well illustrated in Figure 1 below. Of the modules described above only the CPA, and IODE modules are relevant for this study since these cover the relevant phenomena occurring within the confinement.

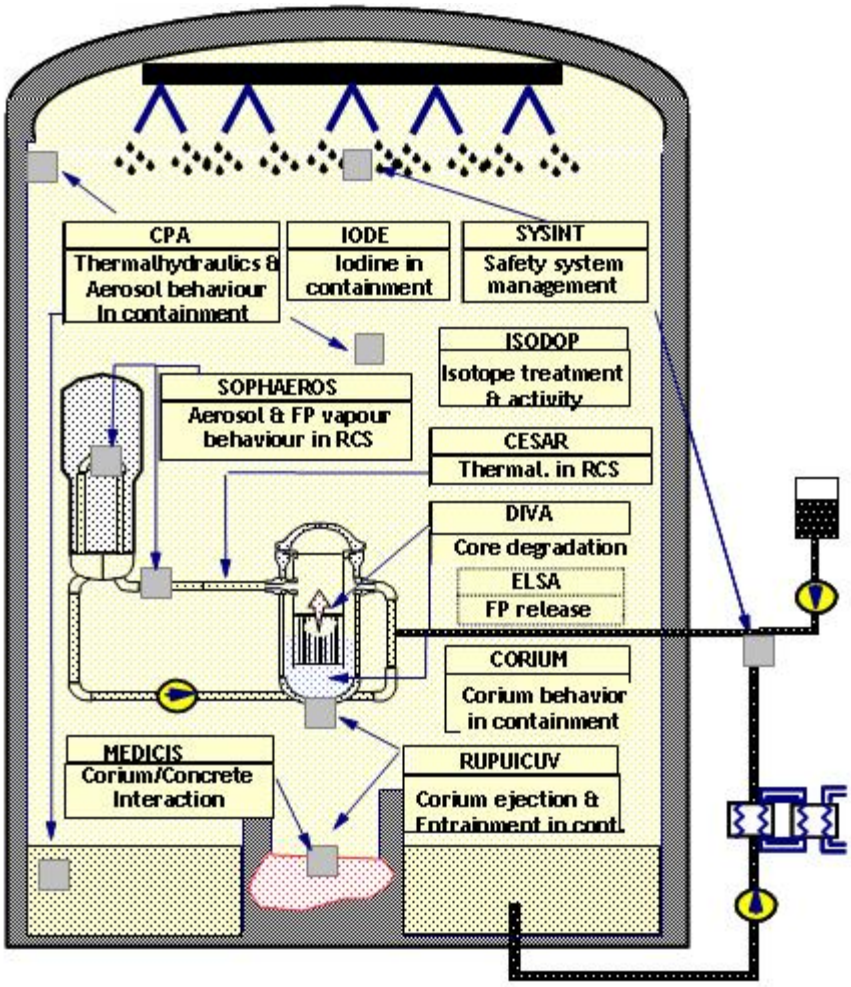

Figure 1: Illustration of the modular nature of ASTEC [15].

2.3 CPA (CONTAINMENT PART OF ASTEC) MODULE

The following paragraphs will describe some of the physical models implemented into CPA for thermalhydraulic and aerosol analysis.

2.3.1 Thermalhydraulic formulation of CPA

The thermalhydraulic (THY) part of CPA is able to evaluate:

- Pressure and temperature build-up and history
- Local temperature and pressure distributions
- Hydrogen combustion
- Energy distribution and local heat transfer to and heat conduction in structures
- Local gas distributions
- Water distribution
- Mass and volume flowrates for the release of fluids via openings and leakages
- Heat and combustion gas production distribution during fires

- Behaviour of systems such as fan systems, catalytic and thermal recombiners, pump systems, heat exchangers, valves, doors, igniters, pressure suppression systems and spray systems
- Feedback from the AFP (Aerosol and Fission Product) module such as hygroscopic effects and the decay heat of fission products

For the description of the physical processes during an accident propagation, arbitrary compartment systems and geometries can be simulated by specified volumes (the so-called 'lumped-parameter' concept). The conditional changes related to location and time are reduced to a purely time dependent behaviour within the control volumes (nodes), these nodes are interconnected by junctions. For the simulation of heat transfer and heat conduction via walls and internal components, specified structures can be coupled to the nodes. The heat conduction is described in one dimension, for the simulation of heat transfer processes different models and correlations are available.

Heat transfer is described by the different physical phenomena of free and forced convection, radiation (wall to gas, gas to wall, wall-gas-wall, wall to wall) and condensation depending on the thermal status of the zone and structures. Heat conduction is described one-dimensionally by the Fourier equation.

Structural materials can be separated by air-filled gaps and can be subdivided into an arbitrary number of layers with different thickness for the calculation of the heat conduction. The structural materials are defined by the values for thermal conductivity, emissivity, specific heat capacity and density.

2.3.2 Aerosol and fission product (AFP) formulation of CPA

The aerosol and fission product part of CPA is capable of evaluating:

- Volume condensation and growth of insoluble and soluble aerosol particles,
- Behaviour of eight chemically different aerosol components,
- Decay heat of gaseous and particulate fission products.

The aerosol calculation is based on the poly-disperse aerosol model. All agglomeration and deposition processes important in a LWR containment are modelled. The condensation of steam on insoluble and soluble aerosols is calculated by the moving-grid-method. The fission product decay heat module of ASTEC distinguishes between alpha, beta and gamma radiation. The heat of the beta radiation is released into the gas whereas the gamma radiation heats the wall structures. The retention of aerosols from a carrier gas channelled through a water pool is simulated. Thus, for example, pool scrubbing in the suppression pool of a boiling water reactor can be simulated.

2.3.2.1 Aerosol modelling

The AFP subroutine of CPA is based on the aerosol model MAEROS [31] which was developed at the Sandia National Laboratory, and is also used in other popular accident analysis codes. MAEROS describes the behaviour of a homogenously mixed poly-disperse aerosol system inside a control volume. The system may contain up to eight chemically different aerosol components. The processes of agglomeration, condensation, deposition and existing aerosol sources and sinks are calculated. A brief overview of the aerosol processes implemented into CPA is given below.

2.3.2.1.1 Agglomeration

Agglomeration or coagulation describes the process of two particles in motion within a gas stream colliding, adhering to each other and forming a single larger particle. CPA simulates four different agglomeration processes.

i. Brown's agglomeration

ii. Gravitational agglomeration

iii. Turbulent shear agglomeration

iv. Turbulent inertial agglomeration

Brown's agglomeration is the result of the Brownian motion of the aerosol particles in the gas stream. This phenomena is proportional to the agglomeration shape factor γ and inversely proportional to the dynamic shape factor χ. These factors are used to model particle behaviour for non-spherical particles. For spherical particles χ and γ are both equal to unity. The agglomeration coefficient for Brown's agglomeration is calculated in CPA by the relationship,

$$b_B = \left(B_i + B_j\right)\left(g_i D_i + g_j D_j\right)\frac{2p}{F} \tag{2.1}$$

where, $B_i = \dfrac{kT_G}{3pD_i h_G c_i} C\left(Kn_i\right)$ (2.2)

$$F = \frac{D_i + D_j}{D_i + D_j + 2d_{i,j}} + \frac{8\left(B_i + B_j\right)}{\overline{v}_{i,j}\left(D_i + D_j\right)} \tag{2.3}$$

$$\overline{v}_{i,j} = \sqrt{v_i^2 + v_j^2} \tag{2.4}$$

$$d_{i,j} = \sqrt{d_i^2 + d_j^2} \tag{2.5}$$

$$d_i = \frac{1}{3D_i l_i}\left\{\left(D_i + l_i\right)^3 + \left(D_i^2 + l_i^2\right)^{\frac{3}{2}}\right\} - D_i \tag{2.6}$$

$$l_i = \frac{8B_i}{pv_i} \tag{2.7}$$

$$v_i = \sqrt{\frac{8kT_G}{p\,m_i}} \tag{2.8}$$

$$C\left(Kn_i\right) = 1 + Kn_i\left(F_{SI} + 0.4\exp\left(-\frac{1.1}{Kn_i}\right)\right) \tag{2.9}$$

$$Kn_i = \frac{2\,l}{D_i} \tag{2.10}$$

Gravitational agglomeration takes into account the collision of large, faster falling particles with smaller slower particles. The coefficient is calculated according to,

$$b_G = e_c\,\frac{p}{4}\left(g_i D_i + g_j D_j\right)^2 \left|v_{Ti} - v_{Tj}\right| \tag{2.11}$$

where the settling velocity is described by,

$$v_{Ti} = \frac{r_{P,i} g D_i^2}{18 h_G c_i} C\left(Kn_i\right) \tag{2.12}$$

The parameter ε_c is the collision efficiency indicating the probability that a collision resulting in a single larger particle is successful.

Turbulent agglomeration is comprised of two parts, a shearing part and an inertia part. These two phenomena are calculated according to the equations

$$b_T = \sqrt{b_{T1}^2 + b_{T2}^2} \tag{2.13}$$

For shearing: $$b_{T1} = \sqrt{\frac{p^2 q_T}{120 u_G}}\left(g_i D_i + g_j D_j\right)^3 \tag{2.14}$$

For inertia: $$b_{T2} = \frac{0.04029\, r_G^{\frac{1}{4}} q_T^{\frac{3}{4}}}{h^{\frac{5}{4}}}\left(g_i D_i + g_j D_j\right)^2 e_c \left|\frac{r_{P,i} C\left(Kn_i\right) D_i^2}{c_i} - \frac{r_{P,j} C\left(Kn_j\right) D_j^2}{c_j}\right| \tag{2.15}$$

2.3.2.1.2 Deposition

There are four deposition processes which are considered in ASTEC:

i. Sedimentation
ii. Diffusive deposition
iii. Thermophoresis
iv. Diffusiophoresis

By combining these four processes, the total deposition rate can be predicted by use of equation (2.16) below

$$R = \sum_{i,k,l} \frac{A_i}{V} \left(v_{Sed} + v_{Dif} + v_{Tph} + v_{Dph} \right) c_{l,k} \tag{2.16}$$

Where A_i is the effective deposition surface area [m^2], V is the zone volume [m^3], $c_{l,k}$ is the aerosol concentration of component k in size class l [kg/m^3] and v_j is the deposition velocity of process j [m/s].

Sedimentation is the deposition of particles under the influence of gravity. In most instances sedimentation is the dominant deposition mechanism for LWR accidents, the sedimentation velocity in ASTEC is described by the Stoke's formula with the Cunningham slip correction.

$$v_{Sed} = \frac{D_p^2 r_p g C(Kn)}{18 h_G c} \tag{2.17}$$

The slip correction is given as,

$$C(Kn) = 1 + Kn\left(F_{Sl} + 0.4 \exp\left(-\frac{1.1}{Kn} \right) \right) \tag{2.18}$$

With Kn the Knudsen number

$$Kn = \frac{2l}{D_p} \tag{2.19}$$

Diffusive deposition occurs due to Brownian motion in the concentration gradient near the deposition surface. It is predominantly a deposition mechanism for small particles, the diffusive deposition velocity is calculated by,

$$v_{Dif} = \frac{k T_G C(Kn)}{3 p h c D_p d_{Dif}} \tag{2.20}$$

Thermophoresis is a deposition mechanism that occurs in the temperature gradient towards a cooler surface. It is predicted in ASTEC according to the relation,

$$v_{Tph} = \frac{1.5 h_G C(Kn)\left(F_{Th} Kn + \frac{l_G}{l_p}\right)\nabla T}{c\, r_G T_G \left(1+3KnF_{Sl}\right)\left(1+2F_{Th}Kn+\frac{l_G}{l_p}\right)} \tag{2.21}$$

Diffusiophoresis occurs through the condensation of steam on a cold wall resulting in the transport of aerosol material towards the wall, this deposition mechanism is predicted in ASTEC according to the relation,

$$v_{Dph} = \frac{g_1\sqrt{M_W}}{g_1\sqrt{M_W}+g_2\sqrt{M_{ncG}}} \cdot \frac{G_{Wd}}{A_{Wd}\,\overline{r}_D} \tag{2.22}$$

where the average steam density in the boundary layer is predicted by,

$$\overline{r}_D = \frac{p_{D,Atm}+p_{D,Wd}}{2} \cdot \frac{M_W}{RT_{Atm}} \tag{2.23}$$

with

$$g_1 = \frac{p_{D,Atm}+p_{D,Wd}}{2p_{Tot}} \tag{2.24}$$

$$g_2 = 1-g_1 \tag{2.25}$$

2.4 IODE (IODINE CHEMISTRY) MODULE

The IODE module simulates the behaviour of iodine in the containment. The chemical reactions account for the reactions in the aqueous phase (sump), gaseous phase, and absorption/desorption mechanisms for contact with surfaces of steel, concrete or painted walls. These reactions are considered kinetically and are thus non-equilibrium based. For organic iodides, IODE models the behaviour of methyl iodide (CH_3I) only, since CH_3I is the most volatile form of the organic iodides. The reaction rate expressions and rate constants are given in the IODE user documentation [30].

2.4.1 Gas phase reactions

The reactions that are considered in the gas phase are given below,

i. Ozone formation, where γ is the dose rate (Gy/s)

$$O_2 \xleftrightarrow{g} O_3 \tag{2.26}$$

ii. Iodine oxide formation by reaction with ozone

$$I_2 + 2O_3 \longleftrightarrow 2IO_3^- \tag{2.27}$$

iii. The formation of organic iodides from the oxides, the CH_3R organic substrate is made available to reaction from painted surfaces in the containment

$$2IO_3^- + CH_3R \longleftrightarrow CH_3I \tag{2.28}$$

iv. The formation of organic iodides from molecular iodine adsorbed onto painted surfaces

$$\tfrac{1}{2} I_2 + CH_3R \longleftrightarrow CH_3I \tag{2.29}$$

v. The destruction of organic iodides

$$2CH_3I \xleftrightarrow{g} I_2 \tag{2.30}$$

$$10CH_3I + O_3 \xleftrightarrow{g} I_2 + 8IO_3^- \tag{2.31}$$

2.4.2 Liquid phase reactions

The reactions that are considered in the liquid phase are given below,

vi. Hydrolysis of molecular iodine

$$I_2 + H_2O \longleftrightarrow HOI + I^- + H^+ \tag{2.32}$$

vii. Disproportionation of HOI

$$3HOI \longleftrightarrow IO_3^- + 2I^- + 3H^+ \tag{2.33}$$

viii. Oxidation of I^- from dissolved oxygen in the aqueous phase

$$2I^- + \tfrac{1}{2} O_2 + 2H^+ \longleftrightarrow I_2 + H_2O \tag{2.34}$$

ix. Decomposition of oxides by radiolysis

$$2IO_3^- \xleftrightarrow{g} I_2 + 3O_2 \tag{2.35}$$

x. Formation of organics in the aqueous phase

$$\tfrac{1}{2} I_2 + CH_3R \longleftrightarrow CH_3I \tag{2.36}$$

xi. Destruction of organics by radiolysis and hydrolysis

$$2CH_3I \xleftrightarrow{g} 2CH_3 + I_2 \quad (2.37)$$

$$CH_3I + H_2O \longleftrightarrow I^- + CH_3OH + H^+ \quad (2.38)$$

2.5 VERIFICATION AND VALIDATION

ASTEC as been successfully validated for use on LWR applications only, and there is no indication yet of the error that could result in the code's use for HTR scenarios. The PBMR Company has extended the use of ASTEC to HTR applications since the underlying phenomenological modelling would be the same for the majority, if not all, of the phenomena occurring within the HTR confinement. The use of ASTEC as a simulation tool has been recorded as a technical risk at PBMR, but in the absence of a validated HTR confinement analysis code, there was little choice but to use a well developed and respected LWR code. There are however plans in the future for confinement analysis validation experiments based on HTR application [11], using helium and graphite dust at the ThAI (Thermalhydraulics And Iodine) facility hosted by Becker Technologies.

An independent study of a 400 MW_{th} PBMR design, using a direct helium cycle was performed by the research entity, CIEMAT [12]. Their study focused on confinement analysis using ASTEC with a comparison against the prediction of the CONTAIN [13] analysis code, in general their results were consistent between both codes. CIEMAT would continue to perform a study on the confinement performance of the 400 MW_{th} plant with the inclusion of a pressure suppression system (water pool) [14].

3. CALCULATION MODEL

This section will describe the model that was created using CPA and IODE of the ASTEC code to simulate the accident scenario for analysis. It will describe the inputs used and the modelling assumptions made.

3.1 DEMONSTRATION MODULE

The PBMR Company initially envisaged the first demonstration module to be a direct Brayton cycle with a gas turbine and recuperator to increase the net cycle efficiency as compared to traditional steam turbines. The power output of this reactor was expected to be in the region of 400 MW_{th} with a core outlet temperature of 900 ^{o}C at 90 bar absolute pressure. However due to the global economic recession the company decided in a change of product strategy during the final quarter of 2008, in order to make their product more affordable to prospective investors. It was therefore decided to design a demonstration module of 200 MW_{th} using the indirect Rankine cycle that is based on the conventional steam generator and steam turbine, with a core outlet temperature of 750 ^{o}C at approximately 70 bar absolute pressure.

This study is therefore focused on this latter reactor of 200 MW_{th}, a basic flow diagram emphasising the reactor, helium circulator, helium purification system (HPS), steam generator (SG), and the de-aerator feed tank (DFT) is shown below in Figure 2.

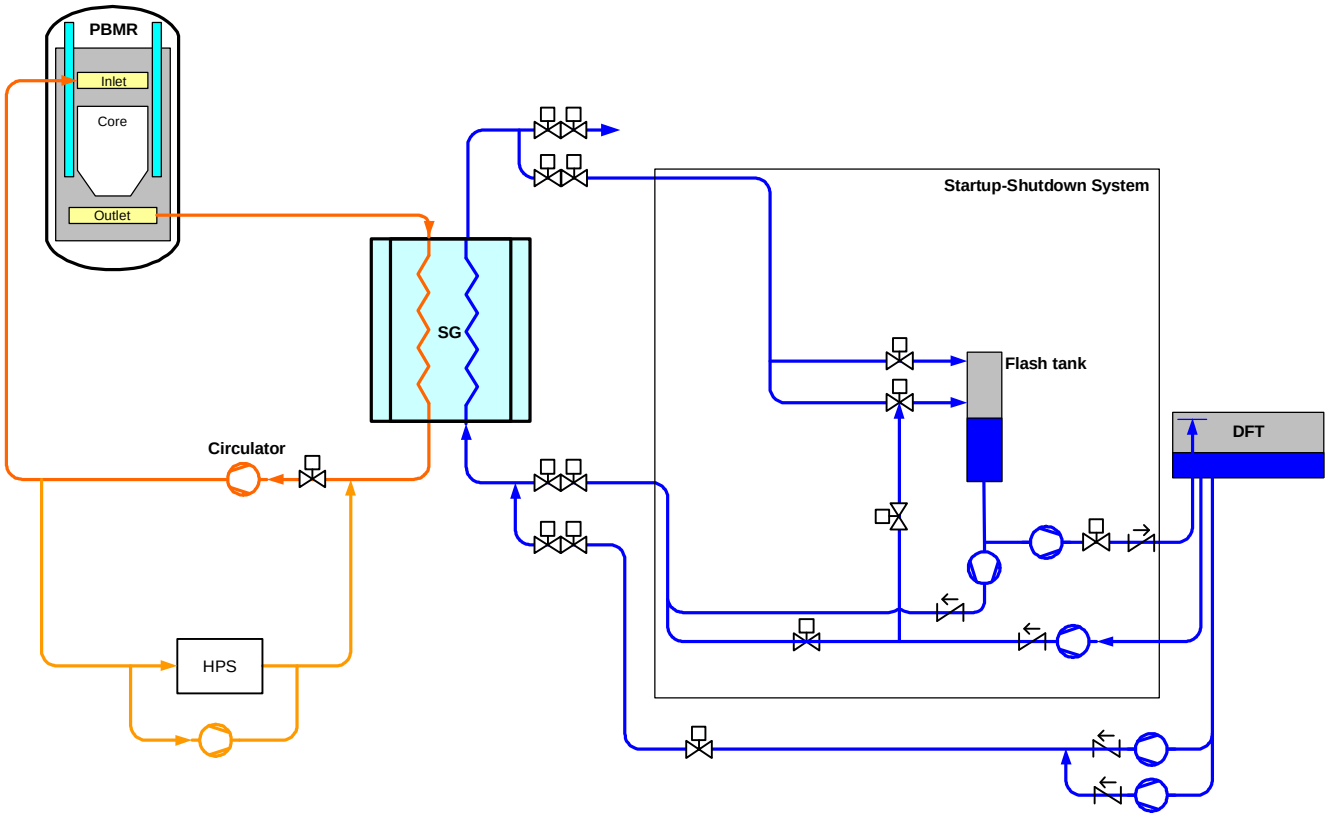

Figure 2: Flowsheet of the PBMR 200MW_{th} Cycle.

3.2 CONFINEMENT MODEL

The containment for nuclear facilities protects the public against uncontrolled exposure to activity and is conventionally a low leakage barrier that can withstand a high differential pressure. When developing the PBMR containment philosophy it became apparent that the conventional high pressure, low leakage containment may not significantly reduce public exposure in an accident any better than a vented filtered containment. The confinement concept of a vented filtered containment does, however, have the advantage of allowing earlier access into the building to close the leak. It was therefore decided that the final barrier for radionuclide retention be a vented filtered confinement.

The compartmental layout for the proposed 200 MW_{th} indirect cycle is shown below in Figure 3. The labels on the far right indicate the building height in metres and shows that the building extends for 12.7 m below ground with a further 60.0 m above ground. This 60.0 m height is the exit of the stack that will be used to disperse the filtered gas and dust in the event of an accident. Each compartment is given a unique number, for instance compartment 111805 is the Reactor Pressure Vessel compartment of Module 1, similarly 111809 is the Reactor Pressure Vessel compartment of Module 2. The compartment names as well as the elevations, floor, ceiling and wall areas are given in Table 3 and Table 4 of Appendix B for Modules 1 and 2 respectively, this information is used in CPA of ASTEC to develop the model of the confinement building.

The location of the pipebreak is the reactor pressure vessel compartment (111809). With the current design choice, this is a location for the 65 mm helium and steam pipes, it should also be mentioned that this location was recommended for analysis by the relevant system design engineers at the PBMR Company. At this stage it is not yet determined whether this is the most conservative location since a sensitivity study, by analysis of many locations with a specific measure of consequence in mind, will be required.

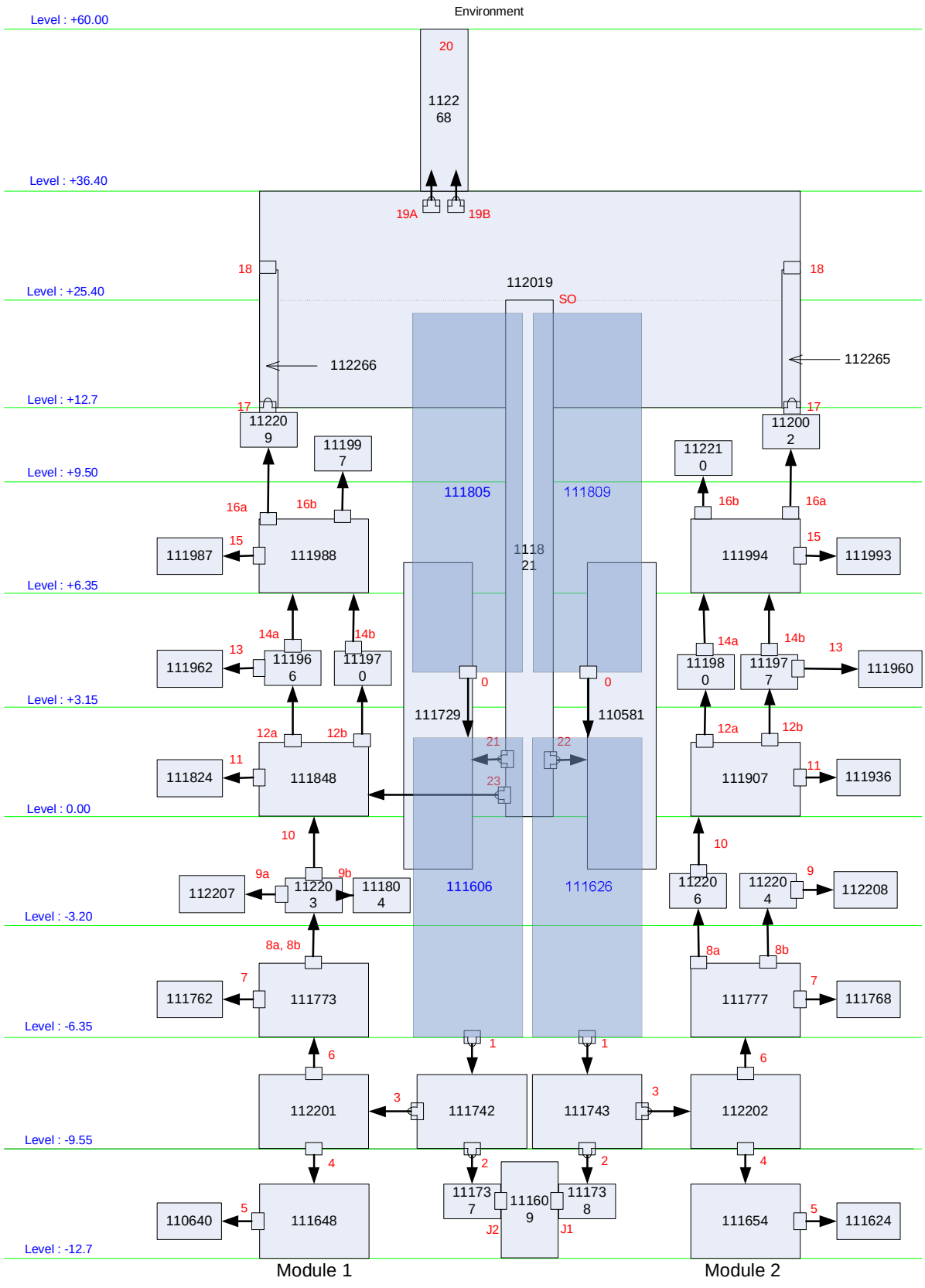

Figure 3: Compartmental layout of the PBMR module.

3.2.1 Junctions

Adjoining compartments within the confinement are interconnected through junctions. These junctions are either unobstructed openings (atmospheric junctions) or pressure sensitive burst discs (rupture panels). The rupture panels have a burst set point of 5.0 kPa differential pressure. Figure 4 below shows the difference in symbolism used in the flow diagram of Figure 3 for atmospheric junctions and rupture panels. As an example, junction 1 of both modules are connected by a rupture panel, while junctions 4 are connected by an atmospheric junction.

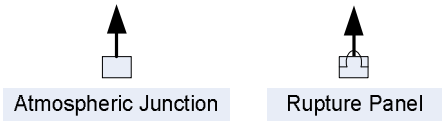

Figure 4: Symbols used to represent the inter-compartmental junctions.

The characteristics of each junction for module 1 and 2 are given in Table 5 and Table 6 of Appendix B respectively.

Please note that junction 2 of both modules, a rupture panel, in Figure 3 was not modelled into ASTEC, according to the system design description [28] this connection would not be used, therefore the only connection between modules 1 and 2 is junction 23.

3.2.2 Concrete data

The material properties for concrete are an important input into the confinement model for ASTEC, since it will determine the heat transfer characteristics of the concrete walls during the accident transient. These properties were obtained from the concrete material datasheet [16] representative of actual concrete that which will be used during construction. The values used are shown below in Table 1.

Table 1: Concrete material properties used

Name	Heat Capacity [J/kg.K]	Heat Conductivity [W/m.K]	Emissivity	Material Density [kg/m^3]
Concrete	1150.0	1.74	0.9	2420.0

3.3 THERMALHYDRAULIC SOURCE

The thermalhydraulic input describes the depressurisation profile for the helium and steam exiting the pipebreak. These were obtained from the analysis reported by the Flownex model for a 65 mm double-ended guillotine break (DEGB) of the reactor outlet pipe at the steam generator inlet and a 65 mm DEGB of the steam generator outlet line [17].

3.3.1 Helium source

The results from the Flownex analyses show that the depressurisation occurs over approximately 630 seconds with almost 3.6 tons of helium entering the reactor building. The characteristic profiles are given in Figure 5 and Figure 6 below. It can be seen that the helium mass flowrate exhibits a characteristic peak from 20 to 30 seconds this is due to the operation of the helium circulator. Once the pipe break occurs, the circulator trips and it begins to ramp down, at 20 seconds the circulator reverses flow direction for 10 seconds thus feeding more helium out of the break location. At 30 seconds the circulator is non-operational and the helium exit mass flowrate resumes a steady decay profile. A corresponding drop in temperature occurs over the same time interval where the flowrate increases; this is due to the fact that when the circulator reverses direction, it drives cooler helium from the cold leg to the break location where it mixes with the hot helium, thus the observed decrease in helium temperature over this time interval.

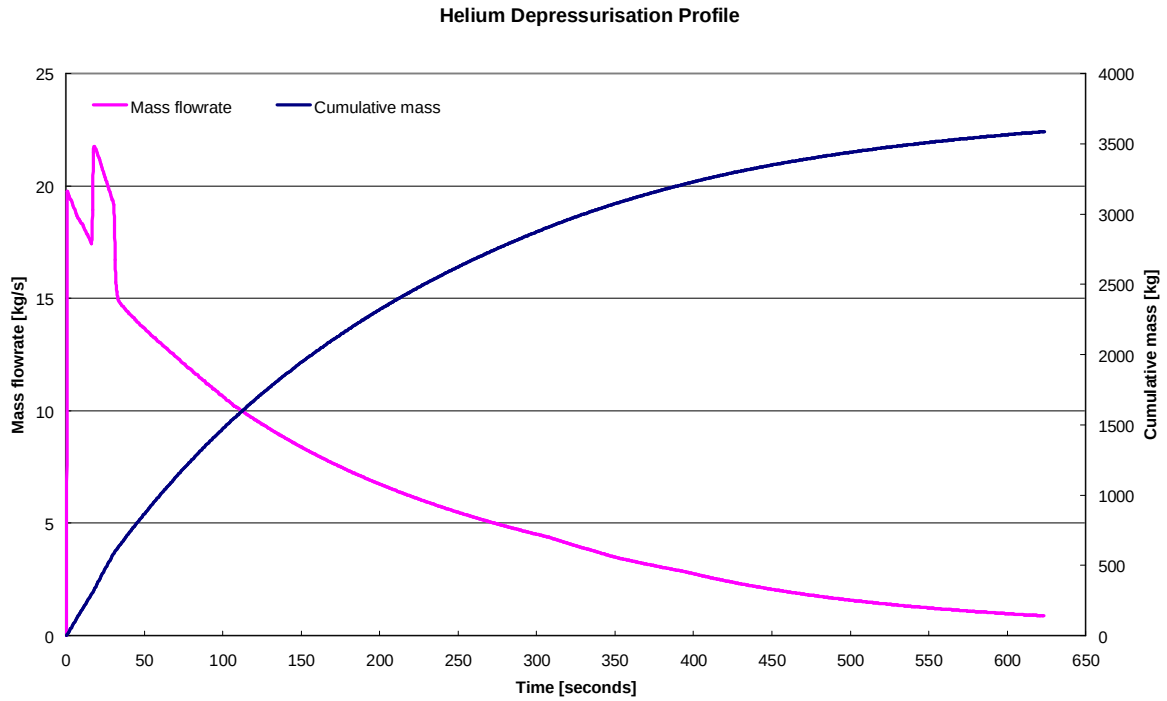

Figure 5: Helium mass flowrate and cumulative mass profile.

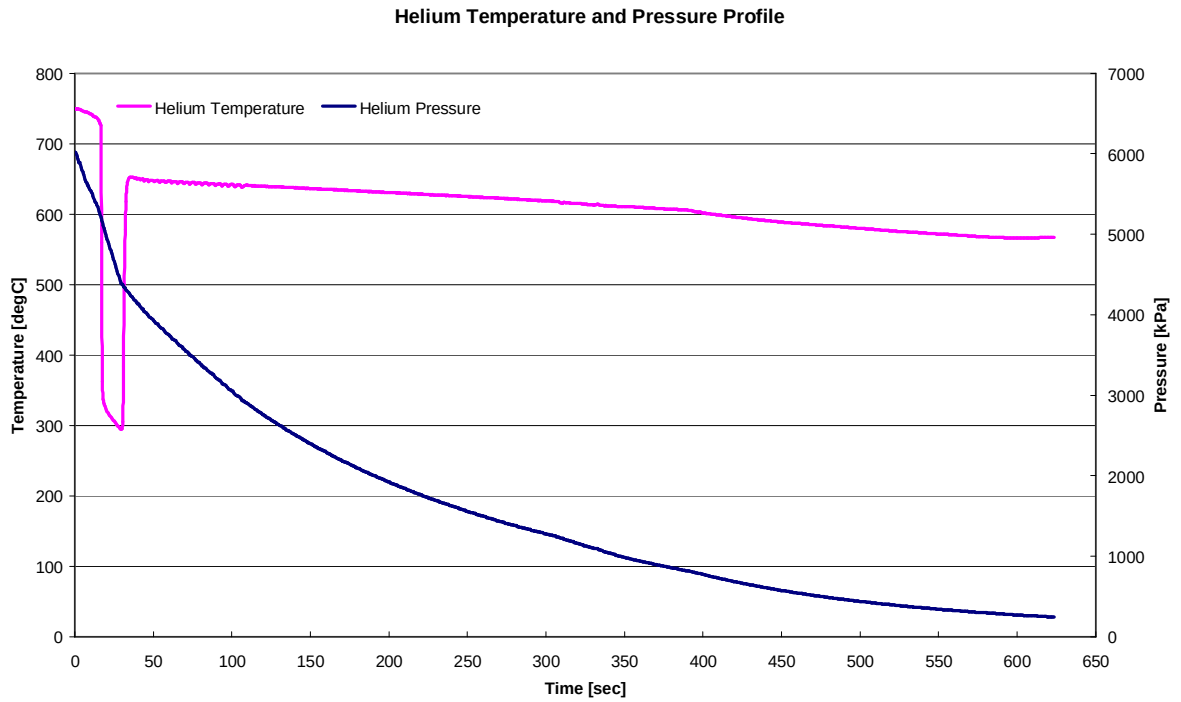

Figure 6: Helium temperature and pressure profile.

3.3.2 Steam source

The results from the Flownex analyses show that there is 10.8 tons of steam entering the reactor building at the end of depressurisation, which occurs over approximately 630 seconds. The characteristic profiles for steam are given in Figure 7 and Figure 8 below. There is a noticeable increase in the steam flowrate at 450 seconds, this is due to residual water in the steam generator that flashes into steam because of the pressure in the steam generator dropping due to the pipe break and resulting depressurisation.

The source terms for helium and steam are used as input into ASTEC for the different model cases. These source terms form the basis of the driving force for the graphite dust and fission product transport through the confinement building during the initial release phase.

3.3.3 Delayed release driving force

Once the depressurisation phase has completed, the reactor core begins to heat-up and the temperature gradient creates a driving force for gas exchange, this results in fission product transport from the core into the reactor building. A detailed computational fluid dynamics (CFD) calculation was not performed for this situation. It was assumed that the leak rate from the confinement to the environment would be one confinement volume (both modules included) per day. This was modelled, in a conservative approach, as an air source injected into the break compartment at a flowrate of 0.44 kg/s, which corresponds to one confinement volume per day, at a temperature of 120 ^{o}C. This source was assumed to commence at 1 hour after the pipe break.

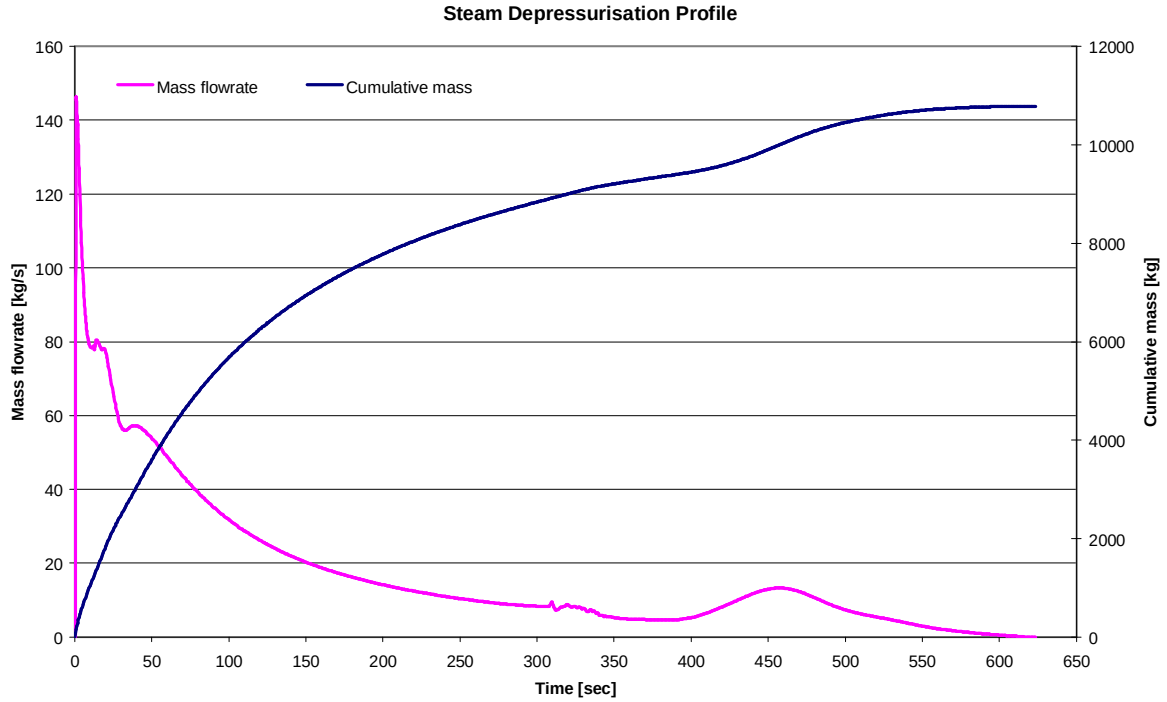

Figure 7: Steam mass flowrate and cumulative mass profile.

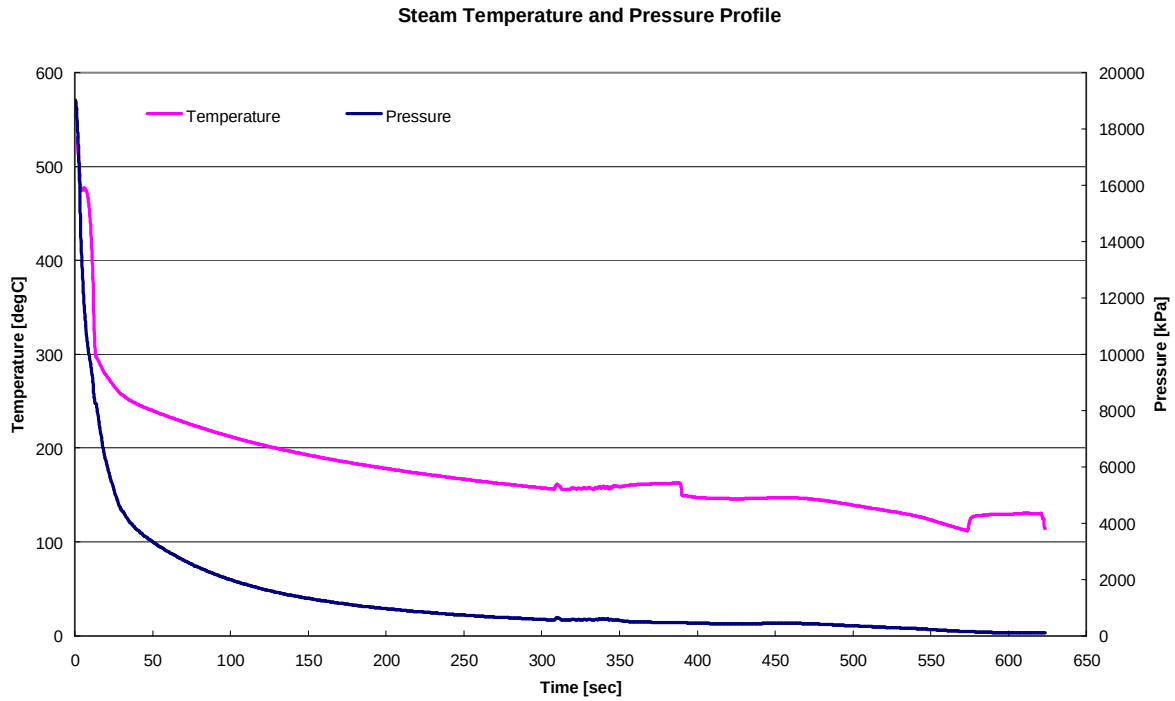

Figure 8: Steam temperature and pressure profile.

3.4 GRAPHITE DUST SOURCE

3.4.1 Dust size distribution

The graphite dust size distribution that was used as input for the models were derived from operational experience of the AVR and reported in [18]. The discrete normalised volume distribution used is shown below in Figure 9.

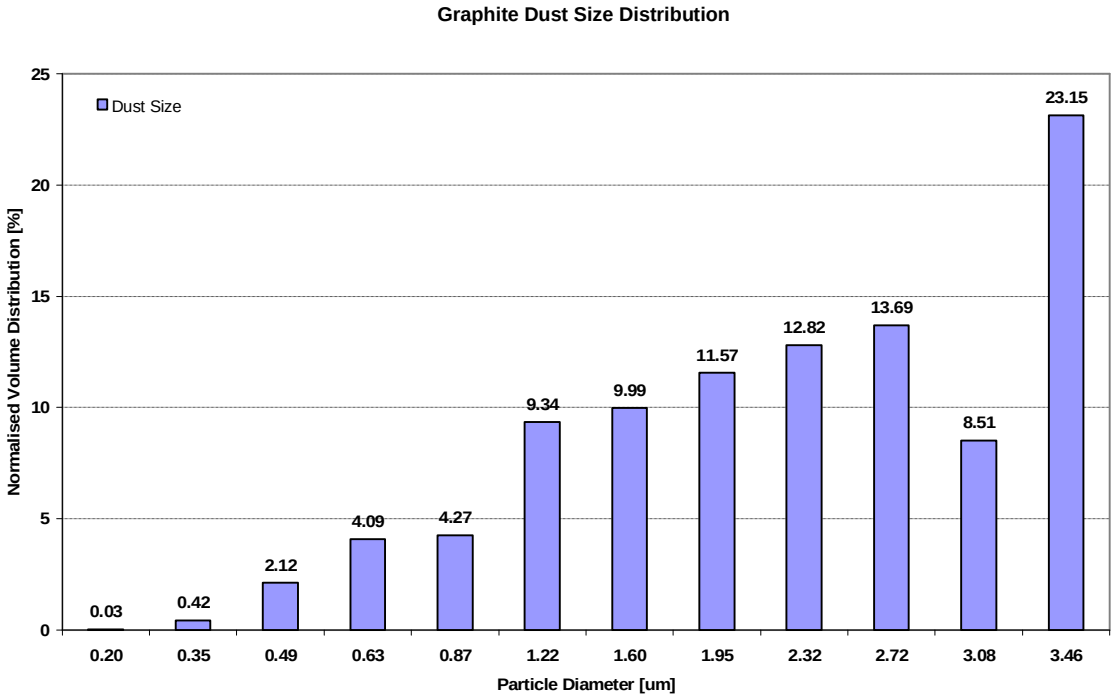

Figure 9: Graphite dust particle size distribution used as input for the models.

3.4.2 Dust injection

A formal estimation of the dust production for the 200 MW_{th} reactor configuration was not performed. To continue this work, a conservative assumption of 100 kg of graphite dust was used as a basis for the model input. This 100 kg will consist both of suspended dust in the helium coolant and dust that is remobilised within the system due to the depressurisation. Indeed 100 kg of dust is a pessimistic assumption since AVR operating experience showed a small concentration of dust suspended in the coolant and an approximate total of 60 kg of dust production during the AVR operational life [5].

The injection characteristic is shown below in Figure 10, the dust injection was assumed to correspond to the helium depressurisation profile, since the primary system helium depressurisation is the driving force for the dust transport. It was assumed that the dust mass fraction released per time interval is

the same as the helium mass fraction that is released (the latter was calculated by Flownex). It is evident that the dust profile corresponds qualitatively to that of the helium profile shown in Figure 5.

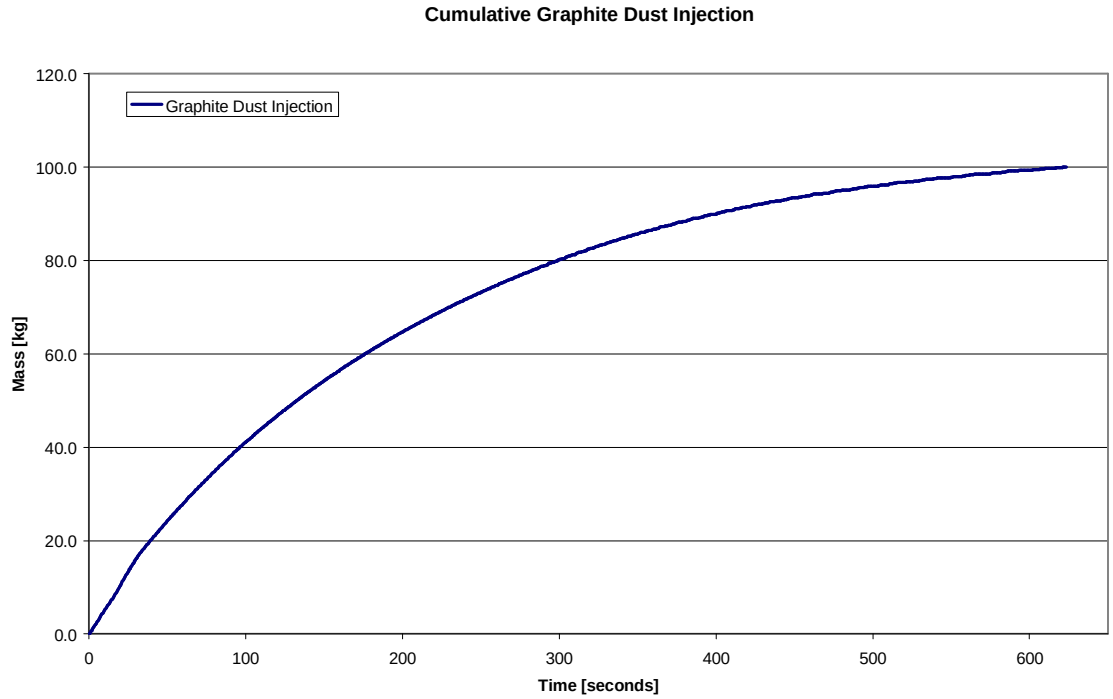

Figure 10: Cumulative graphite dust injection used for the models.

3.5 FISSION PRODUCTS

At the time of this work, fission product release estimates from the fuel for the 200 MW_{th} reactor were not completed, in order to continue with this work, activity releases from a 400 MW_{th} reactor was used instead. The releases from the latter will be considerably larger than that of the former. This approach will not disqualify any of the results obtained but rather provide valuable insight into the retention performance of the confinement building. This was applied to both the initial release and the delayed release. The absolute values of each radionuclide of interest were used.

3.5.1 Initial release

The initial release contains the circulating activity, lifted-off plate out and activity sorbed onto dust particles. The mechanism used for the prediction of the lifted-off plate out is based on a partial pressure model, this falls outside the scope of this work and is discussed in [19]. The radionuclides investigated for the initial release are ^{110m}Ag, ^{137}Cs, ^{90}Sr and ^{131}I, while for the delayed release ^{111}Ag is investigated rather than ^{110m}Ag. These radionuclides were identified as contributing to the majority of the accidental doses [20]. Initial release activities are taken from [21].

3.5.1.1 Gaseous fission products

The fission products that are in the gaseous phase result from the circulating activity and lifted-off plate out, these are released into the confinement from the pipe break. The amounts for the fission

products are shown below in Figure 11 and Figure 12 for ^{110m}Ag and ^{137}Cs, and ^{131}I and ^{90}Sr respectively.

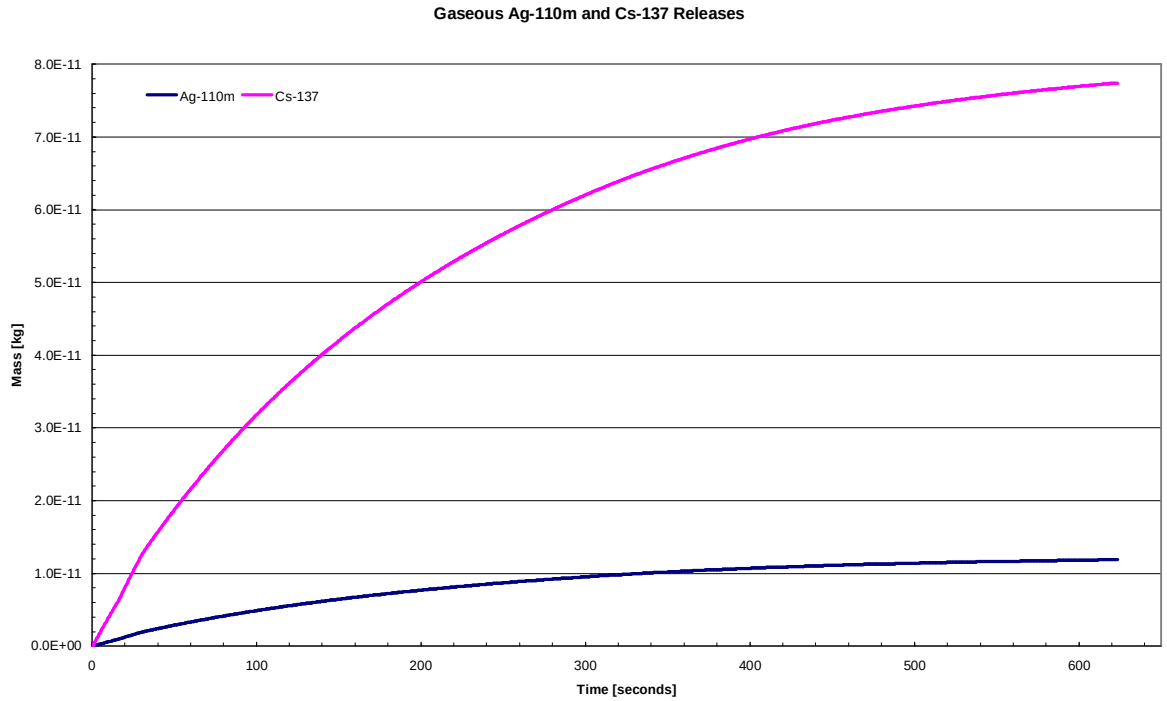

Figure 11: Gaseous ^{110m}Ag and ^{137}Cs releases.

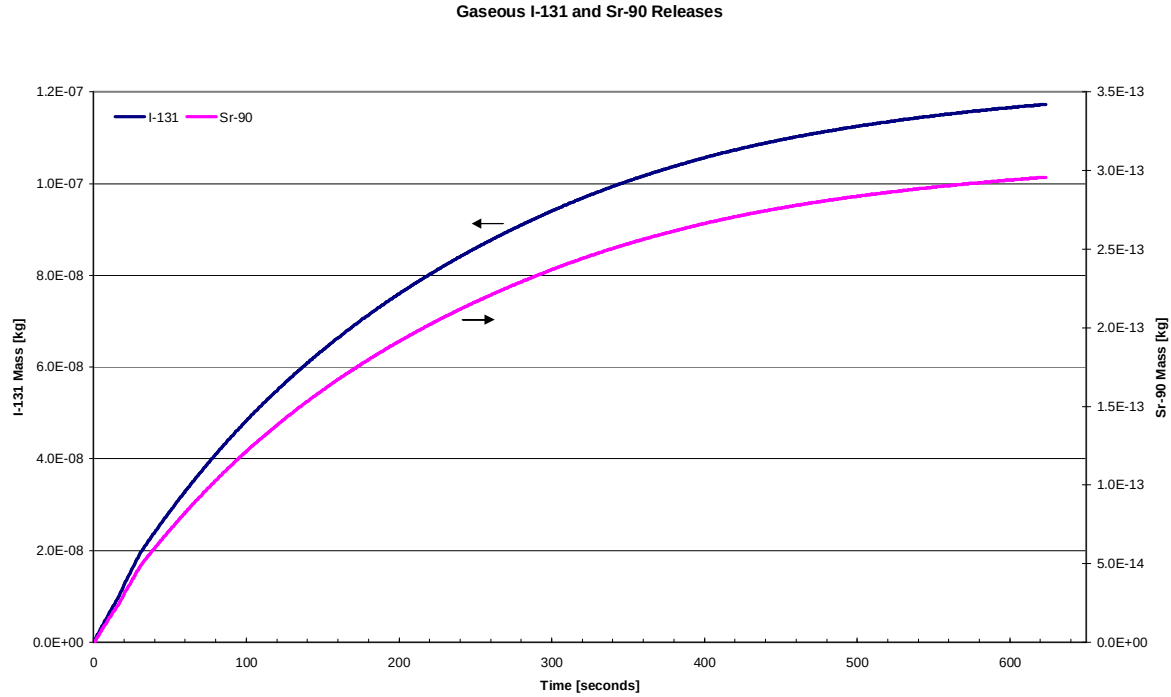

Figure 12: Gaseous ^{131}I and ^{90}Sr releases.

3.5.1.2 Fission products sorbed onto dust

Metallic fission products are also sorbed onto the dust particles entering the confinement. The amounts of these fission products are shown below in Figure 13 and Figure 14 for ^{137}Cs and ^{90}Sr, and ^{110m}Ag respectively.

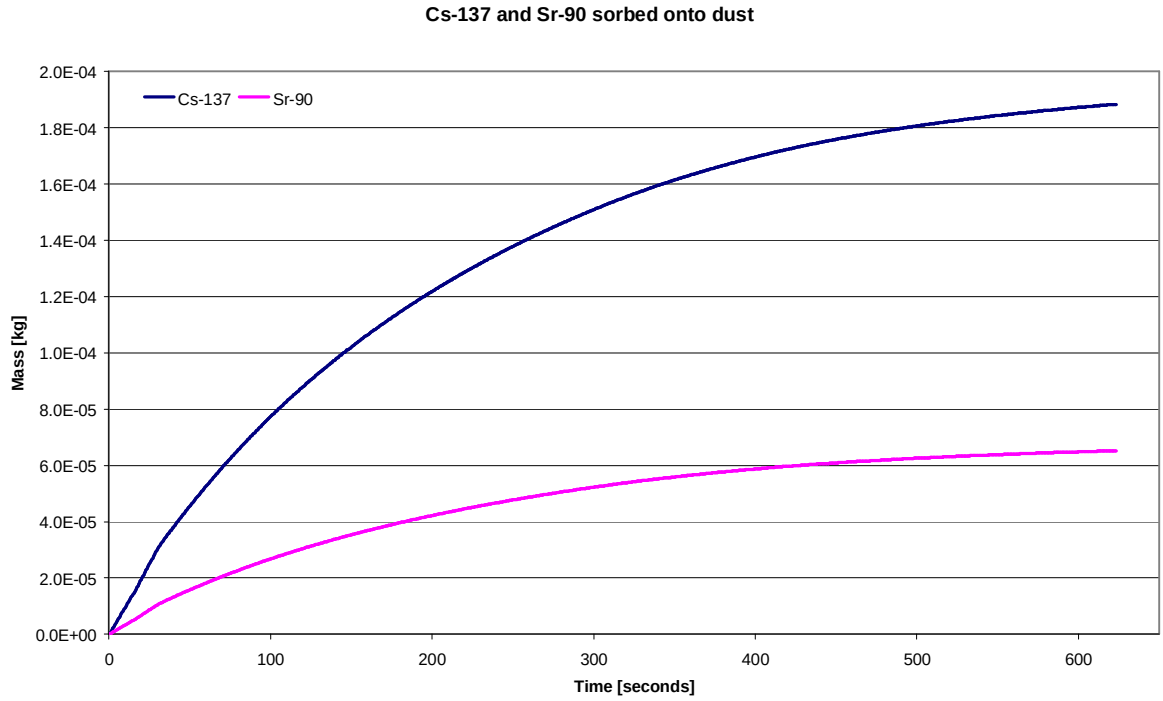

Figure 13: ^{137}Cs and ^{90}Sr sorbed onto dust.

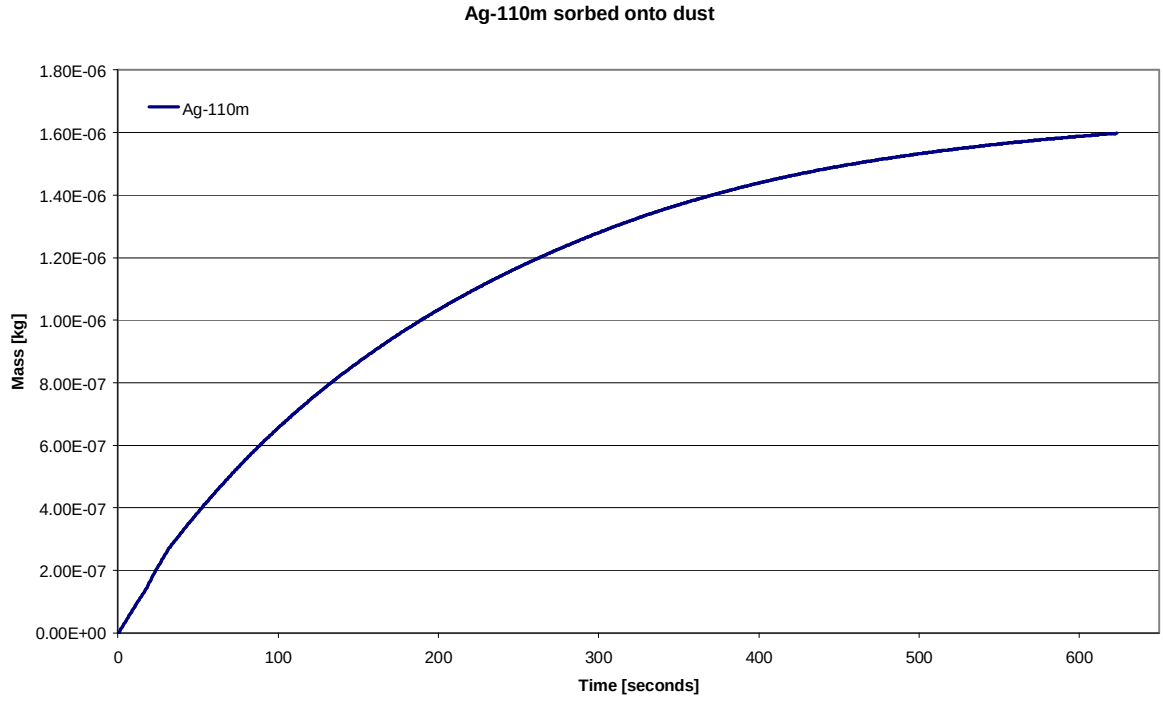

Figure 14: ^{110m}Ag sorbed onto dust.

There was no ^{131}I modelled as sorbed onto dust because all iodine as been assumed to be present in the gaseous phase only, this is a more pessimistic assumption with regard to iodine chemistry.

3.5.2 Delayed release

The delayed release is a significantly higher discharge than the initial release; this is a result of the heat up of the core due to the loss of forced helium cooling. The temperatures of the core begin to exceed normal operational temperatures and the increased fuel temperature promotes diffusion of radionuclides out of the fuel and into the reactor cavity where it can be a potential source for release into the confinement. In addition to the diffusion rate, a small percentage of coated particles become damaged and lose their ability to retain fission products. This increased temperature transient of the core does not continue perpetually, but will drop due to the passive and natural mechanisms of heat transfer from the core. The mechanisms of fission product release out of the fuel kernel, such as diffusion, recoil and knock-out that are used as the basis for the calculation methodology is outside the scope of this work and is described in [22].

3.5.2.1 Size distribution

The metallic fission products as a consequence of the delayed release will be expected to be present as aerosols rather than a gaseous phase since the temperatures in the confinement will be significantly lower after the depressurisation. Metals, due to their low vapour pressure will prefer to condense and this will be expected for the delayed release. The crucial aspect is determining the size of the particles that will result once the metals condense to form aerosols. To consider nucleation theory and postulate a size of aerosol is considered beyond the scope of this study, it is rather more practical for the purpose of this study, to investigate a best estimate size and a conservative size.

3.5.2.1.1 Best estimate size

Information on the aerosol size during HTR accident conditions is scarce; however there was an investigation into the formation of Cs aerosols during HTR accident conditions by Katscher and Stauch [23]. Their recommendation after completion of the experimental tests was that Cs with a particle size of 0.3 µm be used for accident analyses. The authors did not investigate the behaviour of Ag and Sr during their work. Table 2 below indicates the physical properties of the three metals, it can be seen that Ag is the most refractory of the metals with the highest melting and boiling points.

Table 2: Physical properties of Cs, Sr and Ag

	Melting Point [^{o}C]	Boiling Point [^{o}C]	Heat of Vaporisation [kJ/mol]
Cs	28.4	670.9	67.7
Sr	767.9	1376.9	144.0
Ag	960.9	2162.9	250.6

To determine a probable particle size for Sr and Ag, light water reactor experience was used as reference. Data was available for Ag aerosols from experimental tests during the Phébus programme and were used in code validation exercises with a characteristic size of 2.8 μm and a geometric standard deviation (GSD) of 1.9 [24]. During the AHMED experimental tests on aerosol behaviour in LWR containments [25], Ag was investigated at a particle size of 2.7 μm and a 1.7 GSD. The reason for investigating this particle size was not reported, however it is similar to that reported from the Phébus programme [24]. For this study it was decided to use the former size since this was derived from experimental evidence.

The data presented in Table 2 suggests that Sr should have a size range that is between Cs and Ag, but in the absence of experimental data indicating this, it was considered conservative to use a size of 0.3 μm for Sr as found for the Cs aerosol.

3.5.2.1.2 Conservative size estimate

The motivating factor for choosing the conservative size is the aerosol deposition rate, this size can be estimated by analysing the deposition process with respect to gravitational (sedimentation) and diffusional settling, equations (2.17) and (2.20) respectively. Figure 15 below taken from [8] shows that deposition by diffusion is most effective for the smaller particle sizes while gravitational settling dominates for the larger particles. By taking the sum of these two settling rates a minimum deposition velocity in the region of 0.1 μm is evident. This value of 0.1 μm was chosen for the conservative aerosol size estimation because it will result in the lowest deposition rate.

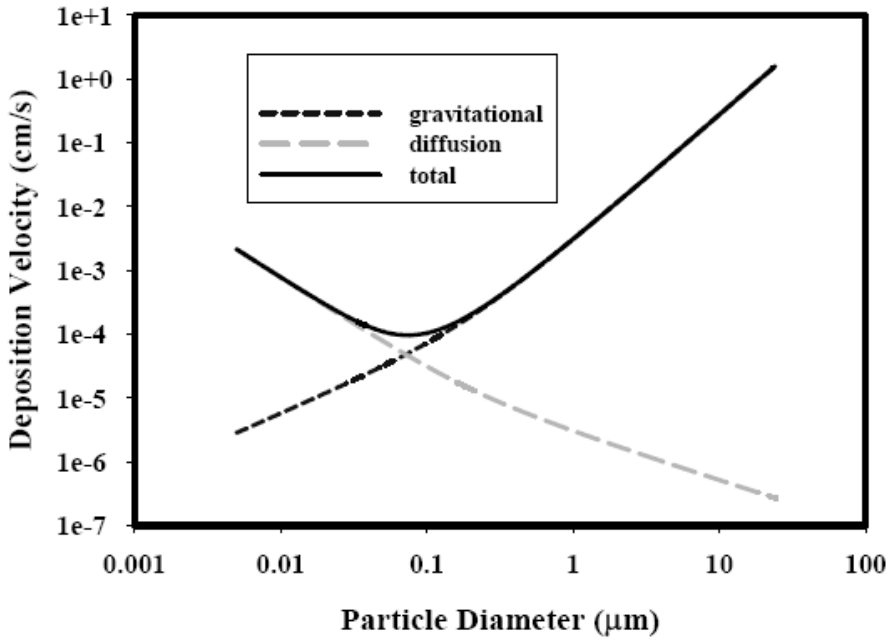

Figure 15: Dependence of deposition velocity on particle diameter [8].

3.5.2.2 Release rates

The delayed release rates used for this study were taken from those calculated for the 400 MW_{th} design [26]. The release amounts are given below in Figure 16 for ^{111}Ag, ^{90}Sr and ^{131}I and in Figure 17 for ^{137}Cs.

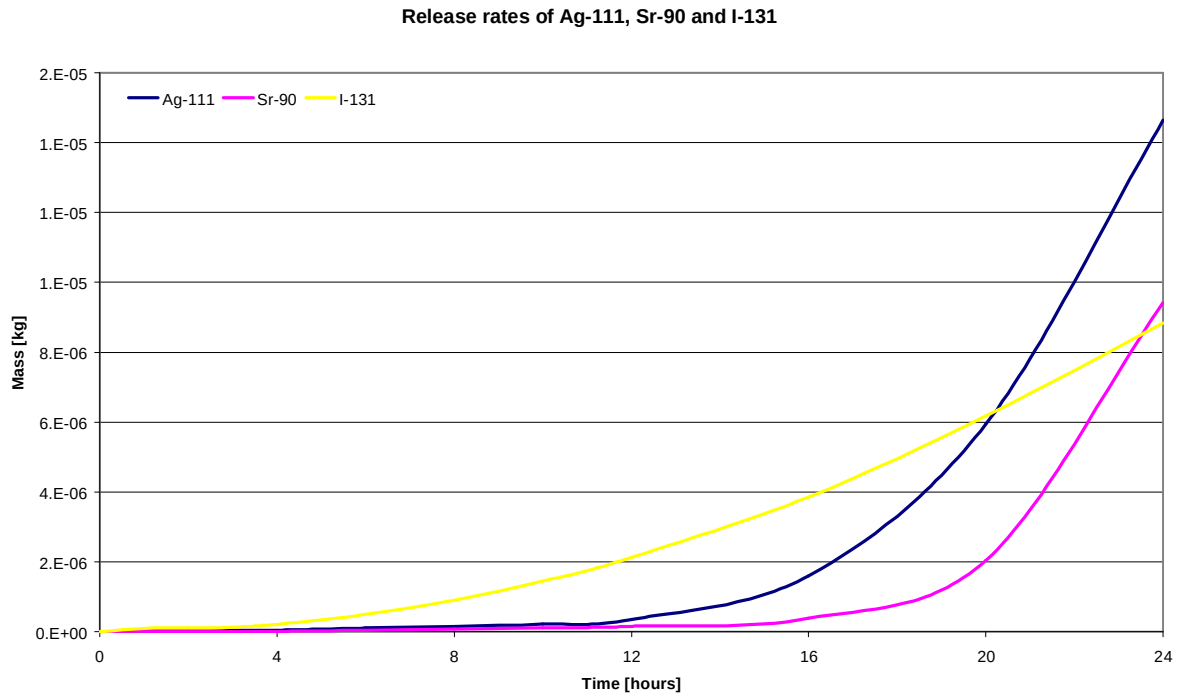

Figure 16: Delayed releases for ^{111}Ag, ^{90}Sr and ^{131}I.

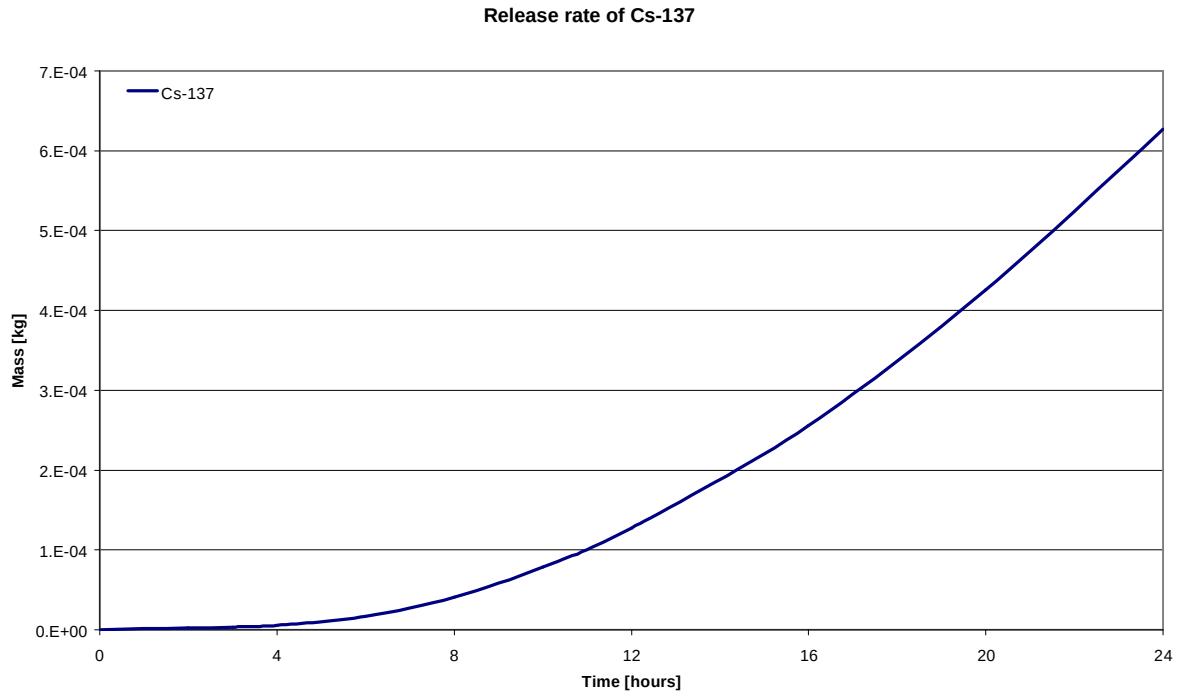

Figure 17: Delayed releases for ^{137}Cs.

3.6 MODEL ASSUMPTIONS

This section outlines the assumptions that were made in order to create the models for analyses.

i. The agglomeration (γ) and dynamic shape (χ) factors are assigned a value of unity; this will imply that all aerosol particles are modelled as being perfectly spherical.

ii. The adsorption and de-sorption rates of molecular iodine (I_2) have been obtained from the recommended values given in the ASTEC user guidelines report [27]. For adsorption a value of 1×10^{-3} m/s and 1×10^{-5} s^{-1} for the de-sorption rate was recommended.

iii. Iodine as been assumed to be present in the vapour form only and not sorbed onto dust particles.

iv. The dust injection during the initial release phase was assumed to correspond to the helium depressurisation profile.

v. The driving force for the delayed release was assumed to be an air exchange of one confinement volume, consisting of both modules, released per day.

vi. The initial condition for each compartment was set to a temperature of 25 ^{o}C and a relative humidity level of 40 %.

The model input file for the ASTEC calculation model is given in Appendix C for reference. Due to the length of the input file, which describes the compartment sizes, wall areas, junction dimensions, and the source terms, only the main input file is given.

4. RESULTS AND DISCUSSION

4.1 HELIUM PIPE BREAK ANALYSIS

This section discusses the results obtained from the analysis for a single 65 mm DEGB of the reactor outlet pipe only. The following sections will highlight the thermalhydraulic, aerosol and fission product, and iodine chemistry behaviour for this accident scenario. The compartment where the break occurs is the reactor pressure vessel compartment (111809) of module 2 (refer to Figure 3).

Due to the long calculation time for this accident scenario, the transient was only analysed for five hours following the pipe break.

4.1.1 Thermalhydraulic results

4.1.1.1 Pressure

The pressure transient within the reactor building is an important parameter for investigation. If the pressures are great enough the structural integrity of the building can be compromised which could result in uncontrolled radiation exposure to the public. The reactor pressure vessel compartments and steam generator compartments of module 1 and 2 are designed to tolerate pressures not exceeding 250 kPa (absolute), while all other compartments are design for a maximum absolute pressure of 140 kPa [28]. The following figures show the response of the building as a result of the helium pipe break as calculated by CPA of ASTEC.

Please note each compartment number is prefixed with the letter “Z”, this has been inherited from the variable nomenclature in ASTEC. Variables are not allowed to be defined as numerical, hence the prefix “Z”.

Figure 18 below shows the pressure response of five consecutive compartments in Module 2 where the pipe break occurs. It can be seen that the steam generator (111626) and the reactor pressure vessel (111809) compartments do not exceed the maximum pressure of 250 kPa, it is difficult to distinguish the profile for 111626 but it is almost identical to that of 111809. Compartments 112202 and 111654 are also almost identical in profile. It is evident that compartment 111743 exceeds the design pressure of 140 kPa for a duration of 10 seconds, beginning at approximately 6 seconds. This is an important finding since it is possible that the structural integrity of this compartment may be compromised during this accident scenario. The peak pressure recorded in this compartment is 149 kPa.

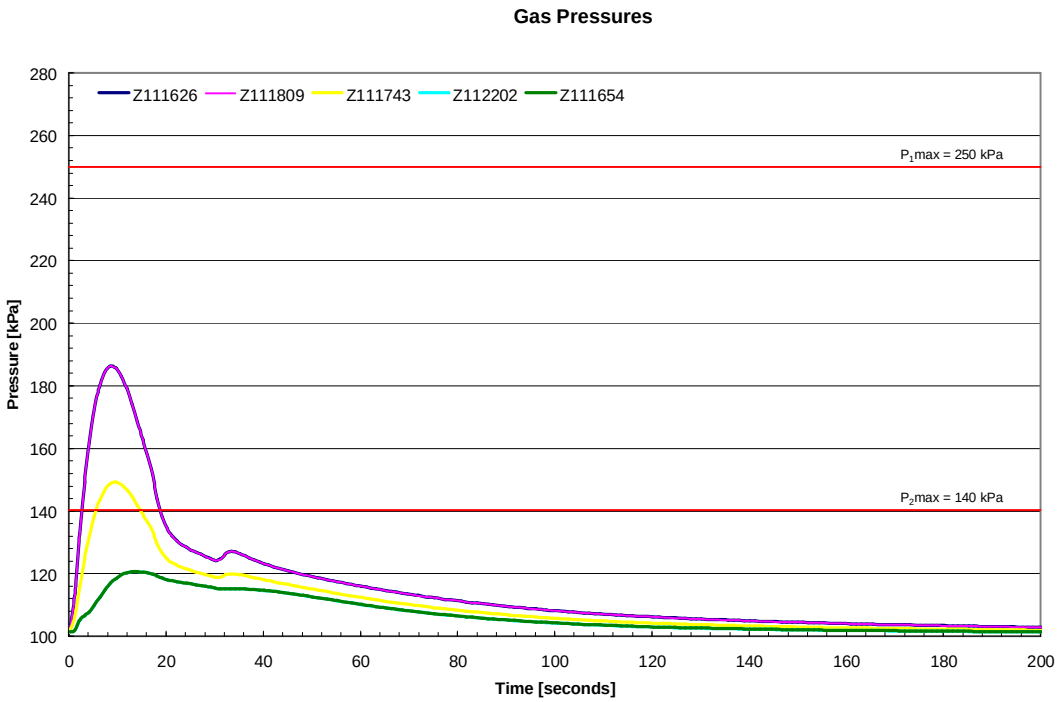

Figure 18: Pressure response of compartments in Module 2.

Figure 18 shows that the violent pressure transient lasts approximately for the first 100 seconds thereafter dropping sharply to atmospheric pressure. The remaining compartments of modules 1 and 2 exhibit behaviour similar to compartments 112202 and 111654 of Figure 18.

4.1.1.2 Temperature

Figure 19 and Figure 20 below show the temperature transient from 0 to 200 and 0 to 18000 seconds (5 hours) respectively. The sharp drop in temperature between 20 and 40 seconds is due to the colder helium that is injected during this phase as discussed in § 3.3.1 and shown in Figure 6. The temperature reaches a maximum of 546 ^{o}C in the break zone, 111809. The profile in Figure 20 shows that the temperature in compartment 111809 (the break zone) remains higher than the other compartments after 4000 seconds, this is because of the delayed release driving force as discussed in § 3.3.3, which is at a flowrate of 0.44 kg/s and 120 ^{o}C.

The remaining compartments of Module 2 have similar temperature profiles however their maximum temperatures range between 250 and 400 ^{o}C, while compartments of Module 1 have maximum temperatures not exceeding 40 ^{o}C.

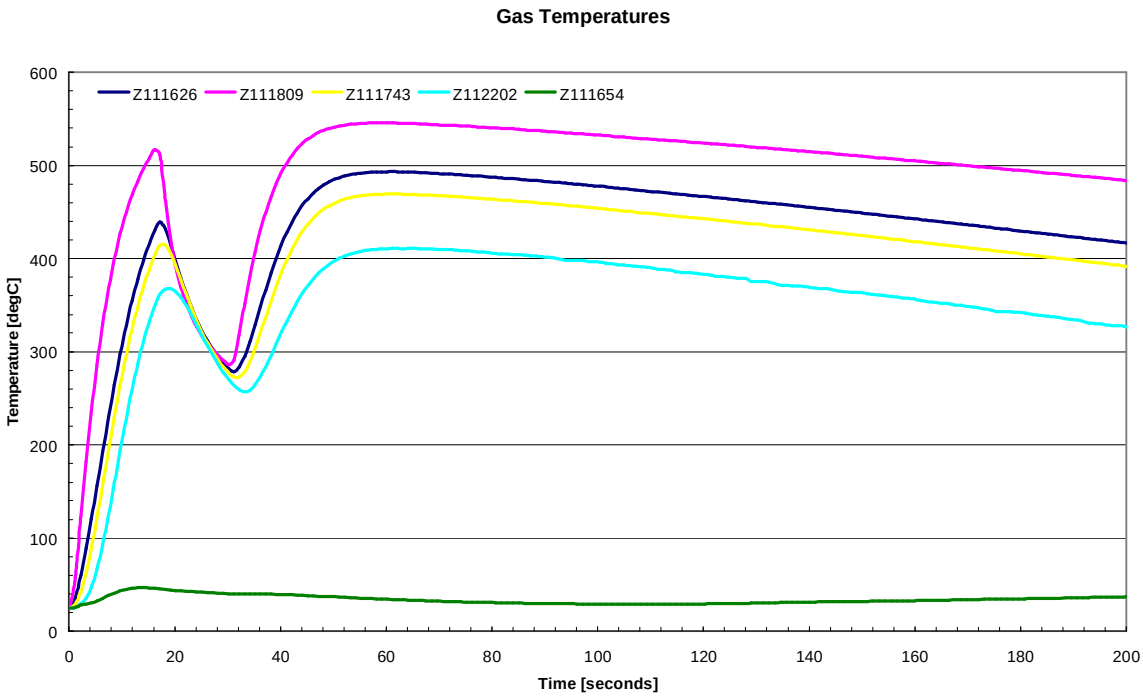

Figure 19: Temperature profile of compartments in Module 2 (200 seconds).

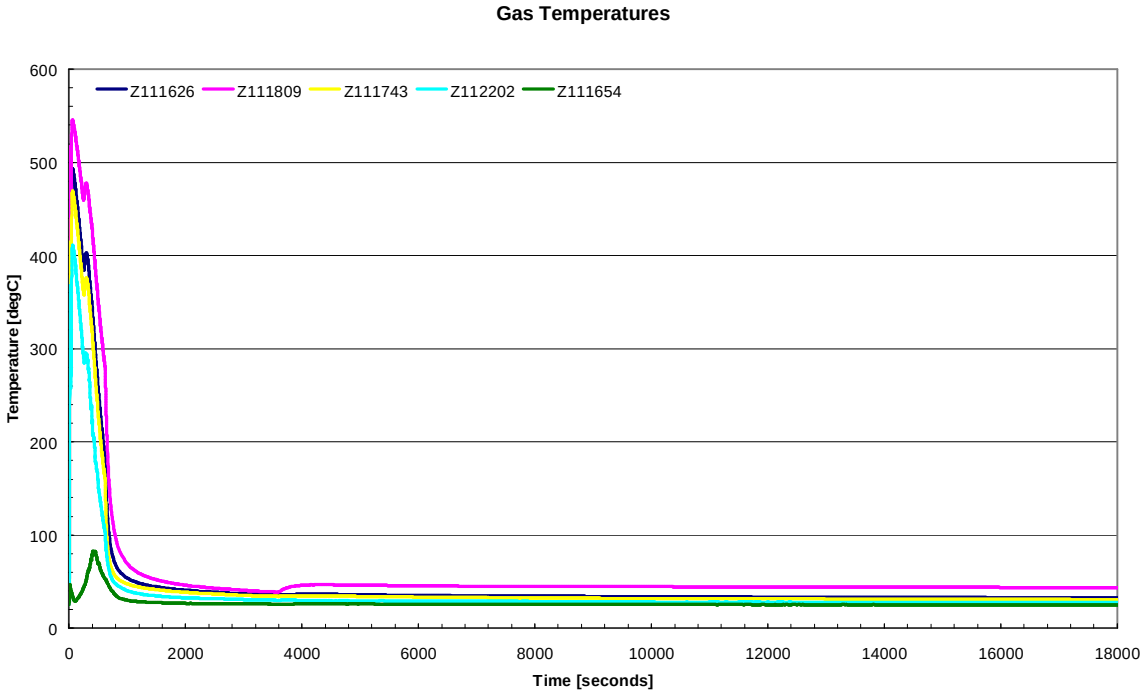

Figure 20: Temperature profile of compartments in Module 2 (18000 seconds).

4.1.1.3 Junction flowrates

The junction mass flowrate data allows one to determine the intervals at which the important rupture panels burst, as well as the flowrate out of the stack and into the environment. Figure 21 below shows the mass flowrate for junctions 19A, 19B, 21, 22 and 23. At 3.8 seconds, junction 23, which connects modules 1 and 2, bursts. Shortly thereafter junctions 21 and 22 burst, these two junctions connect to the stairwells of module 1 and 2 respectively. At 6.5 seconds the panels that lead to the stack and the environment (19A and 19B) burst, allowing the helium to escape into the environment. It is evident from the almost immediate burst times that the depressurisation propagates rapidly through both modules and is relieved into the environment. The profiles for 19A and 19B are exactly the same since these junctions are of the same area and elevation.

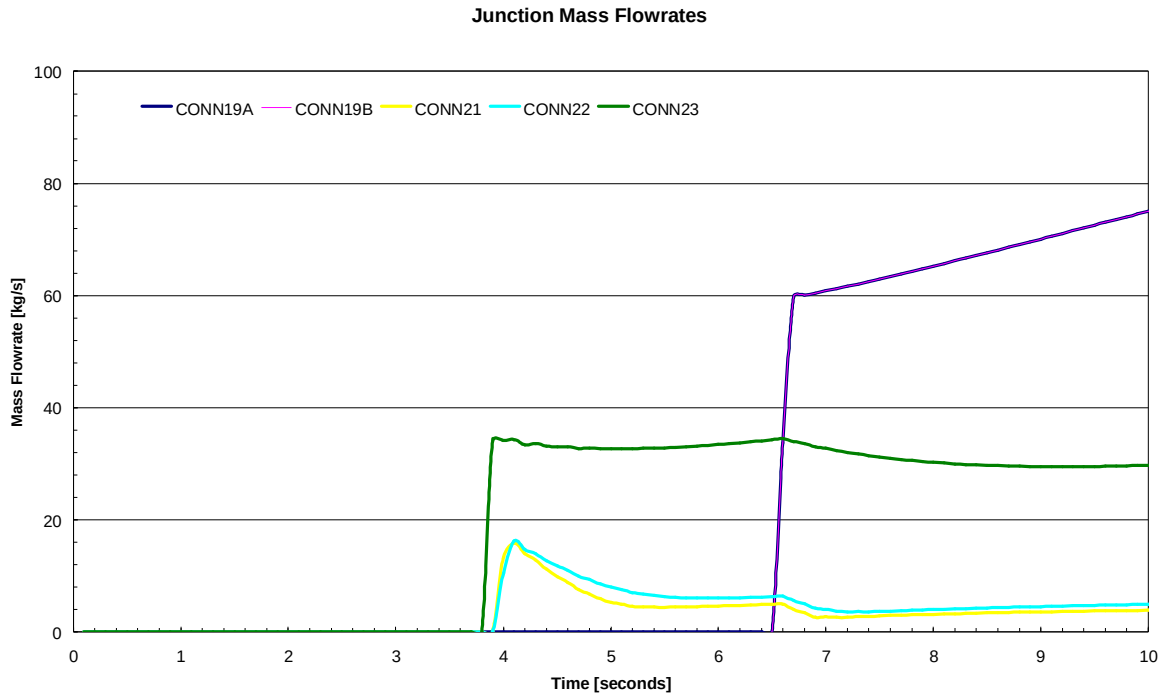

Figure 21: Junction mass flowrates at 10 seconds.

Figure 22 below shows the flowrates up to 700 seconds, the noticeable characteristic is the large mass flowrate out of junctions 19A and 19B into the environment during this initial release phase. The profile for 19A and 19B lie directly over each other.

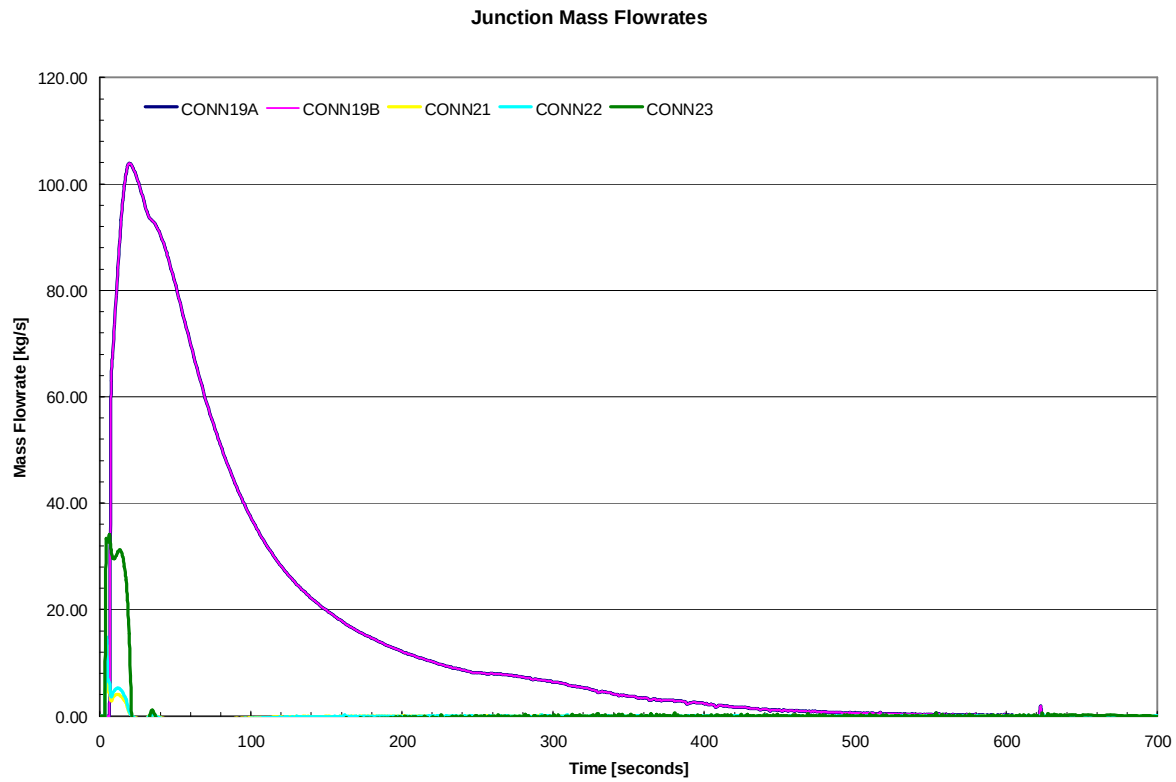

Figure 22: Junction mass flowrates at 700 seconds.

4.1.2 Graphite dust and fission product results

4.1.2.1 Graphite dust

The results for the graphite dust as produced by ASTEC are very detailed for each compartment, reporting the mass deposited on vertical walls, ceilings, and floors, and the mass remaining in suspension within each compartment of the confinement. Due to the large amount of data, it is more practical to provide a summary of the calculation than to report the detailed results per compartment.

Figure 23 below summarises the mass of dust deposited on confinement walls, floors, and ceilings; and the mass of dust remaining in suspension within the first 700 seconds of the transient. The majority of the dust remains in suspension over this time period since this is the depressurisation phase. Figure 24 shows that once the depressurisation is over the dust begins to settle by sedimentation rapidly. It is evident that the floor is the most effective deposition surface with just over 55 kg depositing within 5 hours (18000 seconds), since exactly 100 kg of dust was injected, 55 kg represents 55 % of the total dust.

The amounts that have been deposited onto the ceilings are extremely small.

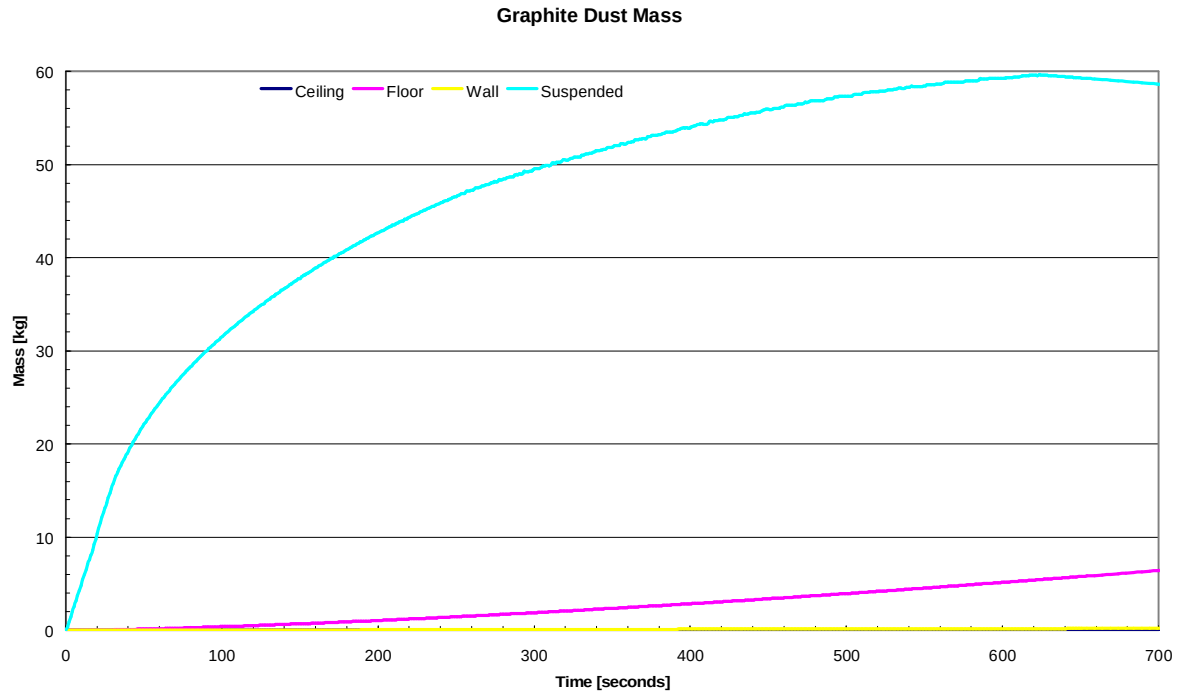

Figure 23: Graphite dust mass within the confinement (700 seconds).

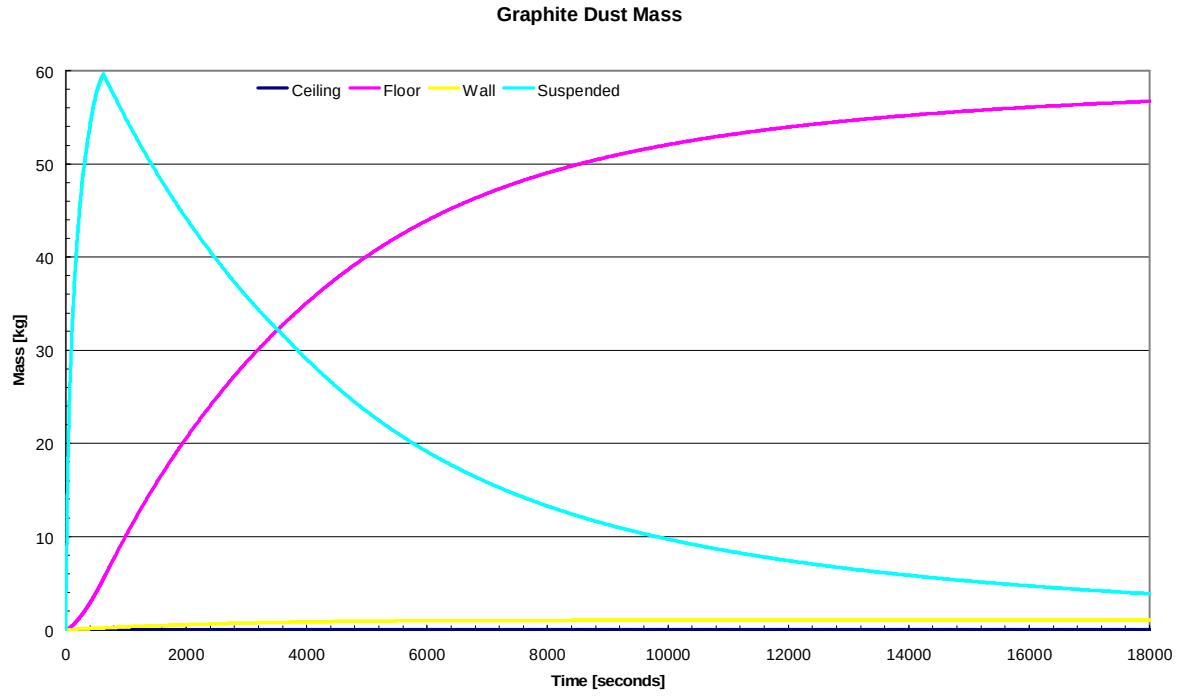

Figure 24: Graphite dust mass within the confinement (18000 seconds).

Figure 25 below shows the amount of dust that is deposited into the filter and the amount of dust that has been released into the environment. Almost 35 % of the dust is deposited into the filter over the first 5 hours; the HEPA filter has a retention efficiency of 90 % for dust particles. The retention of graphite dust after 5 hours within the building and trapped in the HEPA filter is approximately 96.2 % (floors, walls, ceiling, filter and suspended) while the remaining 3.8 % escapes into the environment, this is clearly shown in Figure 26.

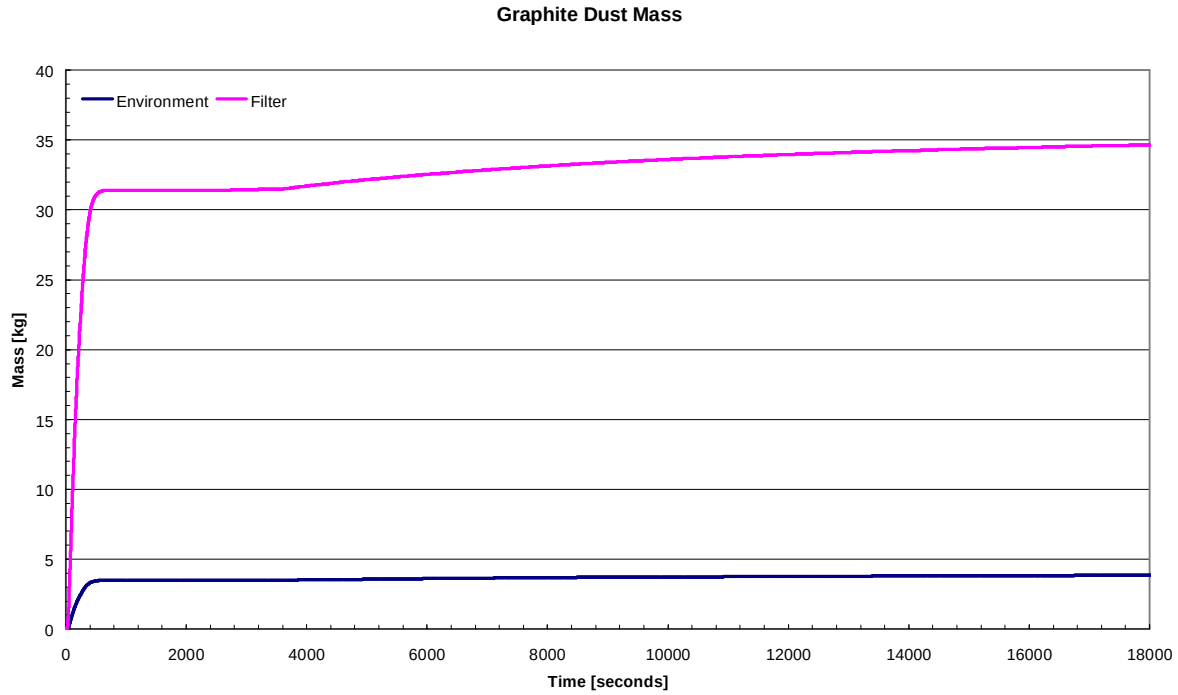

Figure 25: Graphite dust mass deposited in the filter and released into the environment.

Figure 27 below shows the mass balance on the graphite dust, between the amounts that ASTEC reports and that which was actually used as injection material. There is very good agreement between the two values and the balance is thus closed. Balancing injection material is an important aspect of any calculation, as it will be later shown that ASTEC has difficulty in completely balancing small quantities of aerosols.

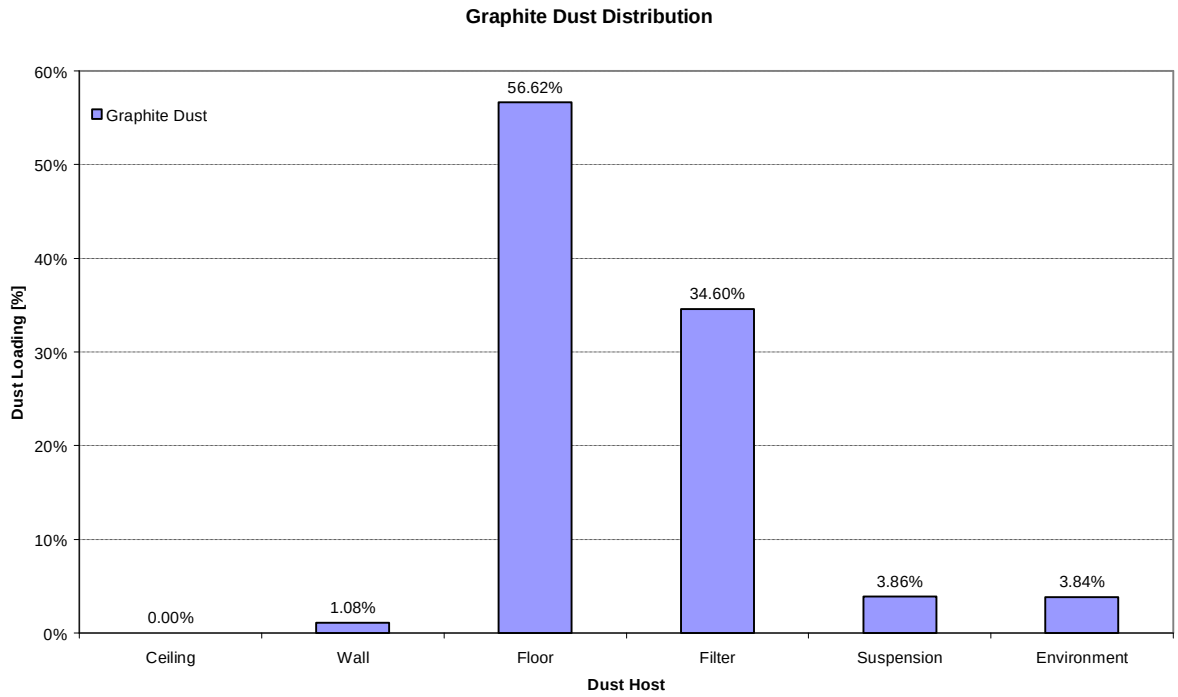

Figure 26: Graphite dust distribution on hosts (18000 seconds).

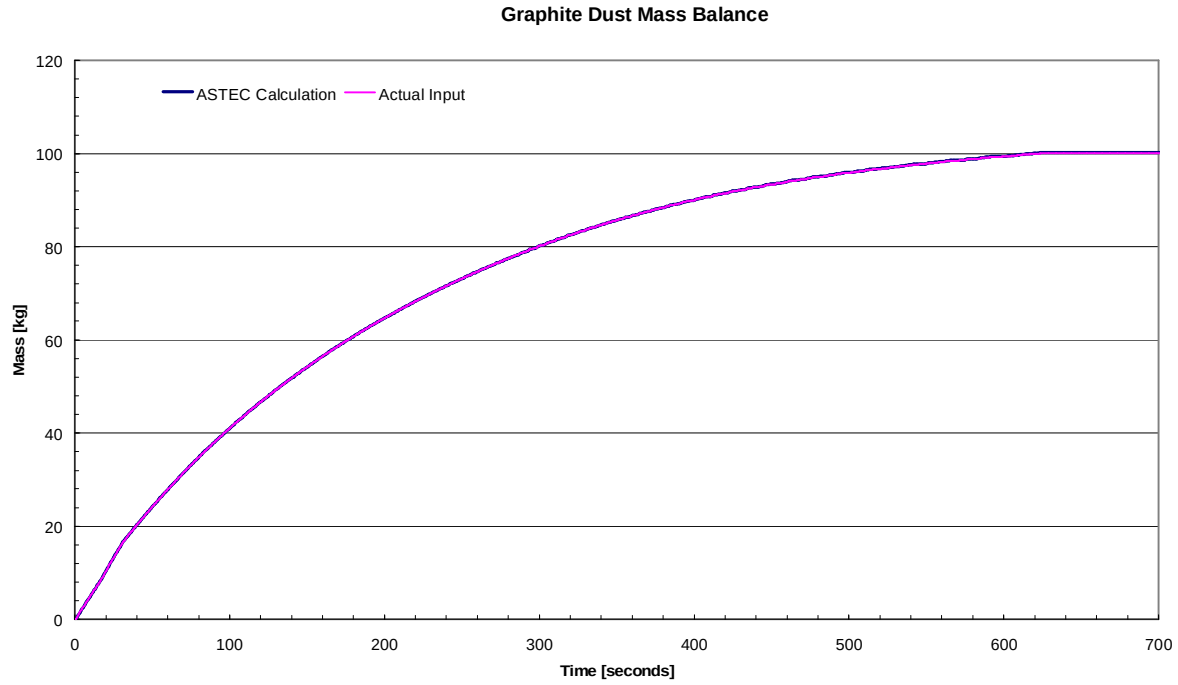

Figure 27: Graphite dust mass balance.

4.1.2.2 Fission products

4.1.2.2.1 Initial release of metallic fission products

Figure 28, Figure 29 and Figure 30 below shows the ASTEC calculation for ^{110m}Ag, ^{137}Cs, and ^{90}Sr respectively, these figures show the amount of fission product remaining in the confinement and that which is released into the environment. Naturally there is an increase in fission products within the confinement over the depressurisation phase, thereafter the mass remains almost constant within the confinement with almost no release to the environment. At 3600 s (1 hour) the amount within the confinement starts to decrease and that into the environment starts to increase again, this is due to the delayed release driving force (see § 3.3.3) which commences at this point and slowly drives fission products out into the environment. There was no filtration modelled for metallic fission products since HEPA filters cannot trap it.

The retention after 5 hours for ^{110m}Ag, ^{137}Cs and ^{90}Sr is 48.2 %, it can be noted from the figures that the fission products continue to escape to the environment due to the driving force of the delayed release. There are design plans for a passive closure system allowing the closure of the area of the burst panels to the environment immediately after the depressurisation, thus preventing air exchange with the environment, however this has not been considered for the scope of this study.

Figure 31, Figure 32 and Figure 33 shows the mass balance for ^{110m}Ag, ^{137}Cs, and ^{90}Sr respectively. It is evident that the mass balances for the metallic fission products are closed.

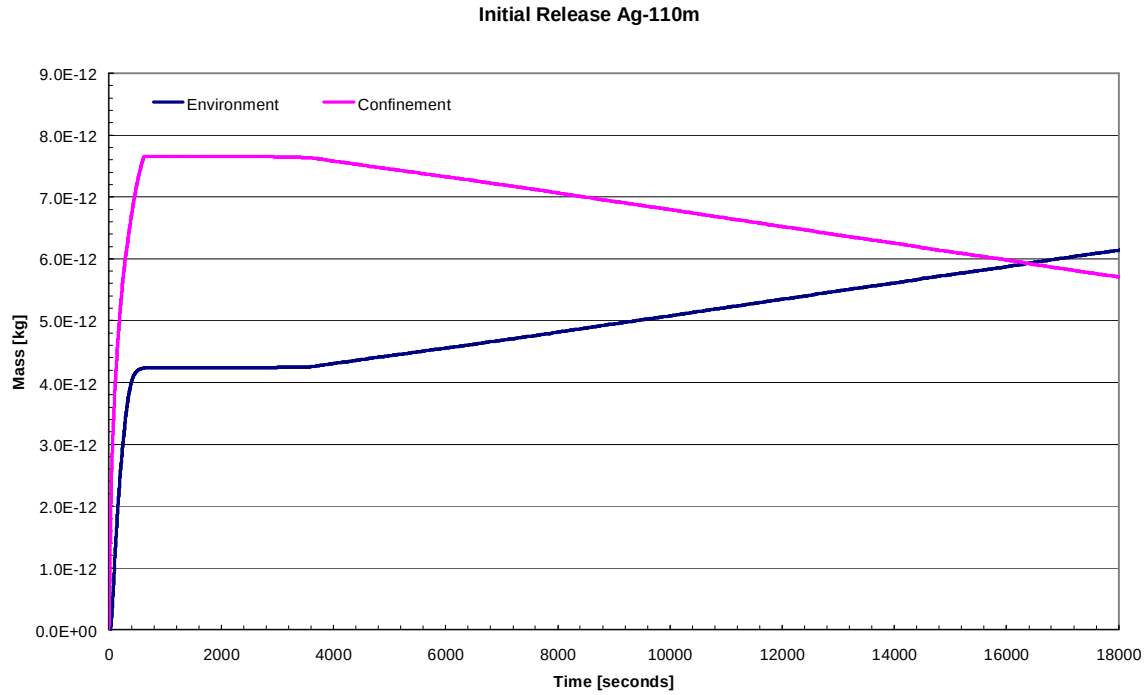

Figure 28: Initial release of ^{110m}Ag.

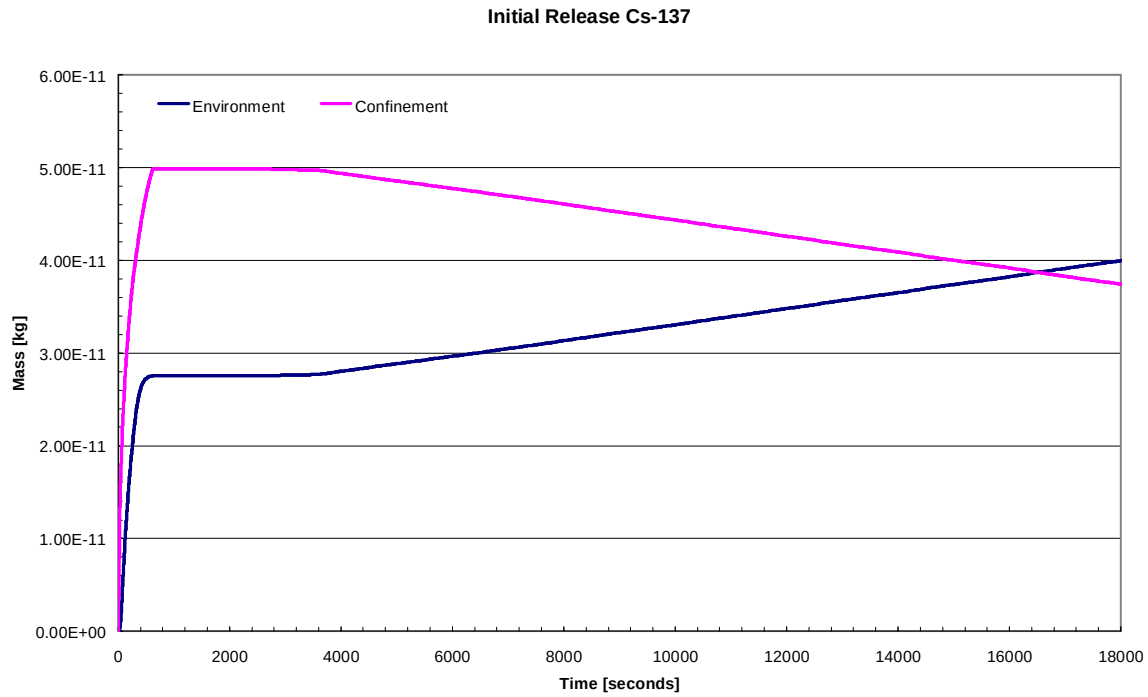

Figure 29: Initial release of ^{137}Cs.

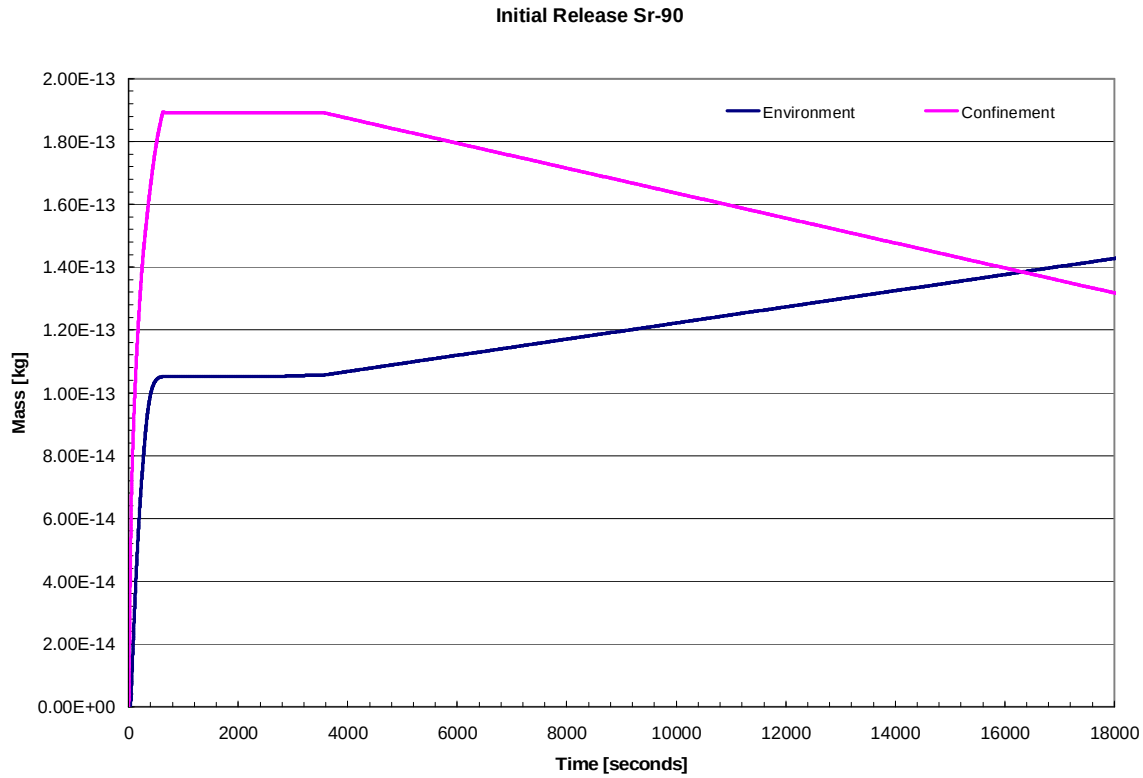

Figure 30: Initial release of ^{90}Sr.

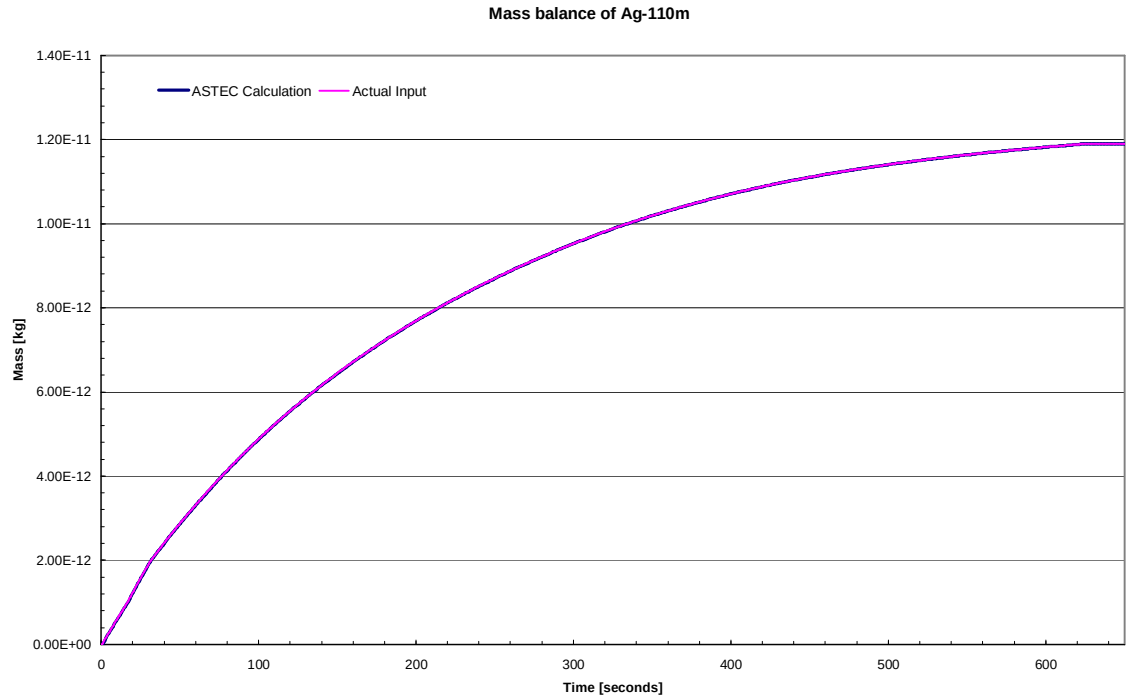

Figure 31: Mass balance on the initial release of ^{110m}Ag.

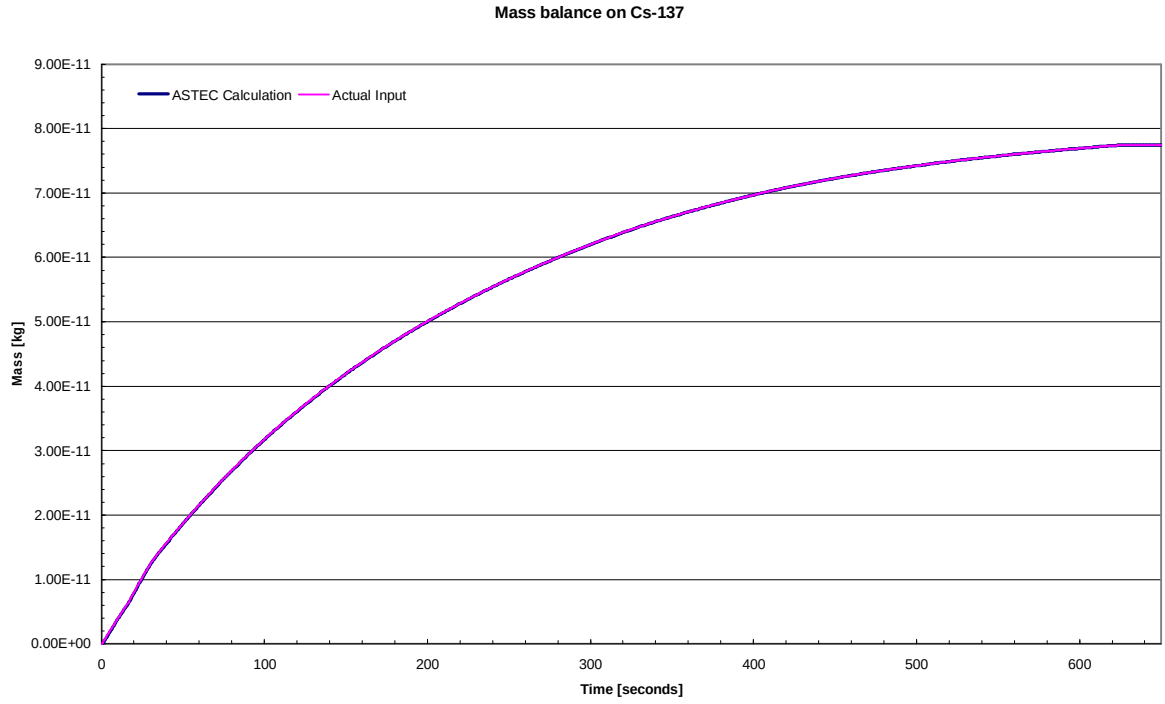

Figure 32: Mass balance on the initial release of ^{137}Cs.

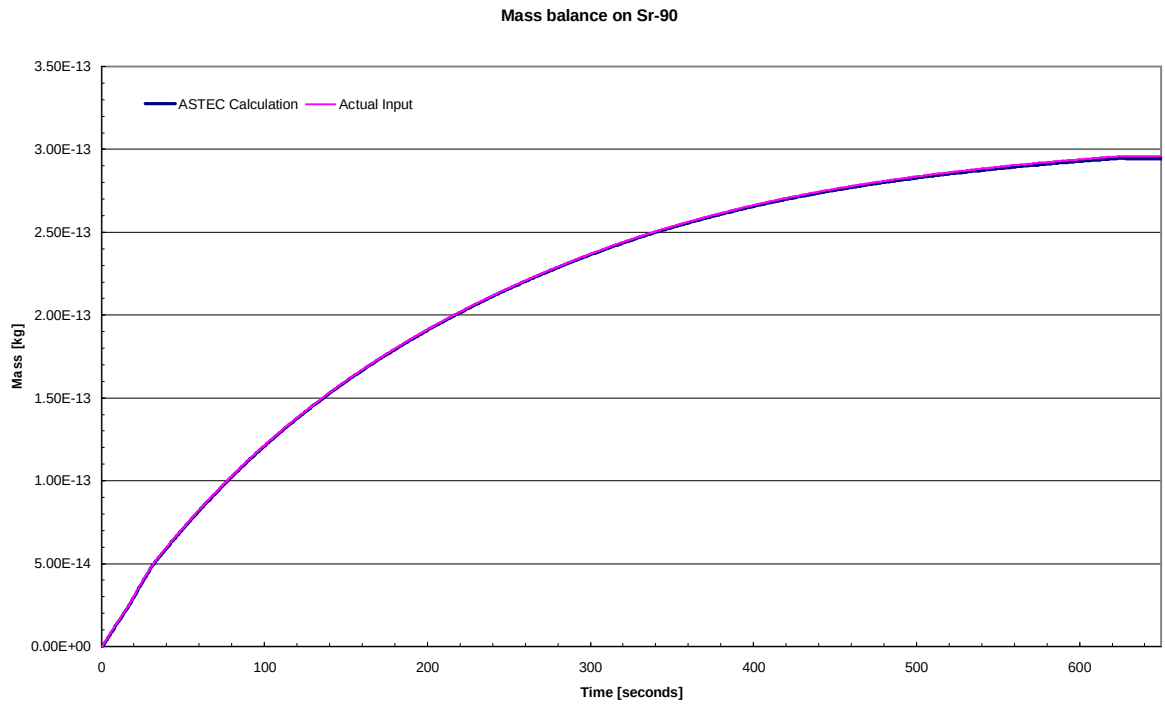

Figure 33: Mass balance on the initial release of ^{90}Sr.

4.1.2.2.2 Initial release of fission products sorbed onto dust

Figure 34, Figure 35 and Figure 36 below shows the distribution of fission products between the deposition surfaces, in suspension, deposited in filters and escaped to the environment for ^{110m}Ag, ^{137}Cs, and ^{90}Sr respectively. The results show a similar trend for all fission products, that the floor is the most significant deposition surface, and that deposition is most predominant after the depressurisation phase. There is a substantial amount of fission products retained on the filter since these fission products are sorbed onto dust particles and are filtered, therefore only a small amount of fission products escape into the environment.

After 5 hours the retention within the building of these 3 fission products are 96.2 %, the remaining 3.8 % escape into the environment

Figure 37, Figure 38 and Figure 39 show the mass balance for the three fission products. There is good conservation of mass in the ASTEC calculation for the fission products sorbed onto dust.

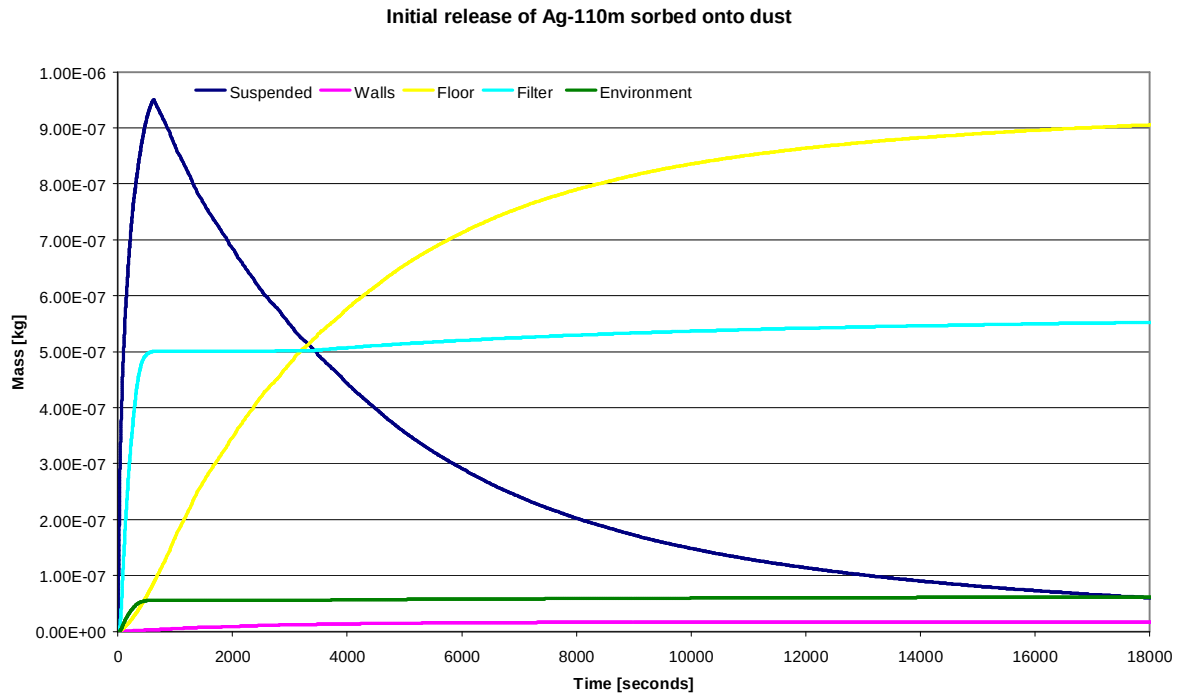

Figure 34: Initial release of ^{110m}Ag sorbed onto dust.

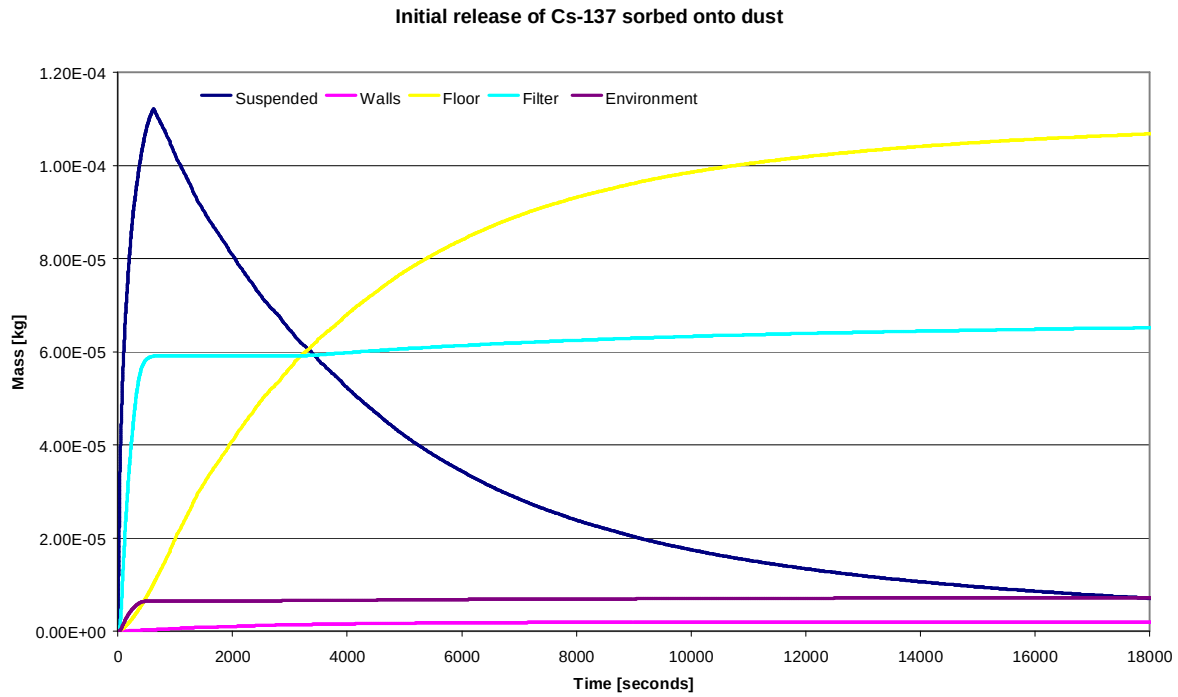

Figure 35: Initial release of ^{137}Cs sorbed onto dust.

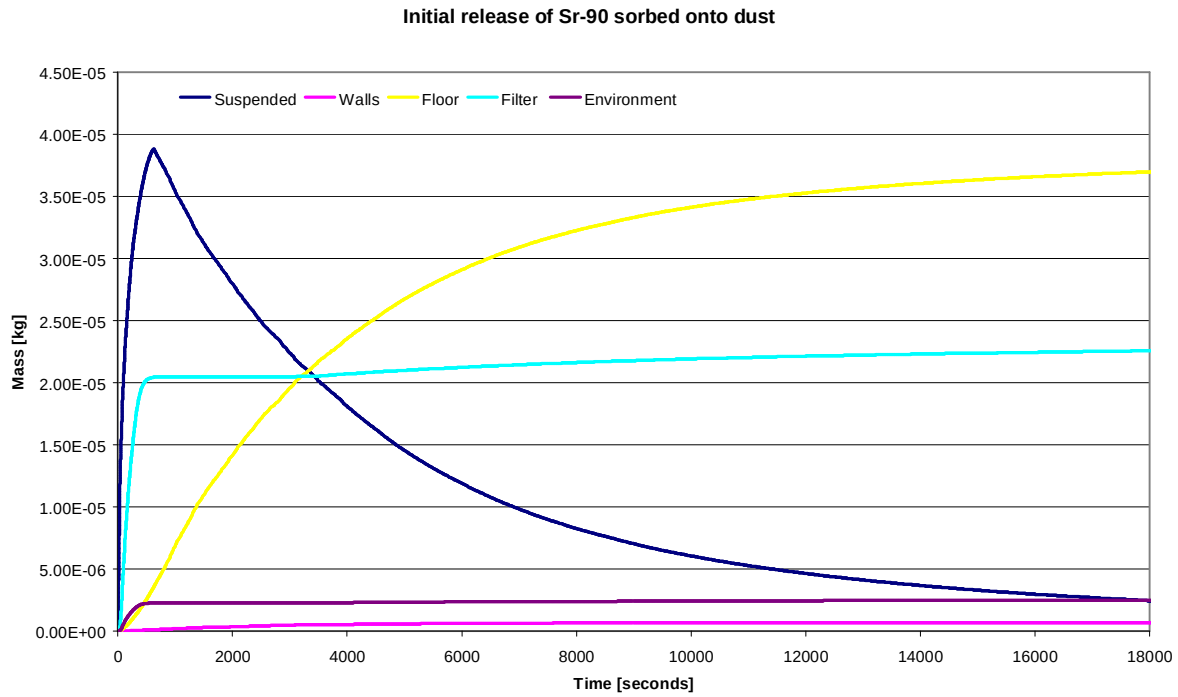

Figure 36: Initial release of ^{90}Sr sorbed onto dust.

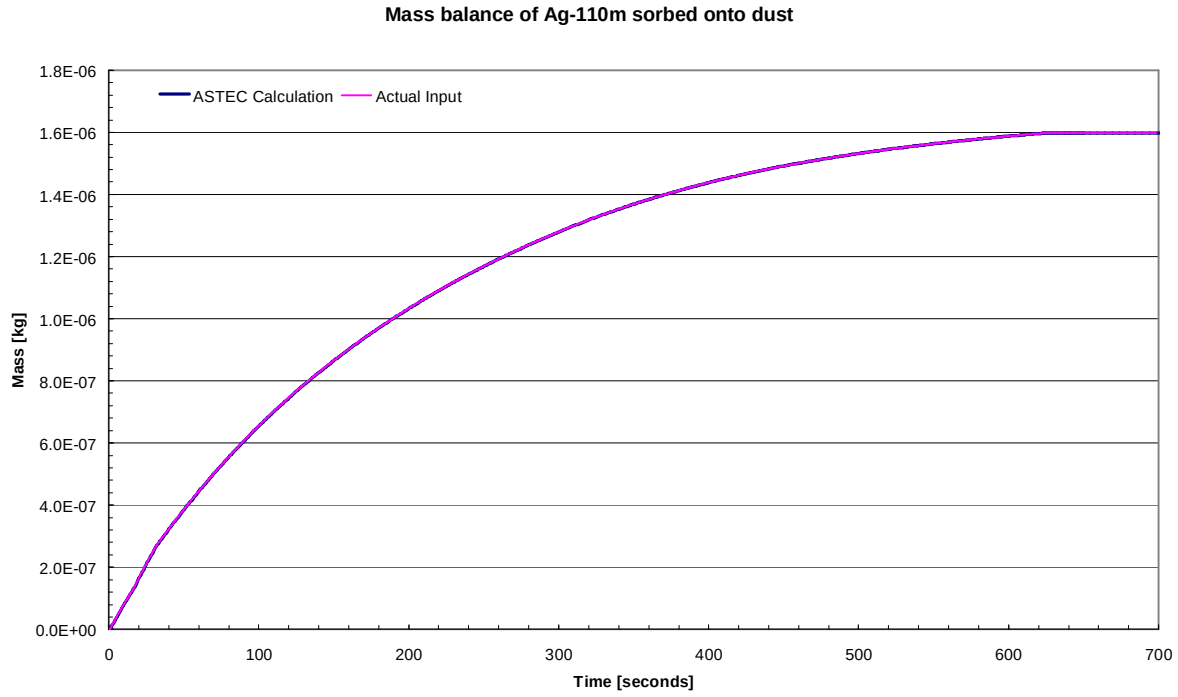

Figure 37: Mass balance of ^{110m}Ag sorbed onto dust.

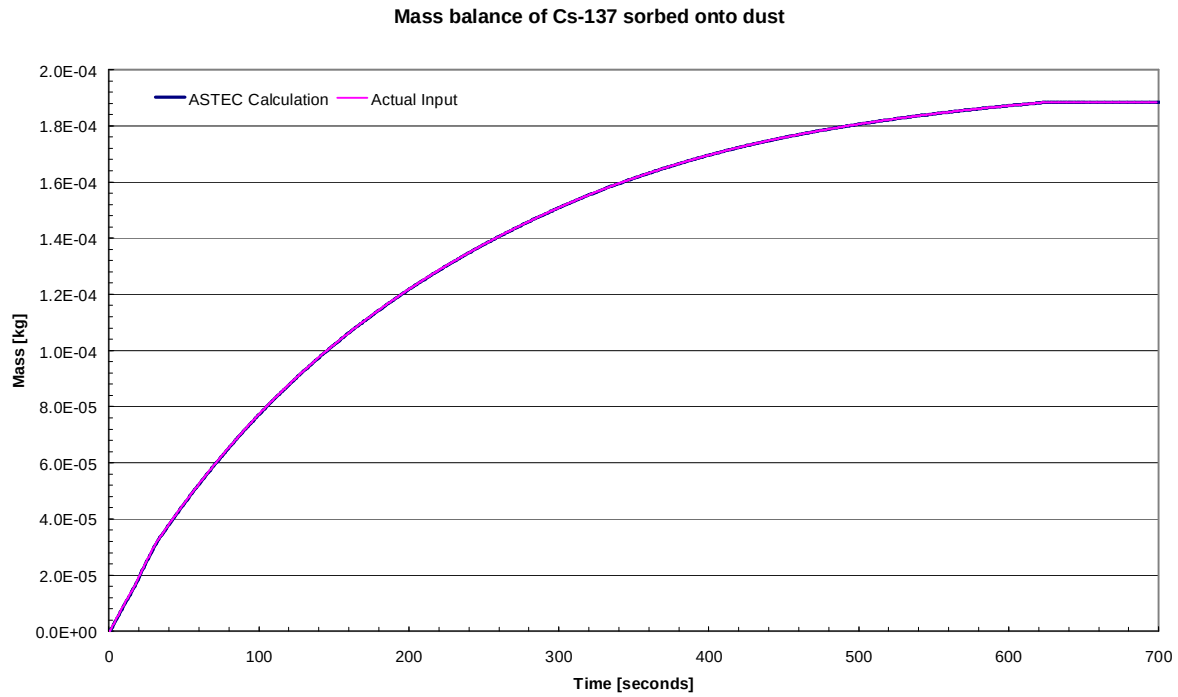

Figure 38: Mass balance of ^{137}Cs sorbed onto dust.

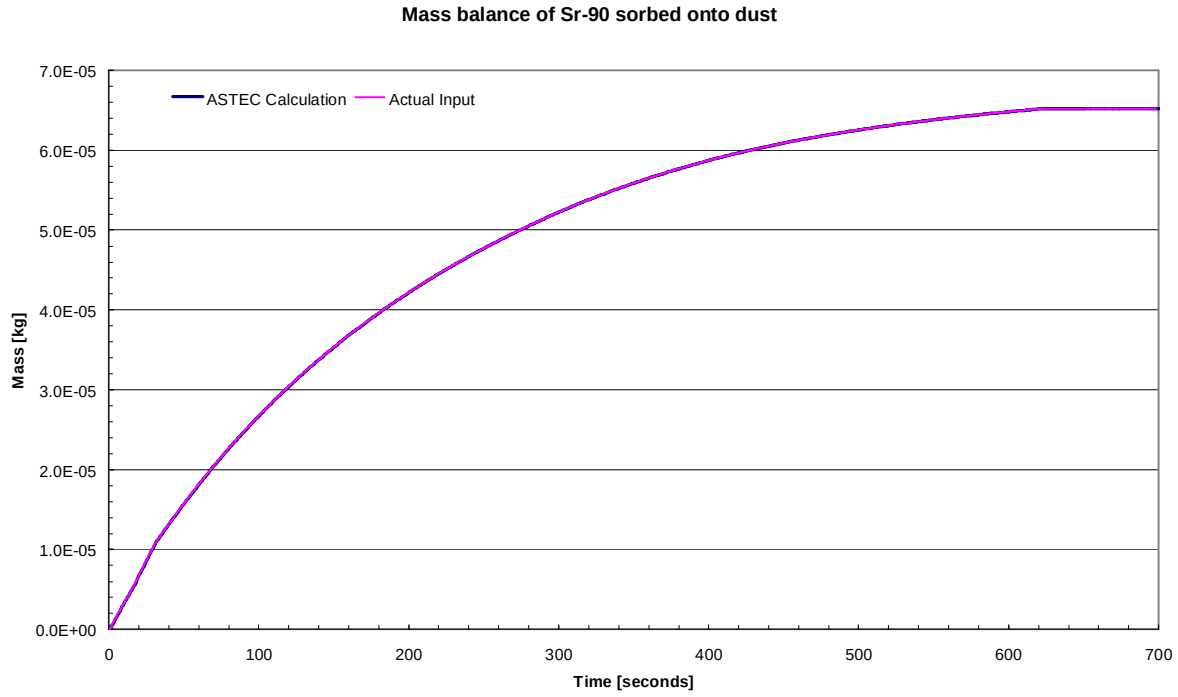

Figure 39: Mass balance of ^{90}Sr sorbed onto dust.

4.1.2.2.3 Delayed release of fission products

The results for the delayed release considering ^{111}Ag, ^{137}Cs and ^{90}Sr as 0.1 µm aerosol particles showed inconsistencies. The mass balance for the fission products, shown in Figure 40, Figure 41 and Figure 42, indicate that the calculation by ASTEC increased the masses of fission products by 34, 27 and 13 times for ^{111}Ag, ^{137}Cs and ^{90}Sr respectively. This inconsistent result is due to the fact that ASTEC, which is a code commercially available for light water reactor analysis, as been applied in this study for use on high temperature reactor analysis. For HTR accident scenarios only a small percentage of fission products escape the silicon carbide layer of the fuel kernel this consequently results in little fission product release compared to LWR accidents. LWR accidents typically involve significant fission product release with the potential for the core to melt, thus ASTEC was designed to handle significantly larger inventories of fission products for accident analysis. The graphs below clearly indicate that the ASTEC mass balance could not converge for the small inventory injected.

The response was exactly the same as for fission products injected with the best estimate sizes discussed in § 3.5.2.1.1.

The fission products sorbed onto the graphite dust during the initial release where of small masses also, but these were sorbed onto the carrier graphite dust, which was injected at 100 kg. This large mass of dust is the reason for the good convergence of the initial release fission product masses. The gaseous fission products during the initial release also showed good convergence since these do not undergo any of the aerosol agglomeration and deposition processes.

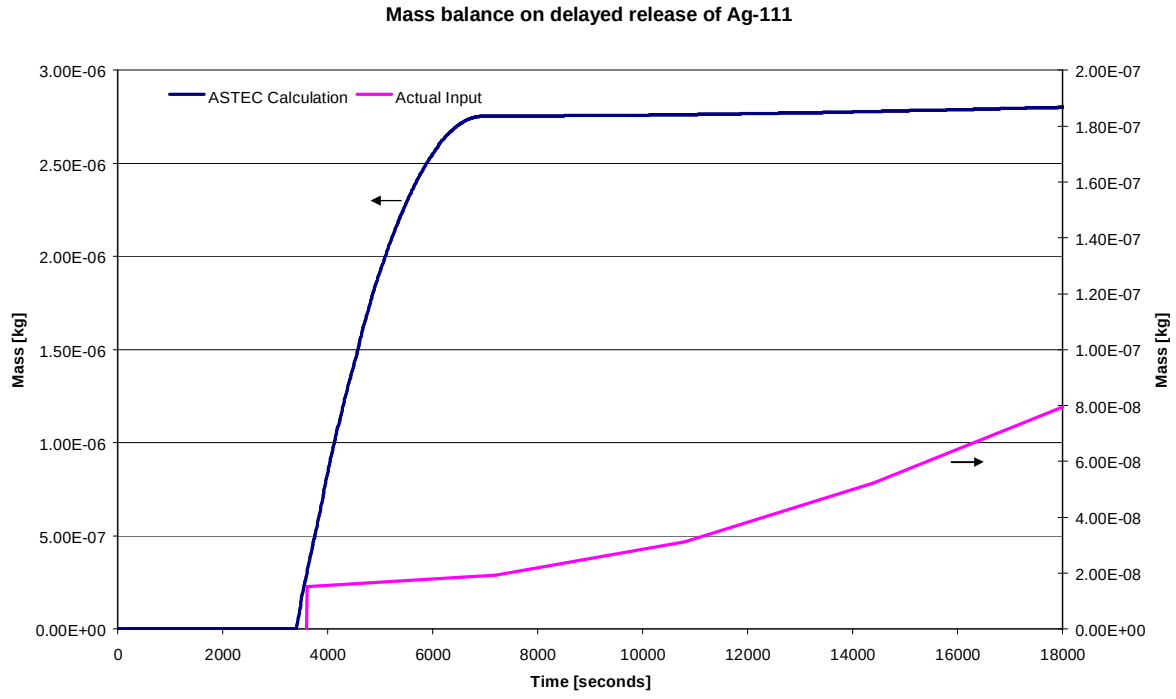

Figure 40: Mass balance on delayed release of ^{111}Ag.

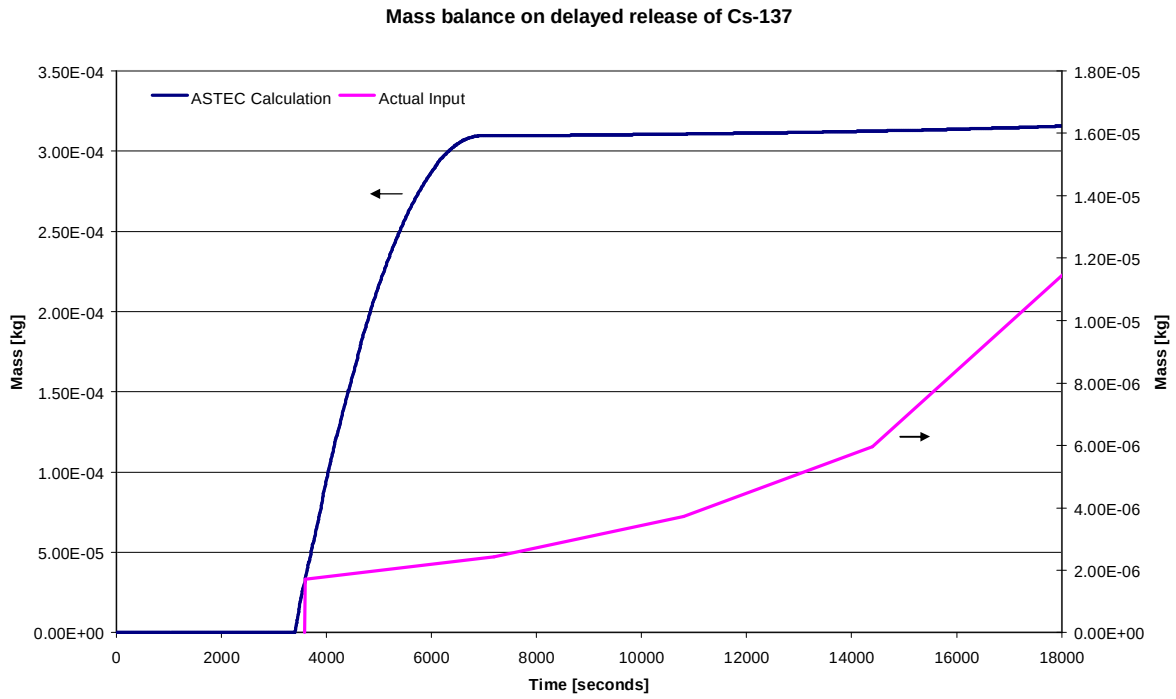

Figure 41: Mass balance on delayed release of ^{137}Cs.

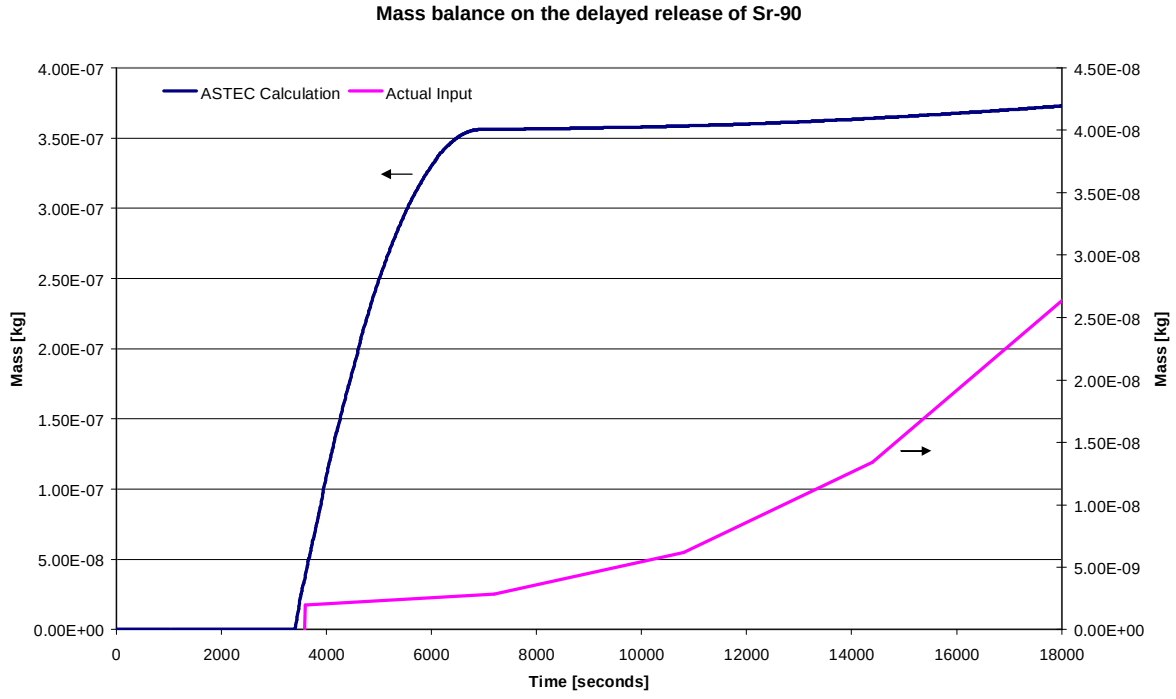

Figure 42: Mass balance on delayed release of ^{90}Sr.

4.1.3 Iodine chemistry results

Figure 43 below summarises the iodine distribution during the transient. One can see that the airborne (gas phase) molecular iodine mass increases until the end of the depressurisation phase at 700 seconds where iodine injection ceases until the addition of the delayed release. At 3600 seconds the iodine mass increases again due to the onset of the delayed release. There is another sharp increase of iodine around 14400 seconds this is due to increase of the injected delayed release at this point which can be seen in from the mass balance of Figure 45.

Figure 43 also shows that painted surfaces assist with retaining iodine, the results show that this process of adsorption of iodine onto paint is more prominent after the depressurisation phase. It is more effective in retaining the delayed release since the gas exchange rates between compartments are lower than compared to the initial release phase. Approximately 65.2 % of the total iodine is sorbed onto painted surfaces at the end of 5 hours, this clearly shows that painted surfaces is an effective retention surface for molecular iodine.

Figure 44 below summaries the methyl iodide distribution between the confinement and the environment. There is a sharp increase in the methyl iodide during the initial release phase, while there is no production during the delayed release phase. The reason for this is that the temperatures are large enough during the initial release phase, as a result of the high temperature helium injection, and thus increases the reaction kinetics in favour of methyl iodide production. During the delayed release the temperatures are not large enough to sustain a high reaction rate thus no production of methyl iodide occurs. Another factor, which is attributed to increasing organic iodide formation, is the dose rate. The dose rate is a significant factor for scenarios in LWRs since there is considerable fission product release into the containment. HTRs such as the PBMR have little fission product release and the dose rate is much lower compared to LWRs thus the dose rate had little influence for this scenario.

Approximately 5 % of the initial release iodine that was injected over the first 700 seconds reacted to form the organic methyl iodide. At the end of 5 hours approximately 64 % of the methyl iodide escapes into the environment.

With no filter retention modelled for iodine, there is approximately 37.4 % retention of all iodine species for the initial release (determined at 700 seconds) and a final retention of 78.5 % determined at 5 hours.

Figure 45 shows that there is good agreement on the mass balance of iodine; this is in contrast with what was seen for the metal fission products of the delayed release. The CPA module of ASTEC simulated the metal fission products while iodine was simulated by the IODE module. These two modules have different convergence criteria, which is why only the metal fission products showed a significant mass balance error.

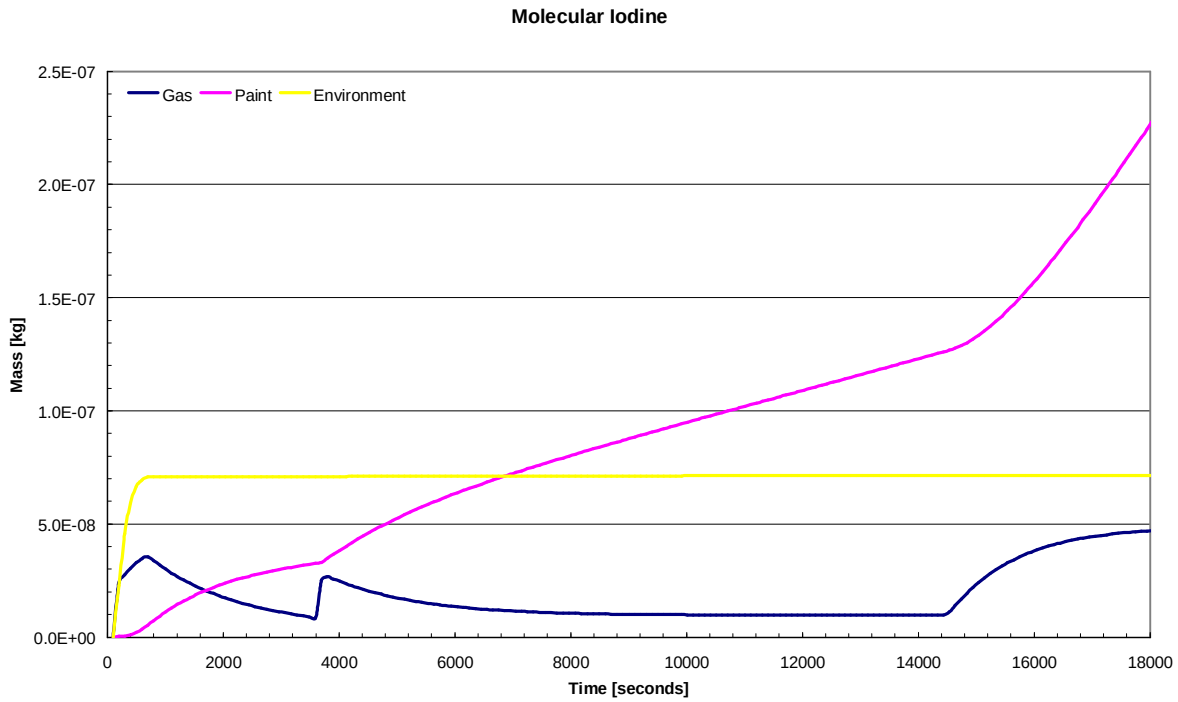

Figure 43: Molecular iodine mass distribution.

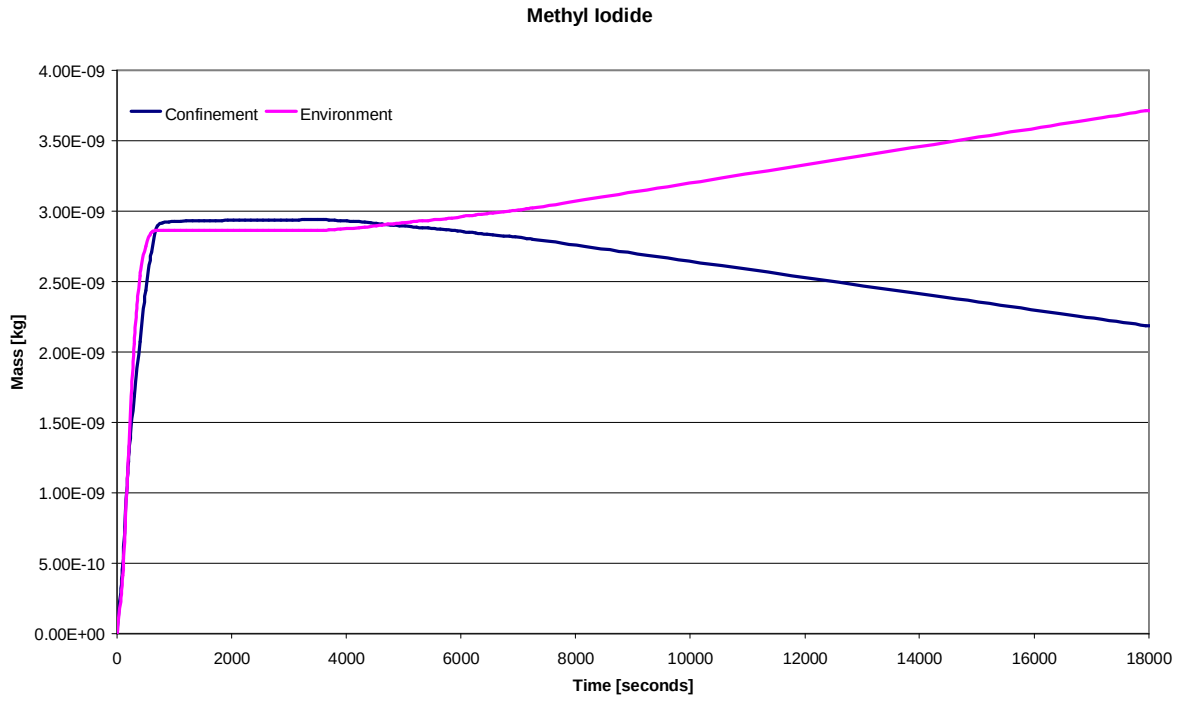

Figure 44: Methyl iodide mass distribution.

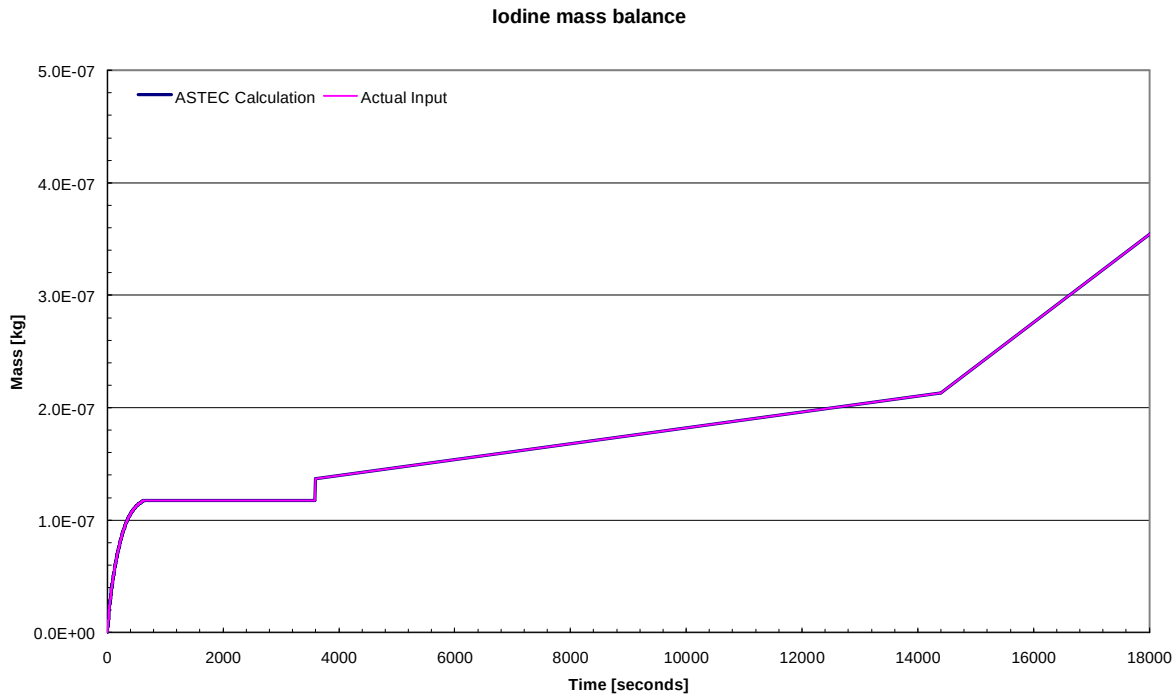

Figure 45: Iodine mass balance.

4.2 HELIUM AND STEAM PIPE BREAK ANALYSIS

This section discusses the results obtained from the analysis of a 65 mm DEGB of the reactor outlet pipe and a 65 mm DEGB of the steam generator outlet pipe. The following sections will highlight the thermalhydraulic, aerosol and fission product, and iodine chemistry behaviour for this accident scenario. The compartment where the pipe breaks occur is the reactor pressure vessel compartment (111809) of module 2 (refer to Figure 3).

4.2.1 Thermalhydraulic results

4.2.1.1 Pressure

The pressure tolerance for the reactor pressure vessel and steam generator compartments of module 1 and 2 is 250 kPa absolute pressure, while all other compartments can tolerate up to a maximum of 140 kPa.

Figure 46 below shows the pressure response of the first five consecutive compartments in Module 2 where the pipe breaks occur. It can be seen that the steam generator (111626) and the reactor pressure vessel (111809) compartments exceed the maximum pressure of 250 kPa at 5 seconds for a duration of 6 seconds. The peak pressure recorded in these compartments is 267 kPa. It is difficult to distinguish the profile for compartment 111626 but it follows almost exactly that of 111809. Compartments 112202 and 111654 are also almost identical in profile. It is evident that compartment 111743 exceeds the design pressure of 140 kPa for a duration of 45 seconds, beginning at approximately 2 seconds. The peak pressure recorded in this compartment is 195 kPa. These are important findings since it is possible that the structural integrity of these compartments may be compromised.

Figure 46 shows that the violent pressure transient lasts only for the first 200 seconds thereafter dropping sharply to atmospheric pressure. The remaining compartments of modules 1 and 2 exhibit behaviour similar to compartments 112202 and 111654 of Figure 46.

The pressures during this scenario are higher than those found during the helium pipe break alone (refer to § 4.1.1.1) since the steam is released simultaneously during this scenario and thus increases the pressure within the compartments.

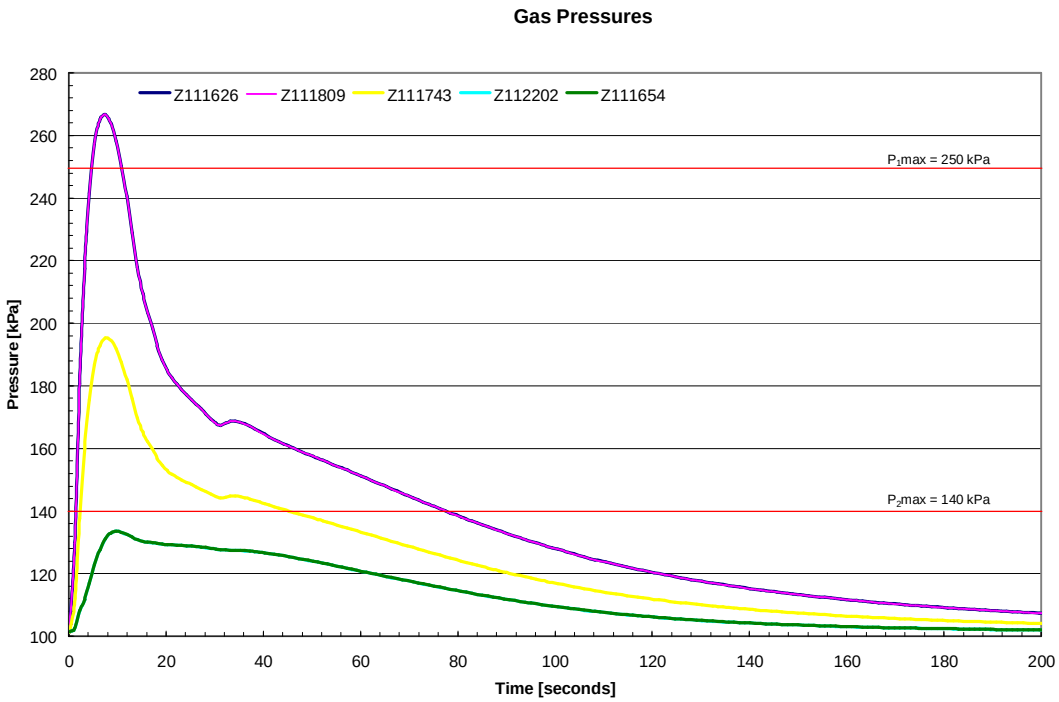

Figure 46: Pressure response of compartments in Module 2.

4.2.1.2 Temperature

Figure 47 and Figure 48 below show the temperature transient from 0 to 200 and 0 to 18000 seconds (5 hours) respectively. The sharp drop in temperature between 20 and 40 seconds is due to the colder helium which is injected during this phase as discussed in § 3.3.1 and shown in Figure 6, while the temperature reaches a maximum of 438 ^{o}C in the break zone, 111809. This maximum temperature is considerably lower than that found from the previous scenario (refer to § 4.1.1.2), this is due to the fact that the steam is released at a lower temperature than that of the helium (Figure 6 and Figure 8) therefore the steam absorbs some of the excess thermal energy of the helium thus reducing compartment temperatures as compared to a helium pipe break alone.

The profile in Figure 48 shows that the temperature in compartment 111809 (the break zone) remains higher than the other compartments after 4000 seconds, this is because of the delayed release driving force as discussed in § 3.3.3, which is injected at a flowrate of 0.44 kg/s and 120 ^{o}C.

The remaining compartments of Module 2 have similar temperature profiles however their maximum temperatures range between 250 and 350 ^{o}C, while compartments of Module 1 have maximum temperatures not exceeding 50 ^{o}C.

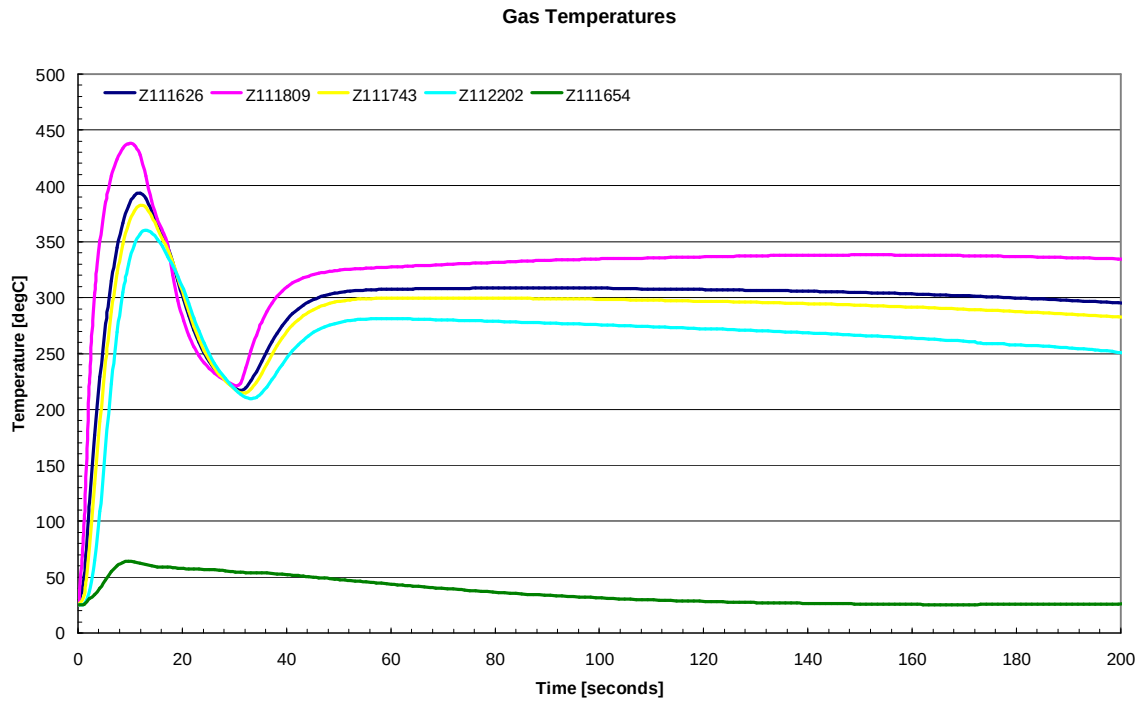

Figure 47: Temperature profile of compartments in Module 2 (200 seconds).

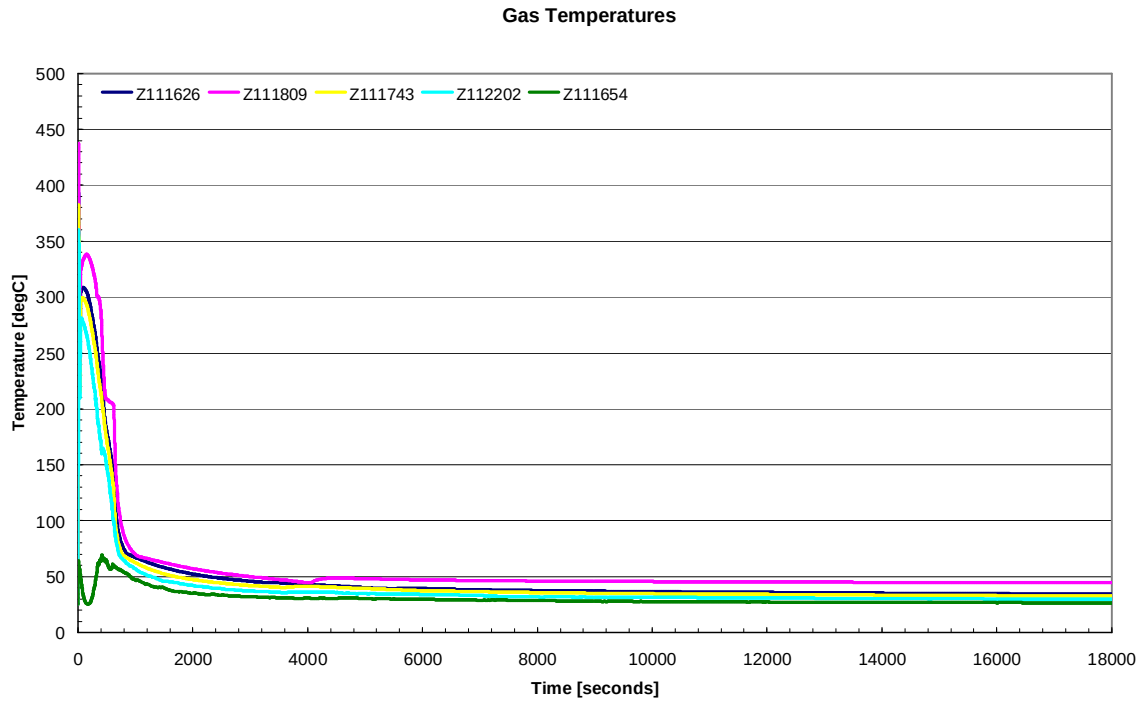

Figure 48: Temperature profile of compartments in Module 2 (18000 seconds).

4.2.1.3 Junction flowrates

The junction mass flowrate data allows one to determine the intervals at which the important rupture panels burst, as well as the flowrate out of the stack and into the environment. Figure 49 below shows the mass flowrate for junctions 19A, 19B, 21, 22 and 23. At 3.1 seconds, junction 23, which connects modules 1 and 2, bursts; shortly thereafter junctions 21 and 22 burst, these two junctions connect to the stairwells of module 1 and 2 respectively. At 4.8 seconds the panels that lead to the stack and the environment burst, allowing the helium and steam to escape into the environment. It is evident from these almost immediate burst times that the depressurisation propagates rapidly through both modules and is relieved into the environment. The profiles for 19A and 19B are exactly the same since these junctions are of the same area and elevation.

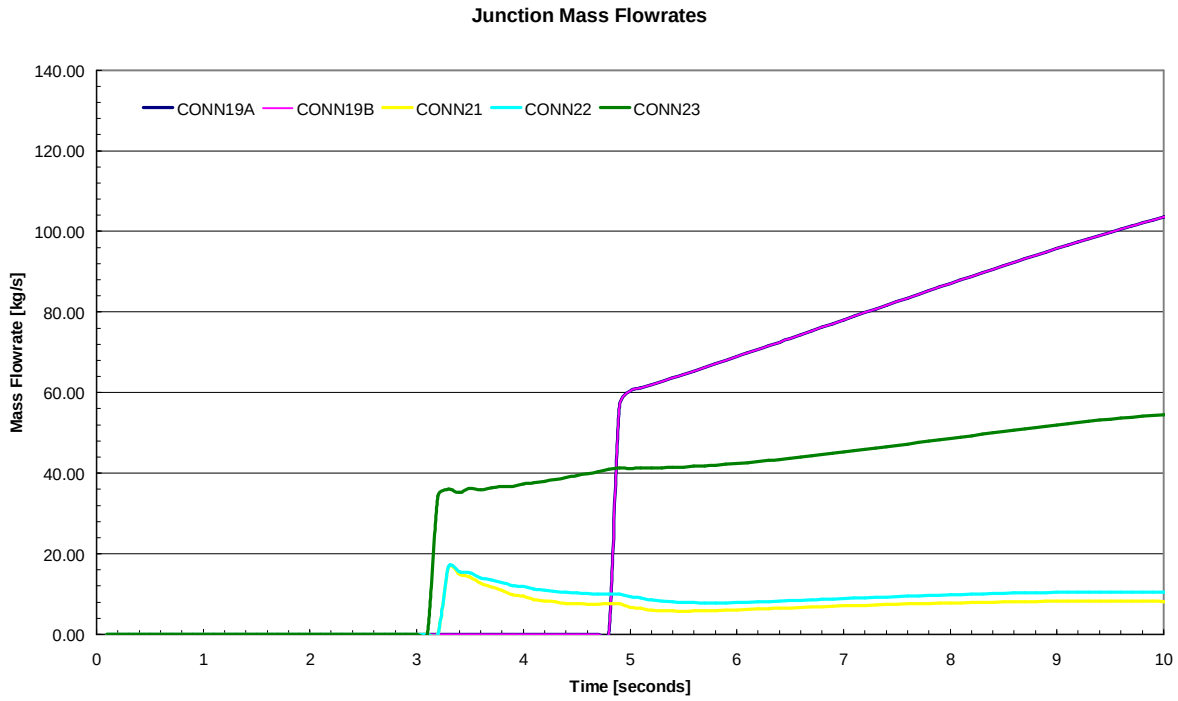

Figure 49: Junction mass flowrates at 10 seconds.

Figure 50 below shows the flowrates up to 700 seconds, the noticeable feature is the large mass flowrate out of junctions 19A and 19B into the environment. The profile for 19A and 19B lie directly over each other and is larger than the case of the helium pipe break alone since some steam exits out the stack as well.

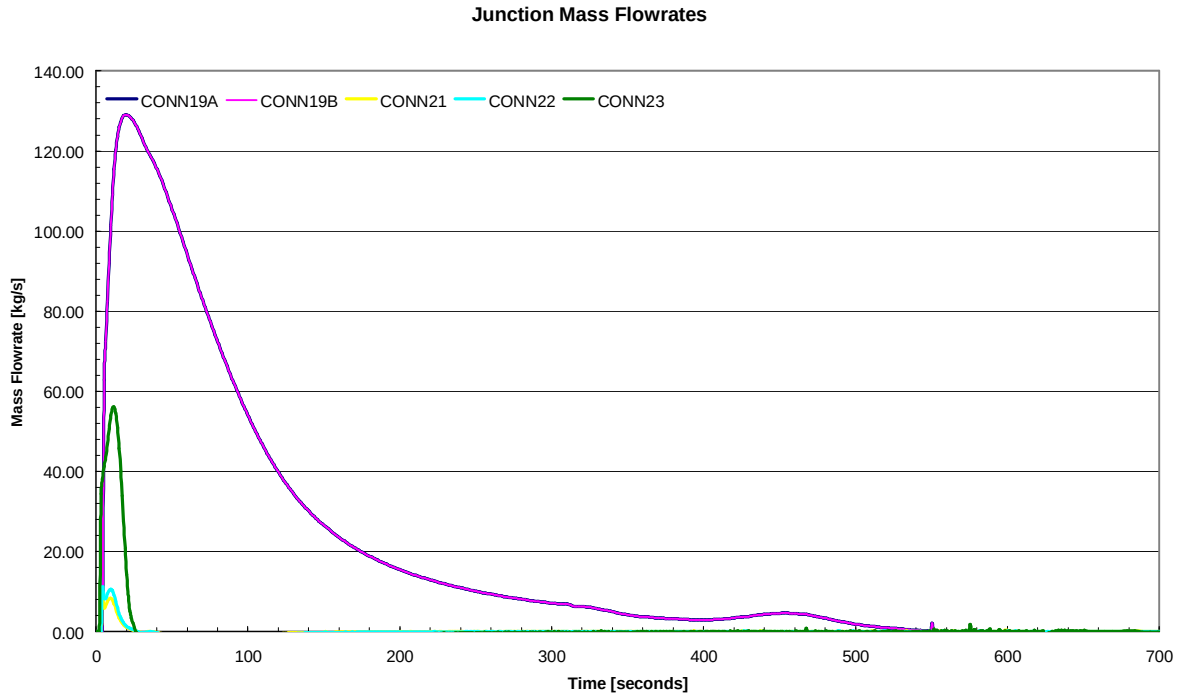

Figure 50: Junction mass flowrates at 700 seconds.

4.2.1.4 Steam mass and liquid volume

The initial humidity of the compartments in the confinement was set at 40 % this amounts to an initial water vapour inventory of 255 kg within the entire confinement. At the onset of the pipe break the mass of steam (water vapour) increases within the confinement according to Figure 51. The mass of steam quickly reaches 3.2 tons in the confinement after 550 seconds, and there is a corresponding increase in the liquid volume in the confinement, this shows that steam condensation begins immediately. The two characteristic peaks in the steam mass profile are a result of the injection characteristic of steam, the injection flowrate of steam increased around 450 seconds as discussed in § 3.3.2. The steam mass drops rapidly after the depressurisation phase due to condensation of steam into water.

The volume of liquid generated will influence the iodine chemistry with the generation of iodine species such as I^- and HIO. Approximately 6 m^3 of liquid is found at the end of 5 hours within the confinement, this represents approximately 6 tons of water condensed inside the confinement from the total injected steam mass of 10.8 tons.

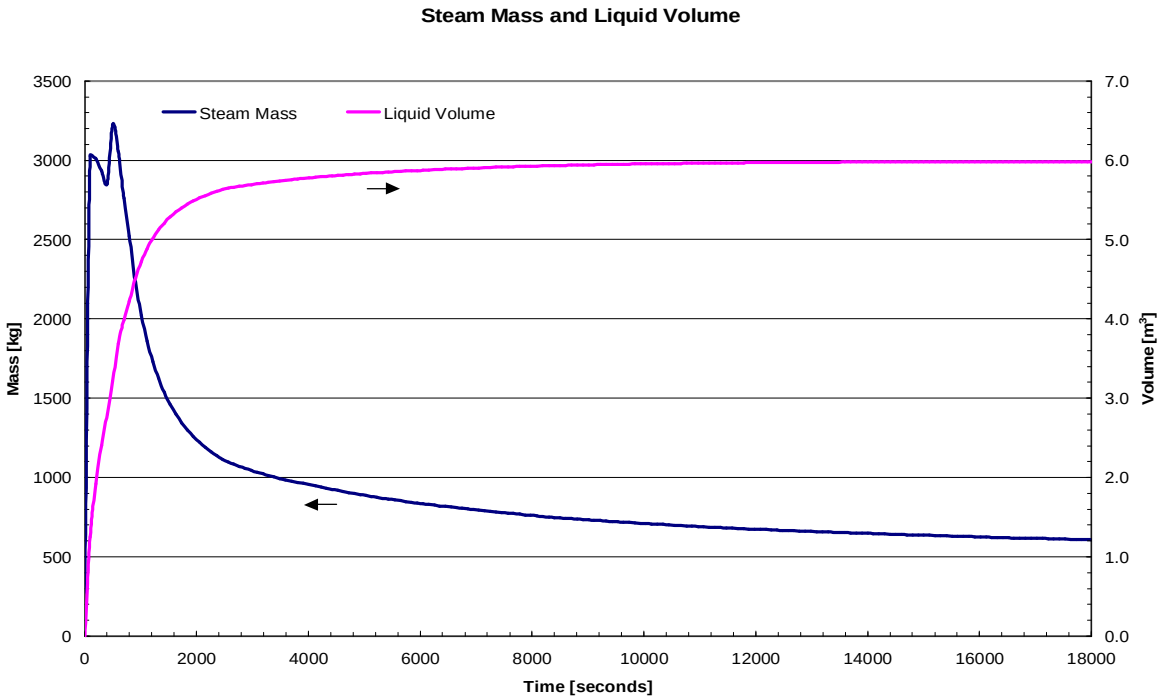

Figure 51: Total steam mass and liquid volume in the confinement.

4.2.2 Graphite dust and fission product results

4.2.2.1 Graphite dust

Although the results generated by ASTEC is a detailed set per compartment, it is impractical to reproduce this amount of data here, and therefore a summary of the result based on the entire confinement is presented.

Figure 52 below summarises the mass of dust deposited on confinement walls, floors, and ceilings, and the mass of dust remaining in suspension. The majority of the dust remains in suspension over the depressurisation phase, once the depressurisation is over the dust begins to settle by sedimentation rapidly. It is evident that the floor is the most effective deposition surface with just over 40 kg depositing within 5 hours (18000 seconds), since exactly 100 kg of dust was injected, 40 kg represents 40 % of the total dust.

The amounts that have been deposited onto the ceilings are extremely small.

Figure 53 below shows the amount of dust that is deposited into the filter and the amount of dust that has been released into the environment. There is 39 kg of dust that is deposited into the filter over the first 5 hours; the HEPA filter has a retention efficiency of 90 % for dust particles. The retention of graphite dust after 5 hours within the building and trapped in the HEPA filter is approximately 95.6 %, while the remaining 4.4 % escapes into the environment. Figure 54 shows the graphite dust distribution by the different hosts at the end of 5 hours, it can be noted that the amount of dust deposited on the walls is much larger than that deposited during the helium pipe break alone (Figure 26), this is due to the presence of steam which increases deposition by diffusiophoresis (equation 2.22) thus resulting in greater deposition onto walls during this accident scenario.

There is good agreement on the mass balance of dust as shown below in Figure 55.

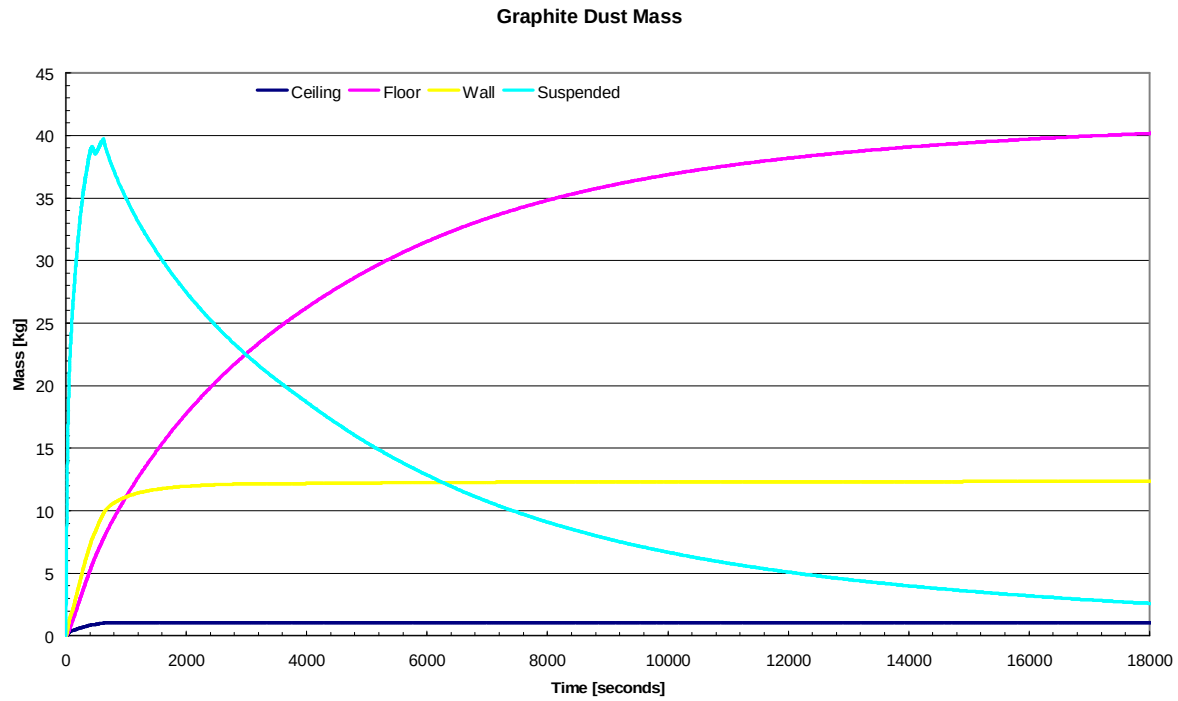

Figure 52: Graphite dust mass within the confinement.

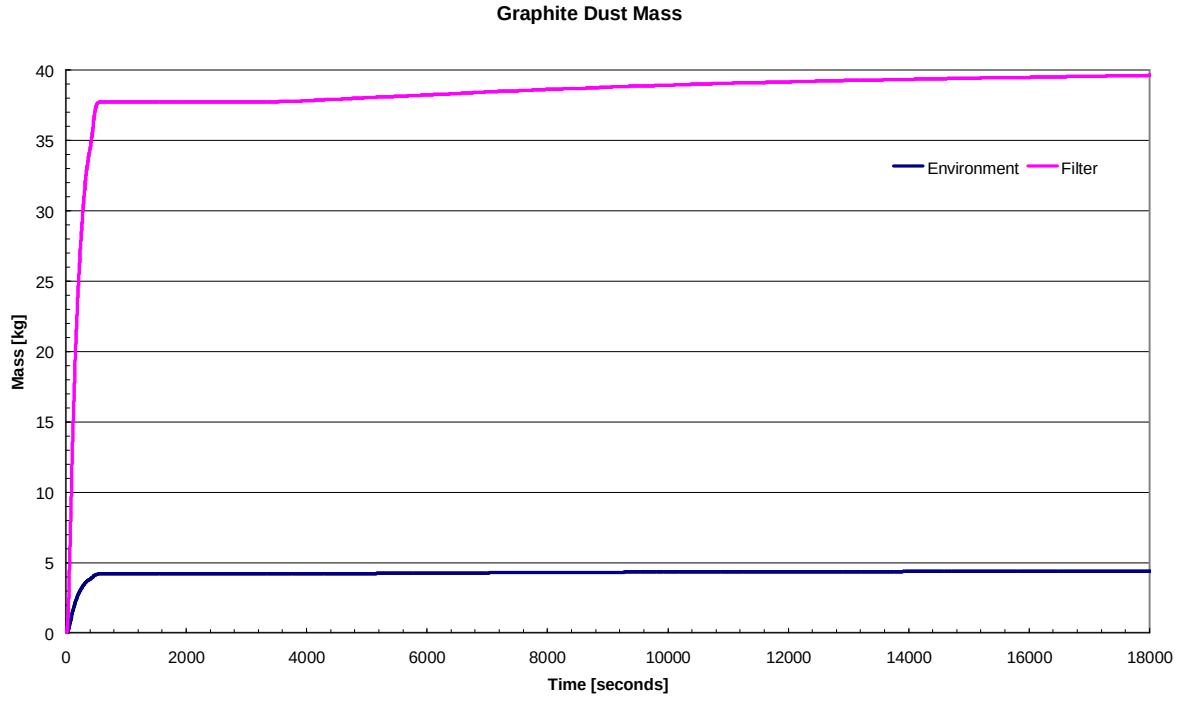

Figure 53: Graphite dust mass deposited in the filter and released into the environment.

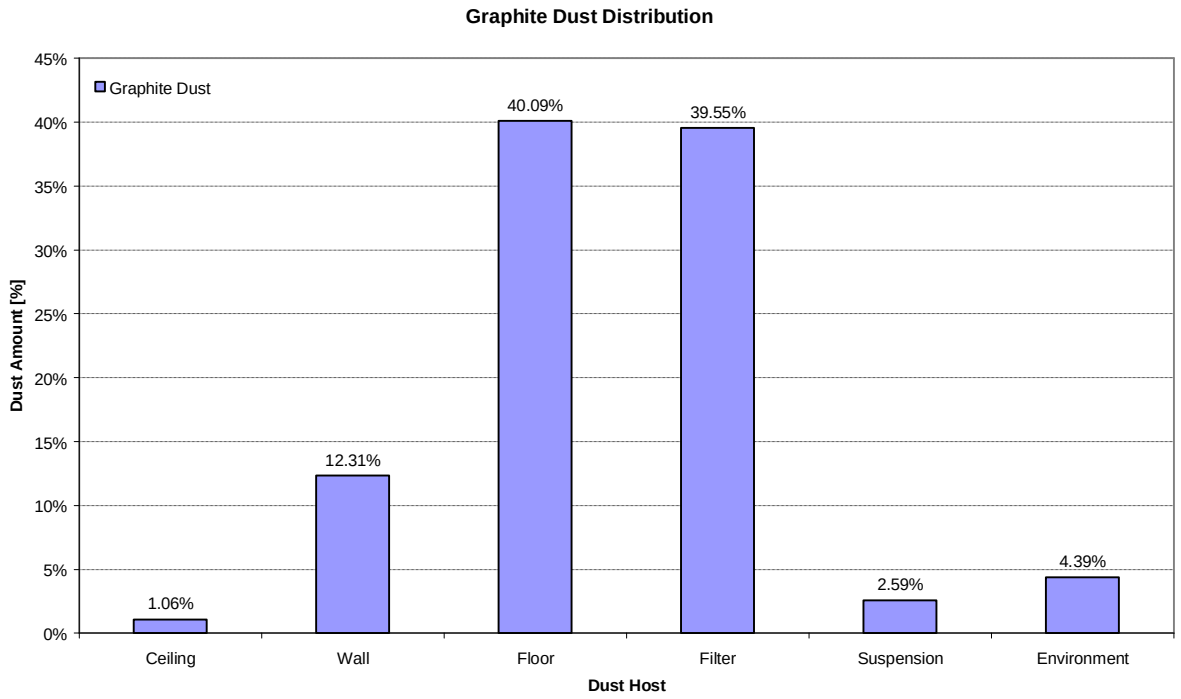

Figure 54: Graphite dust distribution on hosts (18000 seconds).

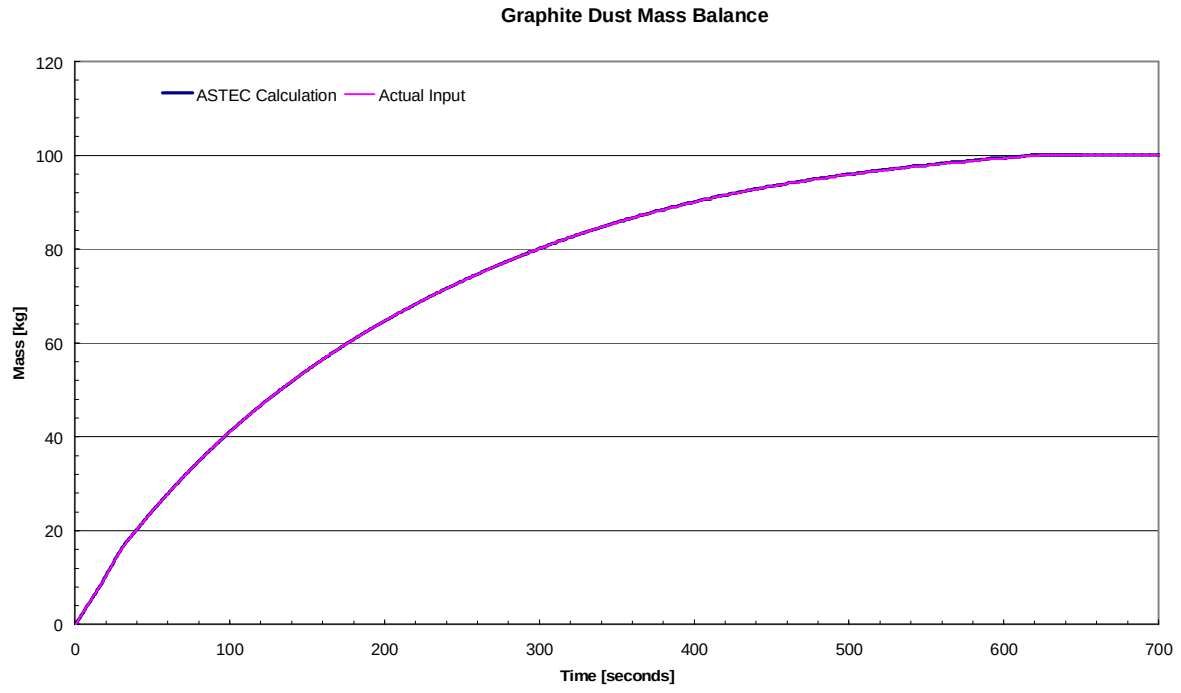

Figure 55: Graphite dust mass balance.

4.2.2.2 Fission products

4.2.2.2.1 Initial release of metallic fission products

Figure 56, Figure 57 and Figure 58 below shows the ASTEC calculation results for ^{110m}Ag, ^{137}Cs, and ^{90}Sr respectively, these figures show the amount of fission product remaining in the confinement and that, which is released into the environment. Naturally there is an increase in fission products within the confinement over the depressurisation phase; thereafter the mass remains almost constant within the confinement with almost no release to the environment. The delayed release driving force (see § 3.3.3) commences at 3600 s and slowly drives fission products out into the environment. There was no filtration modelled for metallic fission products since HEPA filters cannot trap this form.

The retention after 5 hours for ^{110m}Ag, ^{137}Cs and ^{90}Sr is 40.1 %. This is approximately 8 % lower than the scenario with a helium pipe break alone, since the simultaneous break of the steam outlet line results in greater pressures and thus higher mass flowrates into the environment.

Figure 59, Figure 60 and Figure 61 shows the mass balance for ^{110m}Ag, ^{137}Cs, and ^{90}Sr respectively. It is evident that the mass balances for the metallic fission products are closed.

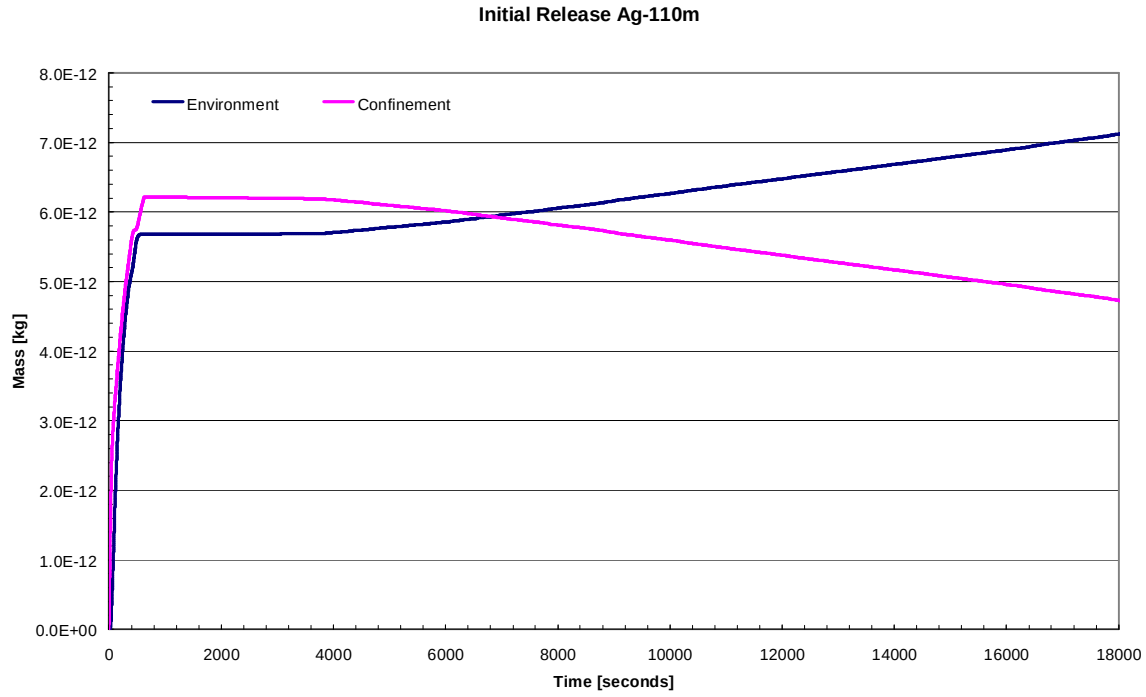

Figure 56: Initial release of metallic ^{110m}Ag.

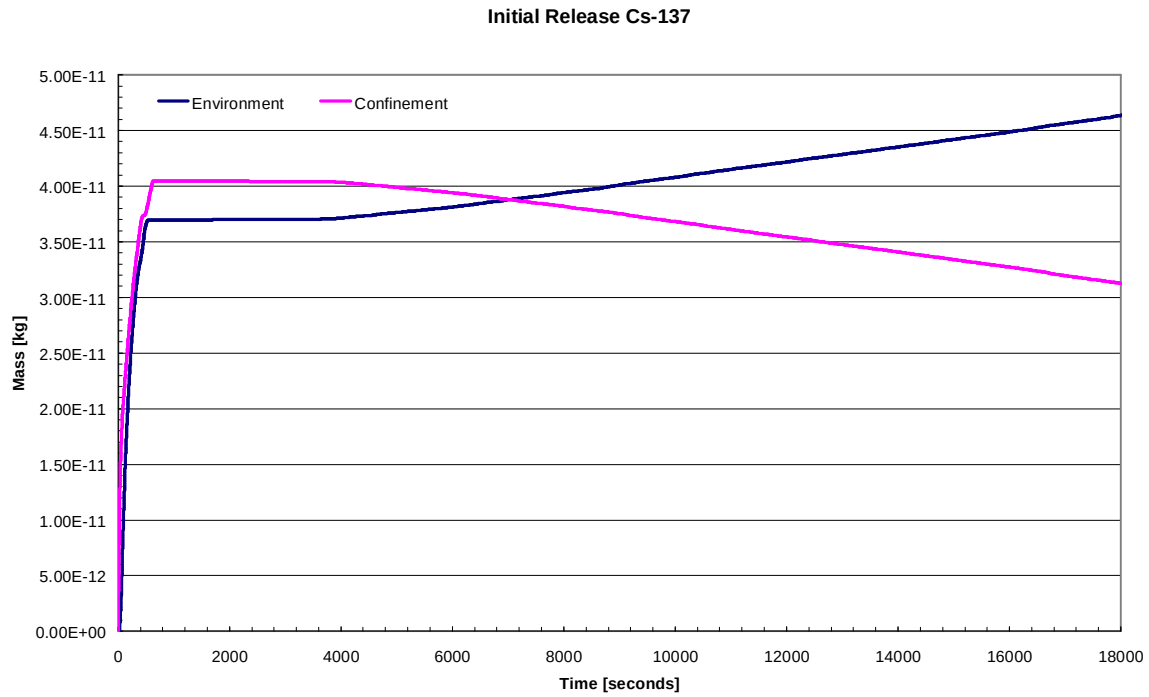

Figure 57: Initial release of metallic ^{137}Cs.

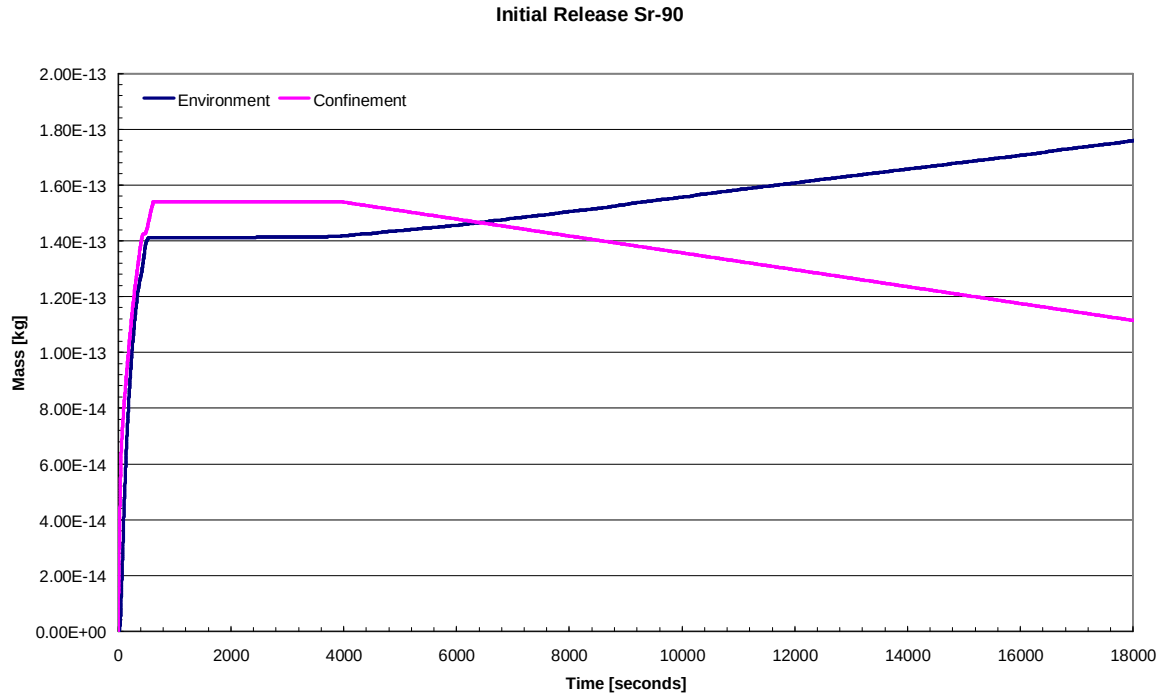

Figure 58: Initial release of metallic ^{90}Sr.

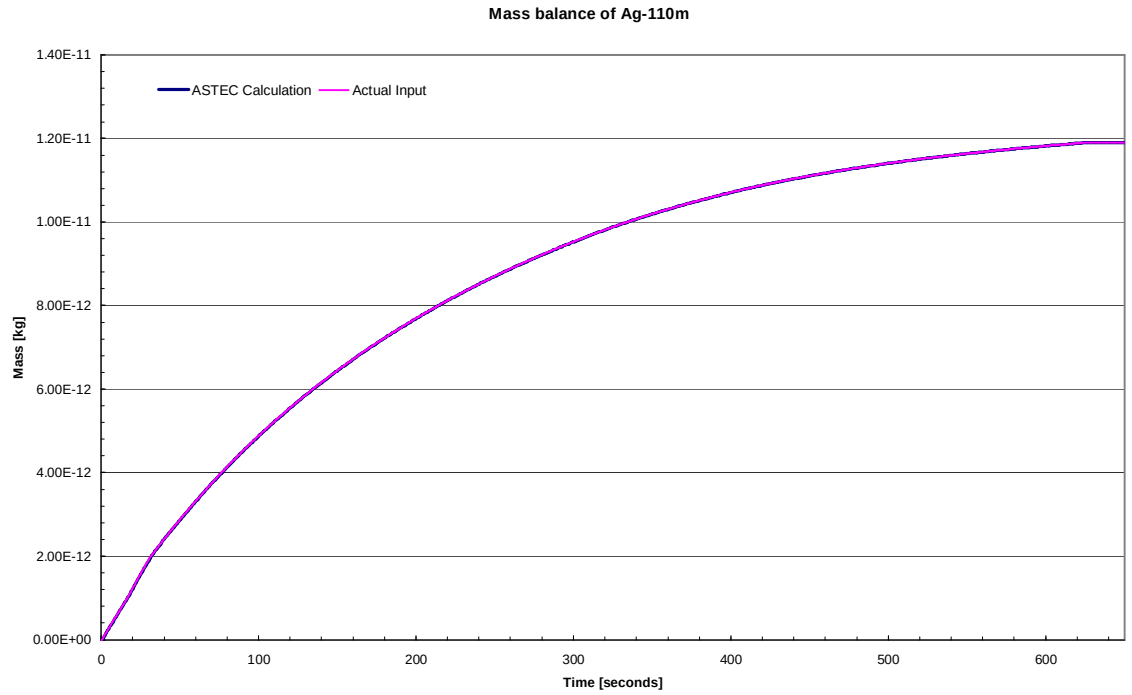

Figure 59: Mass balance on the initial release of metallic ^{110m}Ag.

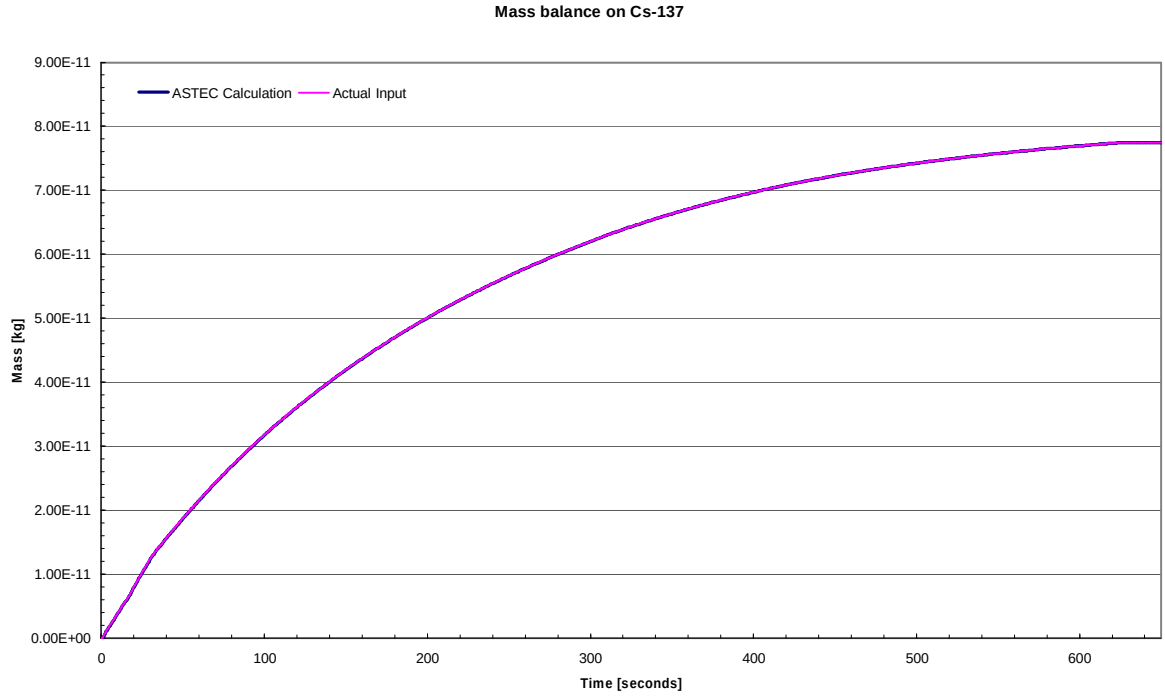

Figure 60: Mass balance on the initial release of metallic ^{137}Cs.

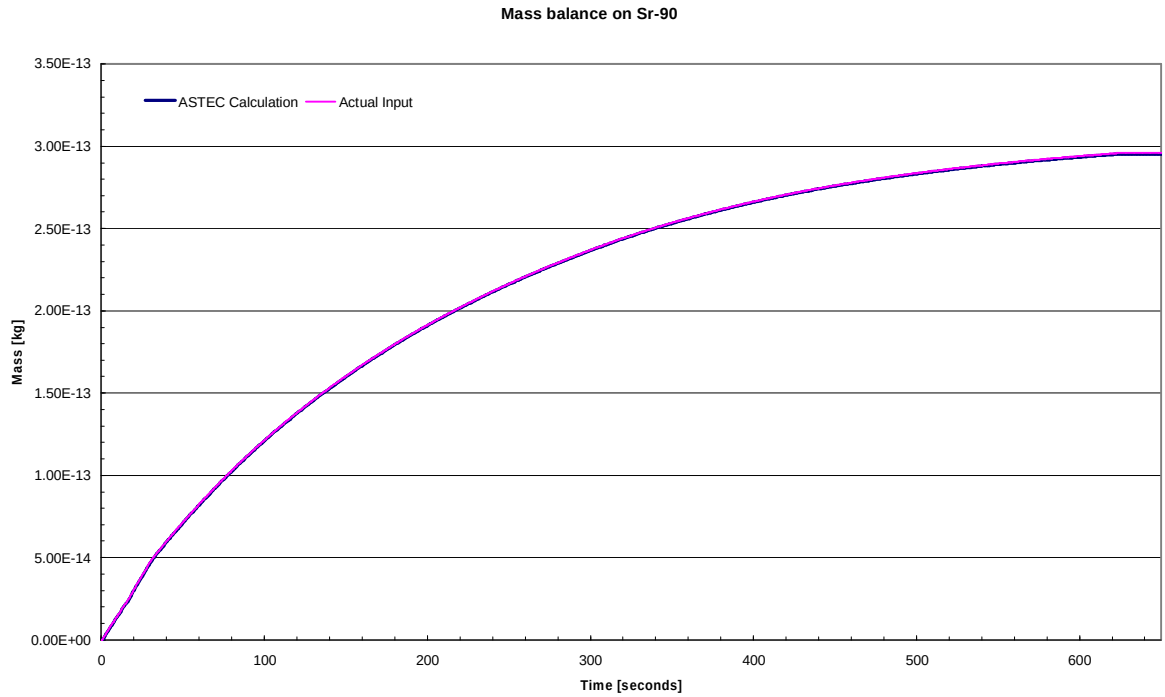

Figure 61: Mass balance on the initial release of metallic ^{90}Sr.

4.2.2.2.2 Initial release of fission products sorbed onto dust

Figure 62, Figure 63 and Figure 64 below shows the distribution of fission products between the deposition surfaces, in suspension, deposited in filters and escaped to the environment for ^{110m}Ag, ^{137}Cs, and ^{90}Sr respectively. The results show a similar trend for all fission products that the floor is the most significant deposition surface, and that deposition is most predominant after the depressurisation phase. Deposition on the walls is made possible through Diffusiophoresis, as was the case for the graphite dust. There is a substantial amount of fission products retained on the filter since these fission products are sorbed onto dust particles, and only a small amount of fission products escape into the environment.

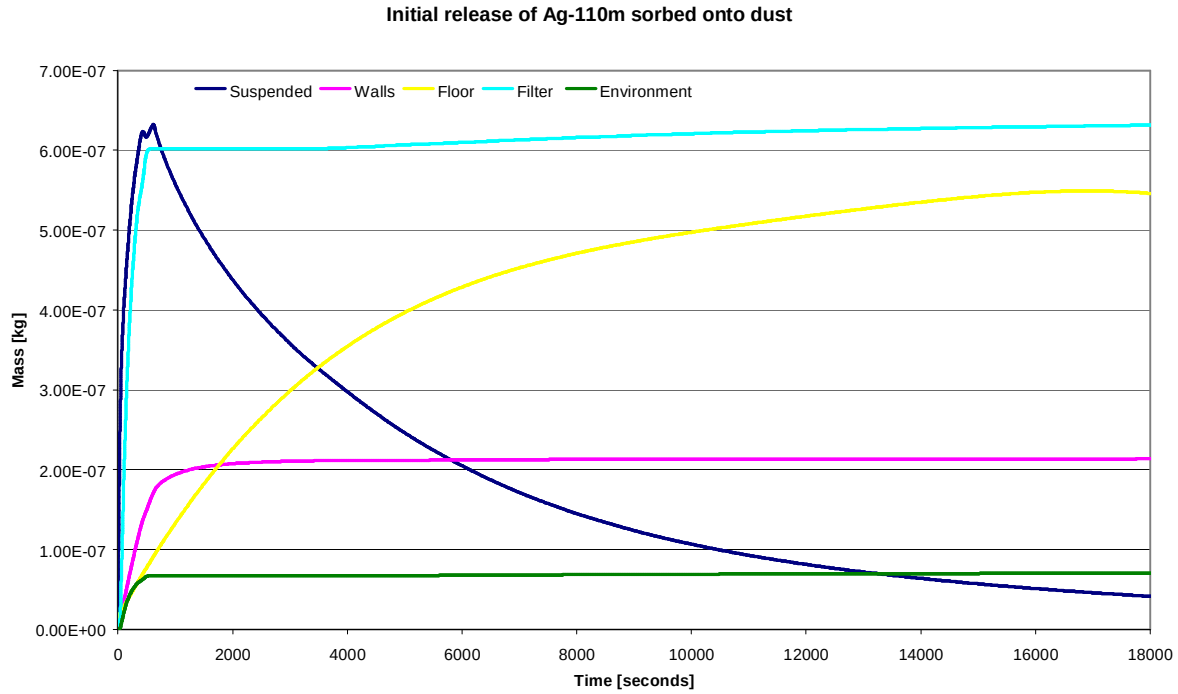

Figure 62: Initial release of ^{110m}Ag sorbed onto dust.

After 5 hours the retention within the building of these 3 fission products are 95.6 %, the remaining 4.4 % escapes into the environment and there is approximately 39.5 % of the total fission products which are collected in the filters.

Figure 65, Figure 66 and Figure 67 show the mass balance for the three fission products, there is good agreement between the values.

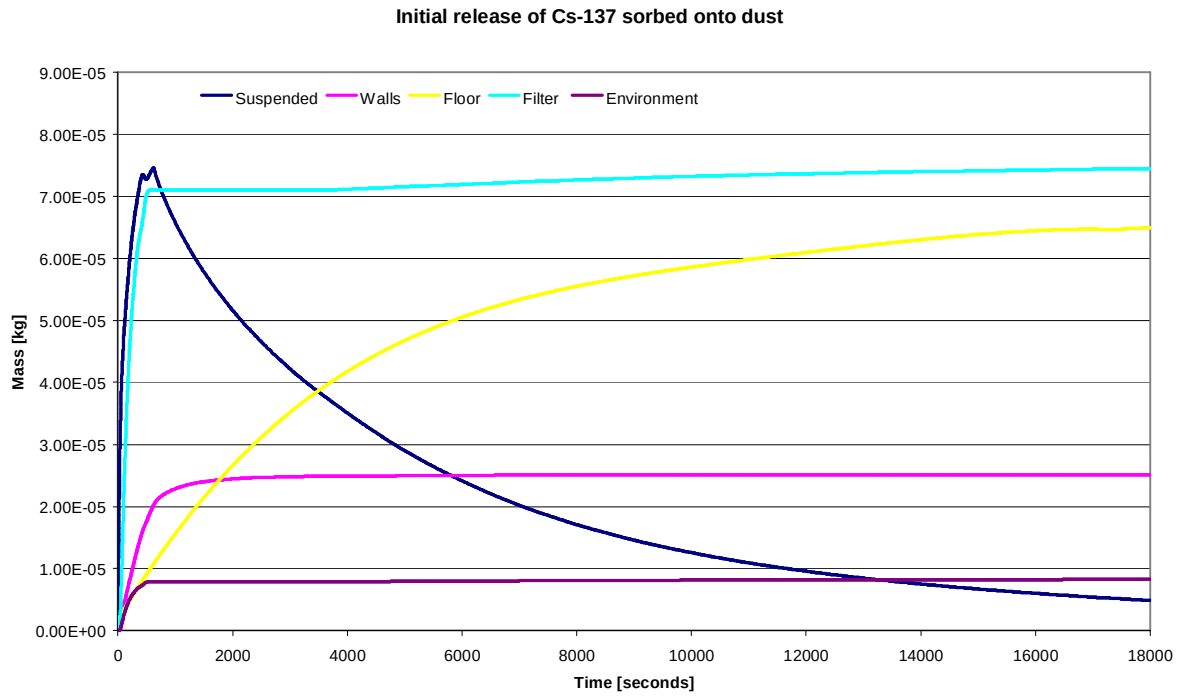

Figure 63: Initial release of ^{137}Cs sorbed onto dust.

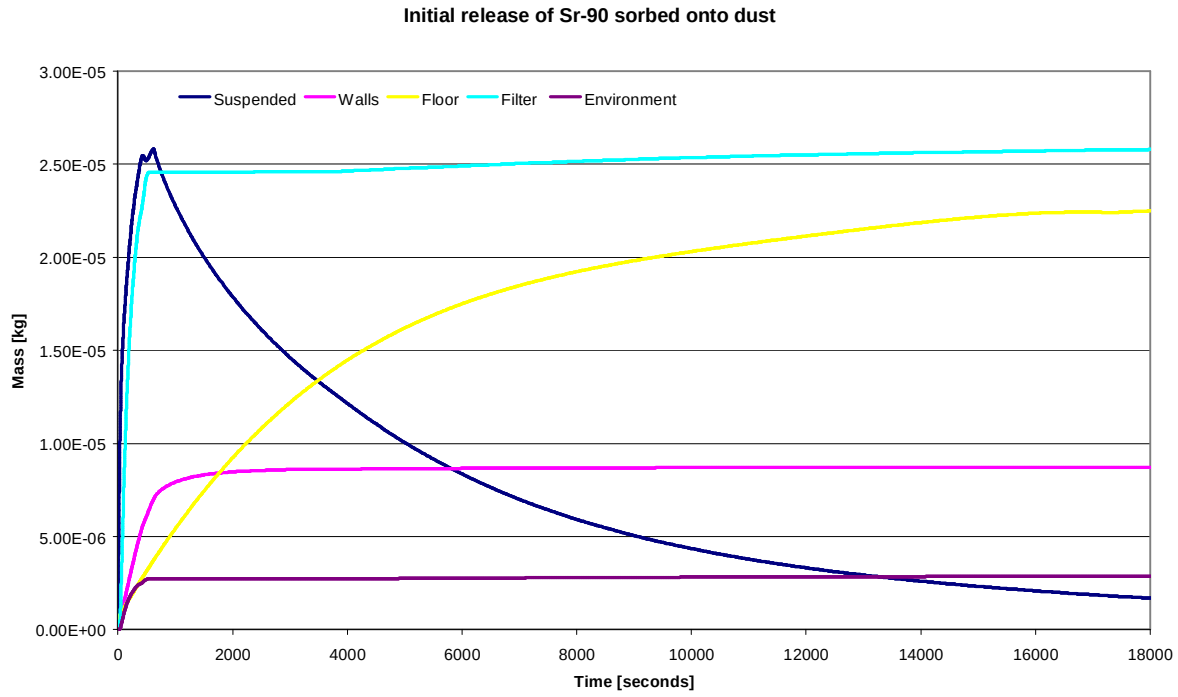

Figure 64: Initial release of ^{90}Sr sorbed onto dust.

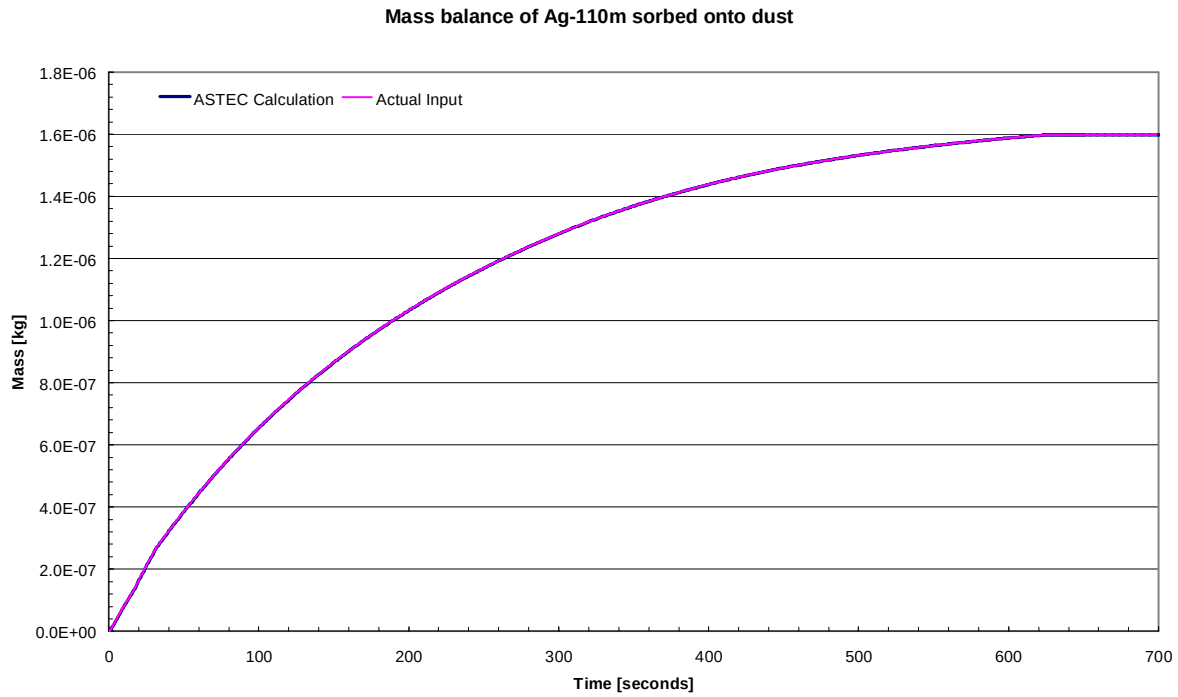

Figure 65: Mass balance of ^{110m}Ag sorbed onto dust.

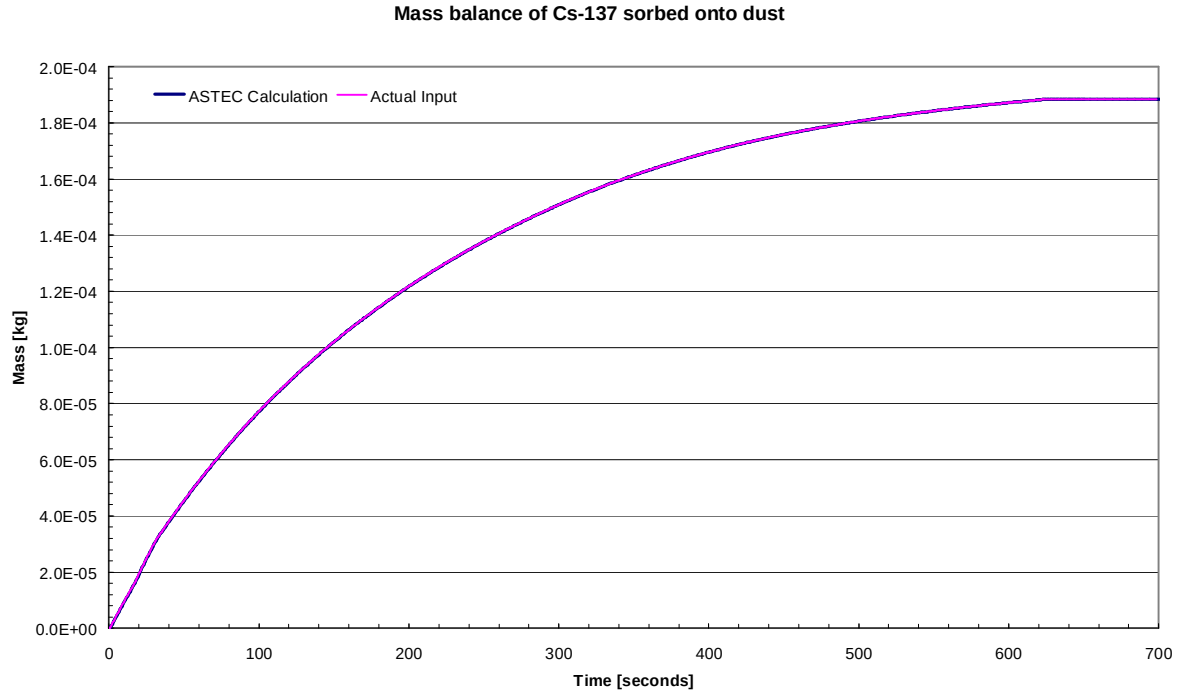

Figure 66: Mass balance of ^{137}Cs sorbed onto dust.

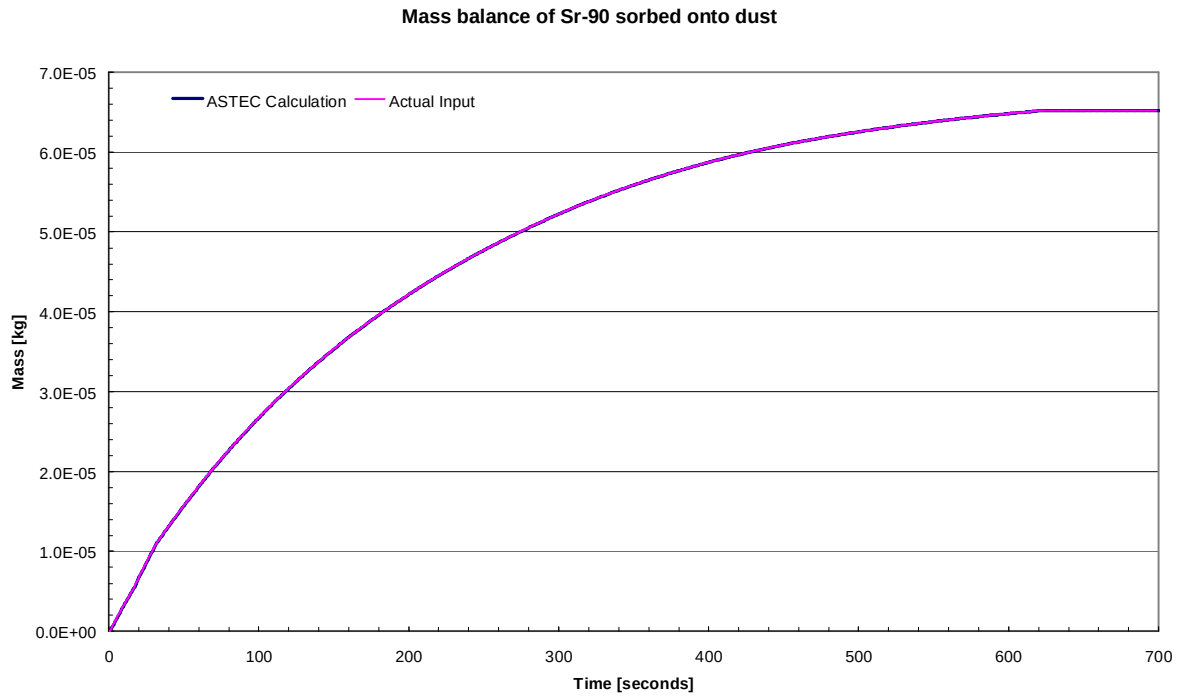

Figure 67: Mass balance of ^{90}Sr sorbed onto dust.

4.2.2.2.3 Delayed release of fission products

The delayed release analysis for this accident scenario showed the same deficiency in the mass balance from ASTEC as the scenario for the single helium pipe break. This is attributed to the low masses of fission products that are injected compared to light water reactor accidents. The results for the mass balance are shown in Figure 68, Figure 69 and Figure 70 for the three fission products.

The response was exactly the same as for fission products injected with the best estimate sizes discussed in § 3.5.2.1.1.

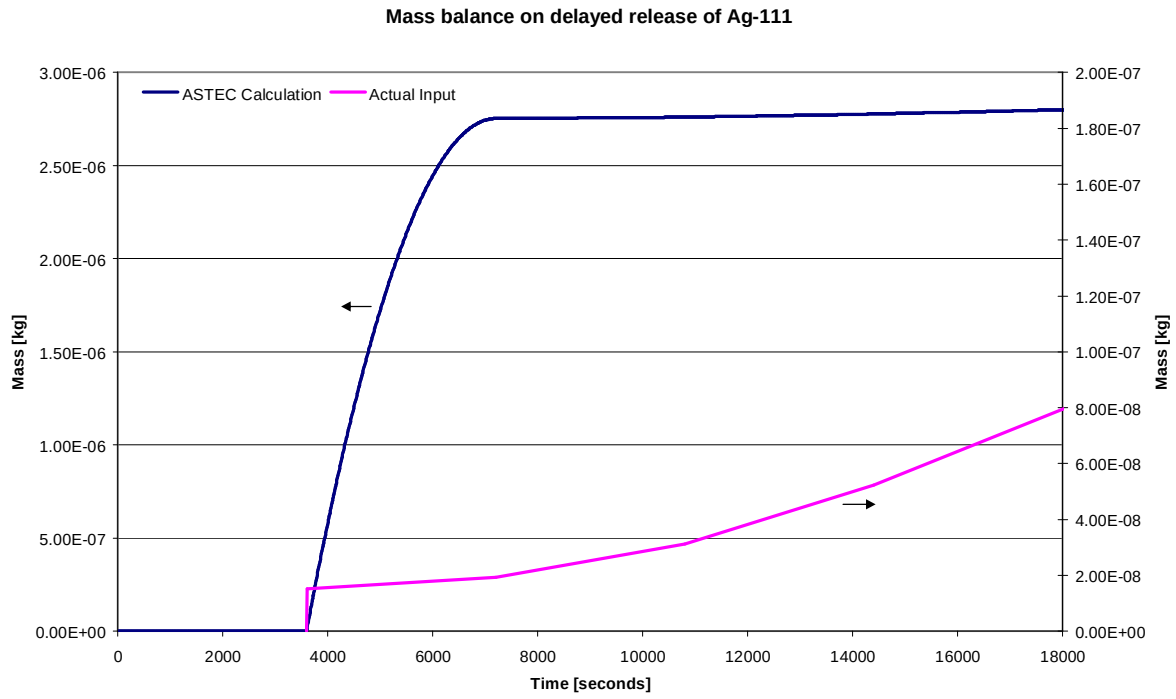

Figure 68: Mass balance on delayed release of ^{111}Ag.

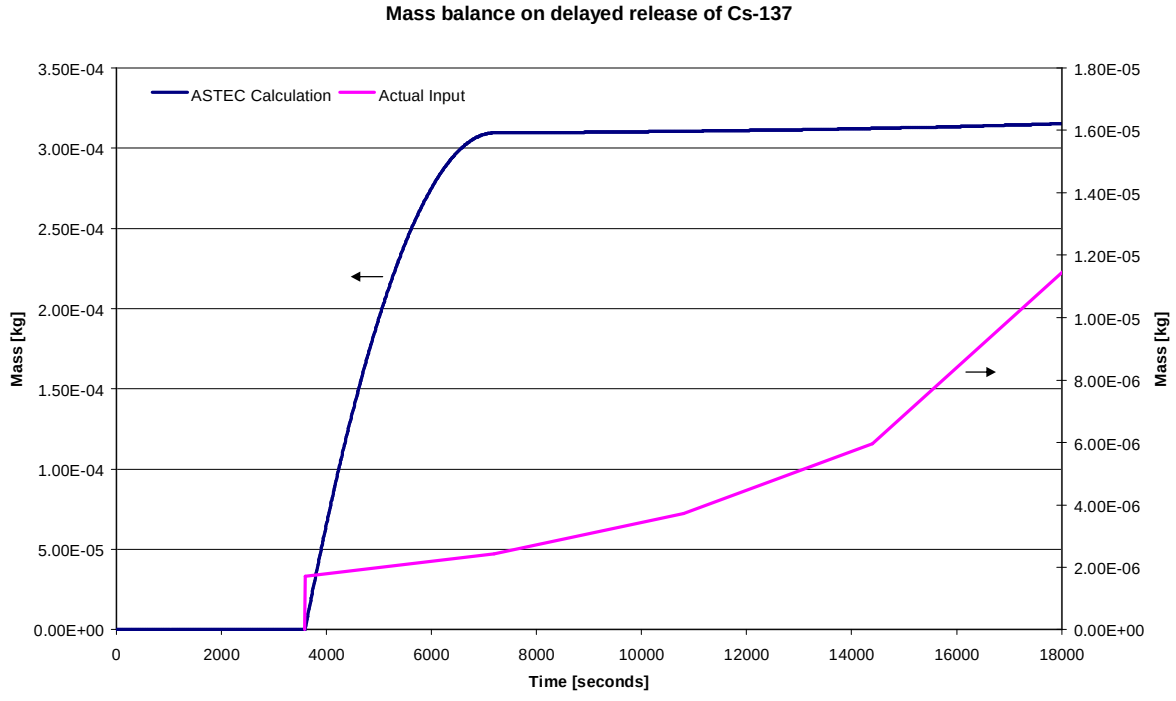

Figure 69: Mass balance on delayed release of ^{137}Cs.

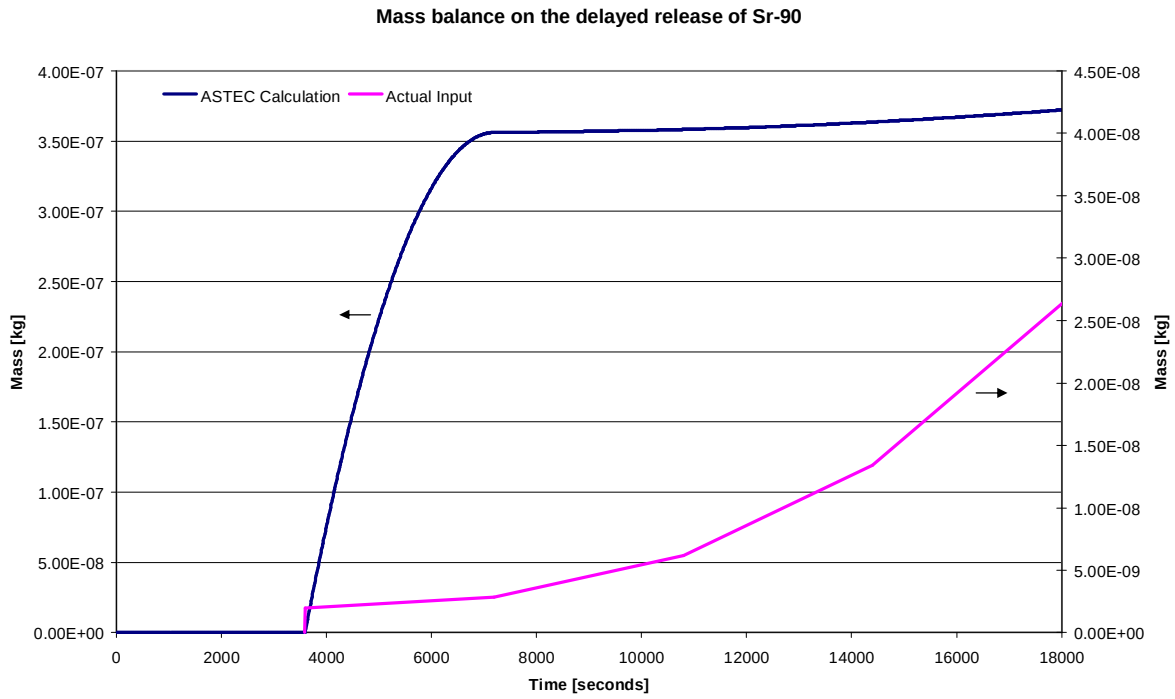

Figure 70: Mass balance on delayed release of ^{90}Sr.

4.2.3 Iodine chemistry results

Figure 71 below summarises the molecular iodine distribution between the gas phase, adsorbed onto painted surfaces and escaped into the environment during the transient. During the initial release phase the airborne (gas phase) molecular iodine reaches a maximum near 600 seconds and then begins to drop until the injection of the delayed release at 3600 seconds. A further increase in molecular iodine occurs around 14400 seconds which is due to the characteristic of the iodine injection, this can be seen from the mass balance of Figure 74. Figure 71 also shows that painted surfaces is most effective in retaining iodine after the depressurisation phase. Approximately 57.5 % of the iodine is sorbed onto painted surfaces at the end of 5 hours.

Figure 72 below summaries the methyl iodide distribution between the confinement and the environment. There is methyl iodide production in the initial release phase only, this can be seen from the sharp increase during the first 700 seconds. The reaction kinetics are greater during this phase as a consequence of the higher temperatures compared to the delayed release phase. Approximately 4 % of the initial release iodine that was injected over the first 700 seconds reacted to form the organic methyl iodide. At the end of 5 hours approximately 67.5 % of the methyl iodide escapes into the environment.

With no filter retention modelled for iodine, there is approximately 39.2 % retention of all iodine species for the initial release (determined at 700 seconds) and a final retention of 79.5 % determined at 5 hours.

In addition to the iodine species formed during the single helium pipe break, the steam break allowed for the condensation of steam into water thus creating a medium for further iodine specie generation as shown in Figure 73. The production of I^- and HOI results in a pseudo retention of iodine since these species are trapped in the liquid phase and cannot escape into the environment. These two iodine species amount to 8.8 % of the total iodine injection at the end of 5 hours.

Figure 74 shows that there is good agreement on the mass balance of iodine; this is in contrast with what was seen for the metal fission products of the delayed release. The CPA module of ASTEC simulated the metal fission products while iodine was simulated by the IODE module.

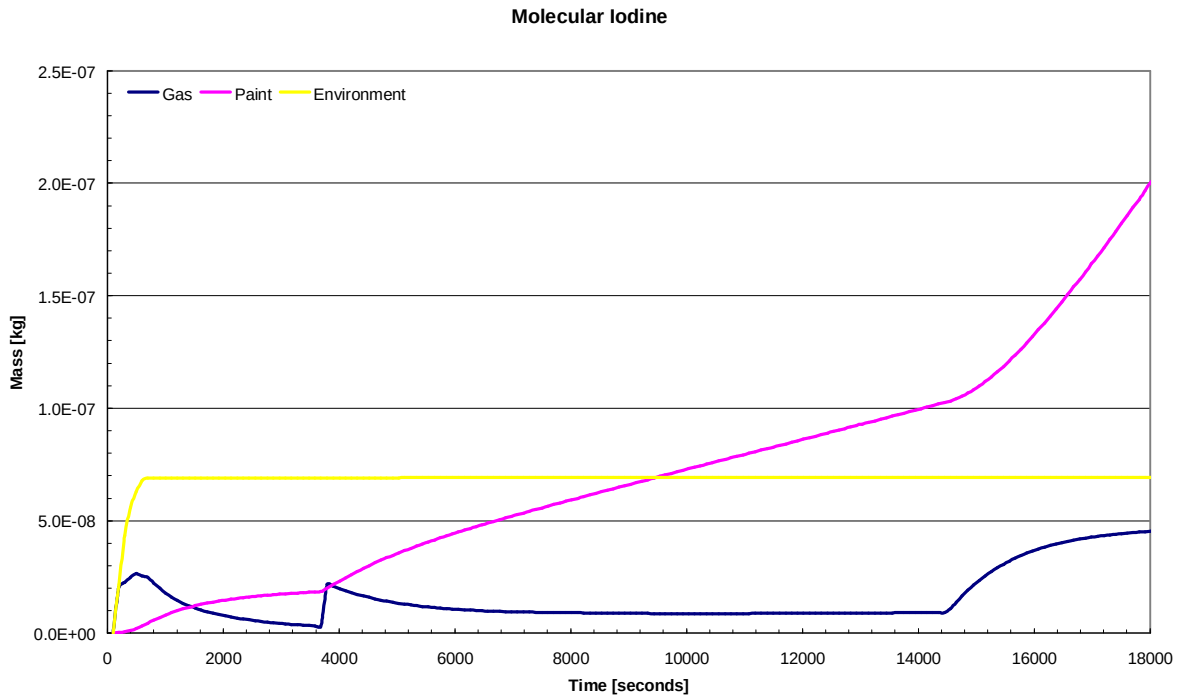

Figure 71: Molecular iodine mass distribution.

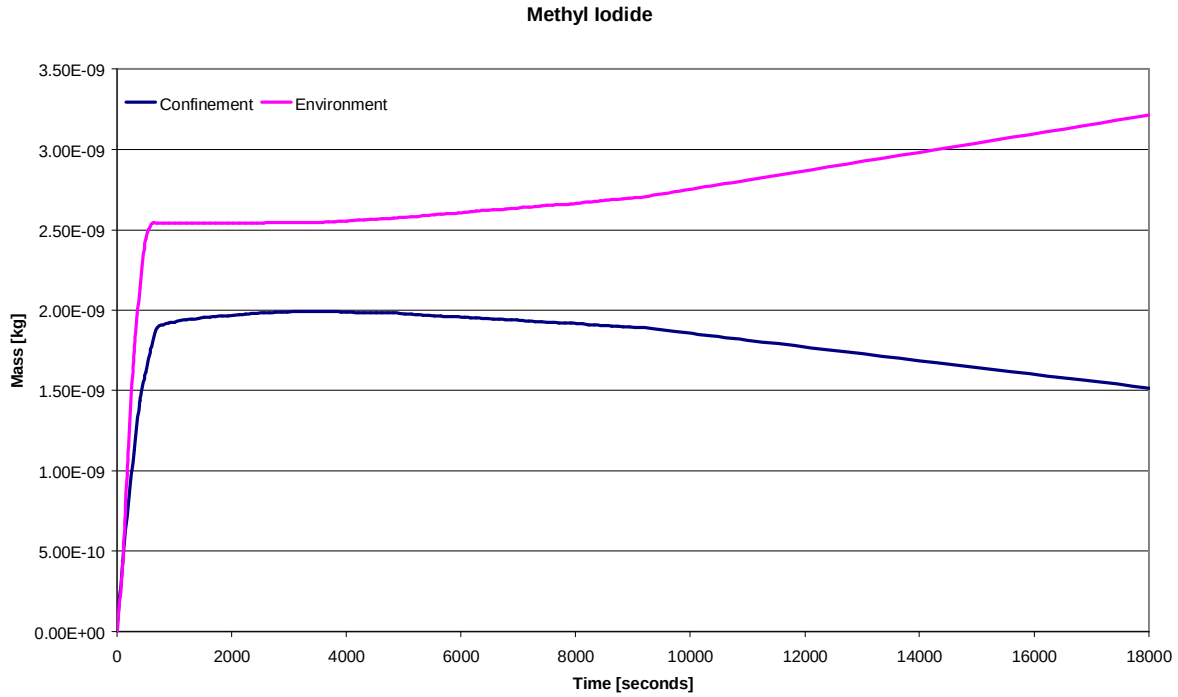

Figure 72: Methyl iodide mass distribution.

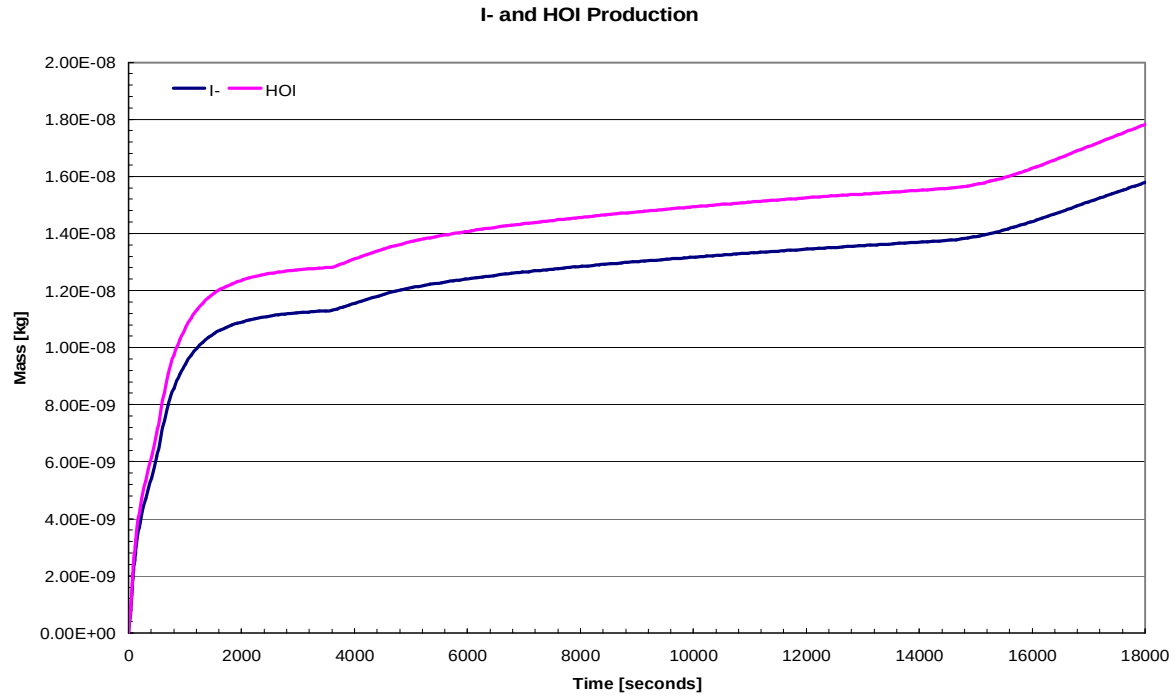

Figure 73: Iodine species found in the aqueous phase.

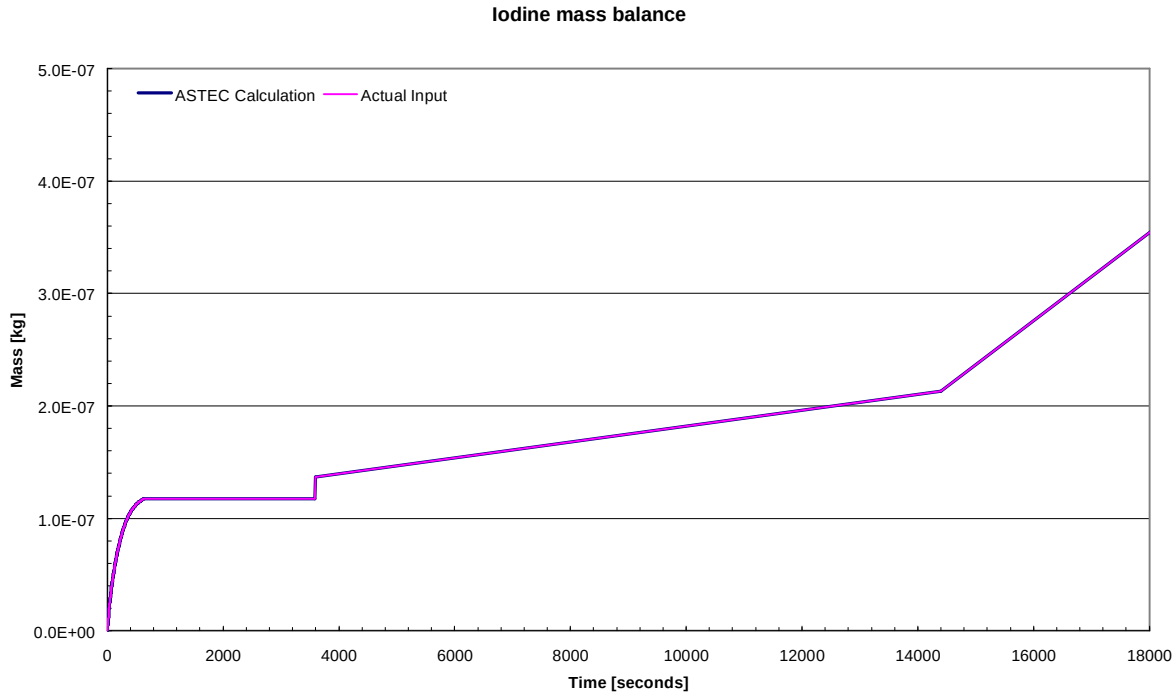

Figure 74: Iodine mass balance.

5. CONCLUSION

It can be concluded from the helium pipe break analysis that the pressure in compartment 111743 exceeds the design pressure of 140 kPa during the transient. There is only one exit point for the gas from this compartment through a rupture panel of 1.5 m^2, this junction area is relatively small and by increasing the area, the pressure in this compartment may remain lower than the maximum value because the flowrate through the junction will increase with an increase in junction area.

The graphite dust retention within the confinement during this scenario was found to be 96.2 % of the total dust injected, in the absence of HEPA filters this would amount to 61.6 % retention because 34.6 % is retained within these filters. For the purpose of this study, the retention has only been calculated for the first five hours of the transient, since computational times are significantly long. Fission products that are sorbed onto the dust also have this retention profile because the fission product host is the graphite dust. It should be noted that these results cannot be scaled to a case of 1 kg of dust, with the assumption in mind that since 96.2 % was retained for 100 kg, that the same will be retained for 1 kg. The deposition mechanisms are not linear.

Fission products that are present in the gaseous phase have shown 48.2 % retention within the building over the first 5 hours. This does not include filtration since the HEPA filters cannot filter fission products present in the gaseous form. At the end of the initial release phase the retention of the fission products are 64.4 % at approximately 650 seconds, this slowly decreases to 48.2 % at 5 hours due to the delayed release driving force which transports fission products out of the rupture panels into the environment.

The iodine chemistry results show that the formation of methyl iodide is possible and that approximately 5 % of the initial release iodine reacted to form methyl iodide. The organic iodide will have a lower filtration efficiency compared to molecular iodine and it is possible for this amount to escape into the environment unfiltered. The organic iodide production was found only during the initial release phase since this is the phase with the highest compartmental temperatures, thus allowing for higher reaction kinetics in favour of methyl iodide production. It was found that painted surfaces are an effective medium for molecular iodine retention with 62.5 % of the iodine adsorbed on such surfaces. At the end of 5 hours the retention of all iodine species within the building was found to be 78.5 %.

The actual design of the confinement will consider a passive closing mechanism to ensure that gas exchange with the environment is not possible after the depressurisation phase when gas pressures within the confinement are close to atmospheric. This passive closing mechanism was not modelled for this study.

The simultaneous helium pipe break and steam pipe break analysis shows that the steam generator and reactor pressure vessel compartments of module 2 exceed their pressure design limit of 250 kPa. Compartment 111743 also exceeds its design limit of 140 kPa. The area of the exit junctions for these

compartments may be increased or additional junctions of equivalent area can be added to allow the pressure to be alleviated more rapidly.

The retention of graphite dust and fission products sorbed onto dust was found to be 95.6 %. In the absence of HEPA filters the retention would amount to 56.1 % because 39.5% is trapped within the filters.

The iodine behaviour during this transient showed similar methyl iodide production as in the helium pipe break analysis. The organic production is greatest during the initial release phase due to the higher compartmental temperatures as a consequence of the helium and steam injection. In addition to the iodine species found in the helium pipe break analysis, I^- and HOI were also found present in the sump liquid phases that were formed from steam condensation. Iodine retention was determined to be 79.5 % at the end of 5 hours.

A significant disadvantage found is that the ASTEC code was unable to tolerate small masses of aerosol fission products. This was exacerbated by the simulation of a large number of compartments for fission product transport. HTR accident scenarios have characteristically lower fission product release rates compared to LWR accidents, and the fact that ASTEC was developed and maintained for use in LWR analysis is the reason for this divergent behaviour on application to HTR scenarios. The examination of the delayed release will be an important aspect of safety analysis at the PBMR Company hence it is justifiable that a more suitable code for tolerating small fission product inventories, such as COCOSYS [29], be used in future.

Local effects such as shockwave analysis and stresses on the reactor internals and the environment cannot be predicted by lumped parameter codes such as ASTEC and COCOSYS. These effects would need to be investigated with an appropriate choice of a CFD simulation tool.

6. REFERENCES

[1] Inglesi, R., Aggregate electricity demand in South Africa: Conditional forecasts to 2030, *Applied Energy*, Vol. 87, p. 197-204, 2009.

[2] A. Koster, et al., PBMR design for the future, *Nuclear Engineering and Design*, Vol. 222, p. 231-245, 2002.

[3] Z. Zhang, et al., Current status and technical description of Chinese 2 × 250 MW_{th} HTR-PM demonstration plan, *Nuclear Engineering and Design*, Vol. 239, p. 1212-1219, 2009.

[4] National Nuclear Regulator, Basic Licensing Requirements for the Pebble Bed Modular Reactor, Report RD-0018, Rev. 1, Centurion, South Africa.

[5] Association of German Engineers Vdi - The Society for Energy Technologies, AVR: Experimental High-Temperature Reactor: 21 Years of Successful Operation for a Future Energy Technology, 1990, ISBN: 978-3-18-401015-7.

[6] J.P. Van Dorsselaere, B. Schwinges, Overview of the Integral Code ASTEC v1.3, Report ASTEC-V1/DOC/06-19, Dec. 2006.

[7] Nuclear Energy Agency, State of the Art Report on Iodine Chemistry, Report NEA/CSNI/R(2007)1, 23 February 2007.

[8] Nuclear Energy Agency, State of the Art Report on Nuclear Aerosols, Report NEA/CSNI/R(2009)5, 17 December 2009.

[9] H. -J. Allelein, et al., European validation of the integral code ASTEC (EVITA), *Nuclear Engineering and Design*, Vol. 221, p. 95-118, 2002.

[10] T. Albiol, et al., SARNET: Severe accident research network of excellence, *Progress in Nuclear Energy*, Vol. 52, p. 2-10, 2009.

[11] G. Poss, ThAI Experiments to investigate gas distribution and graphite dust transport in a generic HTGR Confinement, HTGR Graphite Dust Meeting, Omni Shoreham Hotel, Washington DC, November 19th, 2009.

[12] L., E., Herranz, et al., PBMR Confinment Analysis During Helium Pressure Boundary Breaks, Proceedings of the 4th International Topical Meeting on High Temperature Reactor Technology, Washington DC, September 28 – October 1, 2008.

[13] K. K., Murata, Code Manual for CONTAIN 2.0: A Computer Code for Nuclear Reactor Containment Analysis, Report NUREG/CR-65333, 1997.

[14] L., E., Herranz, et al., Assessment of “Wet Confinement” Performance under Anticipated HTGR Accident Conditions, Proceedings of the 6th International Topical Meeting on High Temperature Reactor Technology, Prague, Czech Republic, October 18-20, 2010.

[15] Klein-Heβling, W., Schwinges, B., CPA Module – Program Reference Manual, Report ASTEC-V0/DOC/01-34, Rev. 0, November 1998.

[16] K. Smith, Normal Density Concrete Material Sheet Report, Pebble Bed Modular Reactor (Proprietary) Limited, Report 022151 Revision 1, Proprietary Class 2, Centurion, South Africa, 12 Dec. 2003.

[17] J. Strauss, Pipe Break Transient Calculation Report, Pebble Bed Modular Reactor (Proprietary) Limited, Report T001922 Revision B, Proprietary Class 2, Centurion, South Africa, 5 May 2010.

[18] N. Coetzee, Dust Particles Sizes and Dust Activities Report, Pebble Bed Modular Reactor (Proprietary) Limited, Report 052230 Revision 5, Proprietary Class 2, Centurion, South Africa, 15 Aug. 2008.

[19] J. Mohan, Dust Re-Suspension and Desorption of Plate Out Calculation Model Report, Pebble Bed Modular Reactor (Proprietary) Limited, Report 025442 Revision 1C, Proprietary Class 2, Centurion, South Africa, 26 Mar. 2009.

[20] I. Petr, Selection of Radionuclides Investigation Report, Pebble Bed Modular Reactor (Proprietary) Limited, Report 055897 Revision 3, Proprietary Class 2, Centurion, South Africa, 31 Aug. 2009.

[21] J. Mohan, Doses From HPB Breaks Evaluation Model Report, Pebble Bed Modular Reactor (Proprietary) Limited, Report T000275 Revision G, Proprietary Class 2, Centurion, South Africa, 17 Jul. 2007.

[22] J., J., van der Merwe, Metallic Fission Product Release Calculation Model Report, Pebble Bed Modular Reactor (Proprietary) Limited, Report T000239 Revision A, Proprietary Class 2, Centurion, South Africa, 22 Dec. 2007.

[23] Katscher, W., Stauch, B., Experimental investigation of aerosol formation from metallic fission products under hypothetical accident conditions in high-temperature gas-cooled reactors, *Journal of Aerosol Science*, Vol. 20(8), p. 1417-1420, 1989.

[24] L., E., Herranz, et al., Experimental interpretation and code validation based on the PHEBUS-FP programme: Lessons learnt from the analysis of the containment scenario of FPT 1 and FPT 2 tests, *Nuclear Engineering and Design*, Vol. 237, p. 2210-2218, 2007.

[25] J., M., Mäkynen, et al., AHMED experiments on hygroscopic and inert aerosol behaviour in LWR containment conditions: experimental results, Nuclear Engineering and Design, Vol. 178, p. 45-59, 1997.

[26] H., van der Merwe, Fission Product Release from the 400 MW PBMR Core Under Medium Break DLOFC Conditions Report, Pebble Bed Modular Reactor (Proprietary) Limited, Report T000181 Revision 2C, Proprietary Class 2, Centurion, South Africa, 22 Dec. 2007.

[27] G., Guillard, et al., Users Guidelines for the integral code ASTEC V2.0, Report ASTEC-V2/DOC/09-07, Rev. 0, March 2009.

[28] H., Antoniol, DPP 200 (HTR Module) Reactor Building Design Description, Pebble Bed Modular Reactor (Proprietary) Limited, Report 111257 Revision A, Proprietary Class 2, Centurion, South Africa, 12 Aug. 2009.

[29] H., J., Allelein, et al., COCOSYS: Status of development and validation of the German containment code system, *Nuclear Engineering and Design*, Vol. 238, p. 872-889, 2008.

[30] L., Bosland, ASTEC V2.0 Code IODE module: iodine and ruthenium behaviour in the containment, IRSN Report ASTEC-V2/DOC/09-13, Revision 0, July 2009.

[31] F., Gelbard, MAEROS User Manual, Sandia National Laboratory Report NUREG/CR-1391, December 1982.

7. APPENDIX A

7.1.1 List of Partners for the SARNET programme

Country	Organisation
Austria	ARC Seibersdorf Research GmbH (ARCS)
Belgium	Association Vincotte Nucleaire (AVN)
Belgium	Tractebel Engineering, a Division of Suez-Tractebel SA (TE)
Belgium	Université Catholique de Louvain (UCL)
Belgium	Université Libre de Bruxelles (ULB)
Bulgaria	Bulgarian Nuclear Regulatory Agency (BNRA)
Bulgaria	Institute for Nucl. Research and Nucl. Energy (INRNE)
Bulgaria	Technical University of Sofia (TUS)
Canada	Atomic Energy of Canada Limited (AECL)
Czech Republic	Ustav Jaderneho Vyzkumu Rez a.s. (UJV)
Finland	Fortum Nuclear Services Ltd. (FORTUM)
Finland	VTT Technical Research Centre of Finland (VTT)
France	Comissariat à l'Energie Atomique (CEA)
France	Electricité de France (EDF)
France	Framatome ANP SAS (FRA ANP SAS)
France	Institut de Radioprotection et de Sûreté Nucléaire (IRSN)
France	PLINIUS
France	Technicatome (TA)
France	Thermodata (THERMODATA)
Germany	Becker Technologies GmbH (BTech)
Germany	Forschungszentrum Jülich GmbH (FZJ)
Germany	Forschungszentrum Karlsruhe GmbH (FZK)
Germany	Forschungszentrum Rossendorf e.V. (FZR)
Germany	Framatome ANP GmbH (FRA ANP-Gmbh)
Germany	Gesellschaft für Anlagen- und Reaktorsicherheit mbH (GRS)
Germany	Ruhr-Universität Bochum (RUB)
Germany	University of Stuttgart (USTUTT-IKE)
Greece	National Centre for Scientific Research DEMOKRITOS (DEMOKRITOS)
Hungary	Budapest Univ. of Technology and Economics, Inst. of Nucl. Techniques (BUTE)
Hungary	KFKI Atomic Energy Research Institute (AEKI)
Hungary	VEIKI Institute for Electric Power Research Co. (VEIKI)
Italy	Centro Elettrotecnico Sperimentale Ital. Giacinto Motta SpA (CESI RICERCA)

Country	Organisation
Italy	Ente per le Nuove Tecnologie, l'Energia e l'Ambiente (ENEA)
Italy	Universitá di Pisa (UPI)
Lithuania	Lithuanian Energy Institute (LEI)
Netherlands	Nuclear Research & Consultancy Group v.o.f. (NRG)
Romania	National Autonomous Company for Nucl. Acitvities, Nucl. Research Subsidiary Pitesti (INR)
Slovakia	Inzinierska Vypoctova Spolocnost Trnava Ltd. (IVS)
Slovakia	Urad Jadroveho Dozoru SR (UJD)
Slovakia	VUJE Trnava, a.s. Inzinierska, Projektove a Vyskumna Organizacia (VUJE)
Slovenia	Josef Stefan Institute (JSI)
Spain	Centro de Investigaciones Energeticas Medio Ambientales y Tecnologicas (CIEMAT)
Spain	Consejo de Seguridad Nuclear (CSN)
Spain	Empresados Agrupados International S.A. (EA)
Spain	Universidad Politecnica de Madrid (UPM)
Sweden	Chalmers University of Tehcnology (CHALMERS)
Sweden	Kungl Tekniska Högskolan (KTH)
Sweden	Swedpower AB (SWP)
Switzerland	Paul Scherrer Institute (PSI)
United Kingdom	National Nuclear Corporation Ltd. (NNC)
United Kingdom	University Of Newcastle Upon Tyne (UNEW)
United Kingdom	Waste Management Technology Limited (WMT)
European Commission	EURATOM Joint Research Center of ISPRA EEC (JRC ISPRA)
European Commission	EURATOM Joint Research Center of Petten EEC (JRC PETTEN)
European Commission	EURATOM Joint Research Centre - Institute for Transuranian Elements EEC (JRC ITU)

8. APPENDIX B

Table 3: Compartmental characteristics for Module 1

Compartment ID	Compartment Description	Floor Area [m^2]	Roof Area [m^2]	Wall Area [m^2]	Compartment Height [m]	Floor Elevation [m]	Centre Elevation [m]	Net Compartment Volume [m^3]
111729	Stairwell	14.36	14.85	1047.49	40.75	-12.70	7.68	464.31
110640	Transducer Compartment	46.10	46.10	91.69	2.65	-12.70	-11.98	103.84
111606	Steam Generator	35.26	40.10	460.42	24.40	-12.70	-0.50	739.00
111648	Valves & Instrumentation	227.85	227.85	1100.27	2.65	-12.70	-11.38	434.31
111742	Core Unloading Device	61.90	61.90	99.43	3.80	-9.00	-7.10	186.56
111737	Hot Pipe Channel (Fuel lines)	7.02	7.02	21.02	2.70	-9.55	-8.20	11.64
112201	Service Floor	222.80	222.80	293.29	2.70	-9.55	-8.20	482.43
111762	Valves	47.16	47.16	93.65	2.65	-6.35	-5.03	106.22
111773	Valves	167.50	167.34	215.12	2.65	-6.35	-5.03	376.70
111804	Pipe Channel	20.62	20.62	70.25	2.70	-3.20	-1.85	47.33
111805	Reactor Pressure Vessel	70.88	70.88	738.62	27.60	-3.70	10.10	1660.88
112203	Access Floor	139.31	139.31	172.19	2.70	-3.20	-1.85	319.73
112207	Pipe Channel	47.16	47.16	95.60	2.70	-3.20	-1.85	108.22
111824	Stairwell Remote Shutdown Station	69.41	71.26	428.73	18.55	0.00	9.28	316.53
111848	Valve Room	181.17	181.17	265.26	2.65	0.00	1.33	407.49
111962	Corridor	38.84	38.84	79.29	2.70	3.15	4.50	89.15
111966	Pipe Route	67.92	67.92	103.59	2.70	3.15	4.50	155.87
111970	Corridor	68.76	68.76	107.80	2.70	3.15	4.50	157.80
111987	Corridor	35.87	35.87	78.41	2.65	6.35	7.68	80.80

Compartment ID	Compartment Description	Floor Area [m^2]	Roof Area [m^2]	Wall Area [m^2]	Compartment Height [m]	Floor Elevation [m]	Centre Elevation [m]	Net Compartment Volume [m^3]
111988	Recirculation Cooling Unit	173.18	173.18	201.92	2.65	6.35	7.68	390.09
111997	Valves	33.66	33.66	74.60	2.70	9.50	10.85	77.24
112209	Recirculation Cooling Unit	30.83	30.83	71.87	2.70	9.50	10.85	70.75
112266	Pressure Relief System (PRS) Shaft	10.33	10.34	182.55	15.60	12.20	20.00	113.41

Table 4: Compartmental characteristics for Module 2

Compartment ID	Compartment Description	Floor Area [m^2]	Roof Area [m^2]	Wall Area [m^2]	Compartment Height [m]	Floor Elevation [m]	Centre Elevation [m]	Net Compartment Volume [m^3]
110581	Stairwell	16.55	21.90	1152.29	46.15	-12.70	10.38	596.96
111609	Fuel Handling Valve Blocks	15.43	15.43	168.46	12.20	-12.70	-6.60	160.01
111624	Transducer Compartment	70.22	70.22	119.82	2.65	-12.70	-11.38	156.08
111626	Steam Generator	35.26	40.10	460.42	24.40	-12.70	-0.50	521.65
111654	Valves & Instrumentation	190.33	190.26	456.32	2.65	-12.70	-11.38	428.18
111738	Hot Pipe Channel (Fuel lines)	21.40	21.40	51.50	1.95	-9.55	-8.58	35.46
111743	Core Unloading Device	61.90	61.90	99.43	3.80	-9.00	-7.10	186.56
112202	Service Floor	224.55	224.55	308.87	2.70	-9.55	-8.20	486.90
111768	Valves	72.00	72.00	131.20	2.65	-6.35	-5.03	162.19
111777	Valves	164.92	164.68	234.47	2.65	-6.35	-5.03	370.29
111809	Reactor Pressure Vessel	70.88	70.88	738.62	27.60	-3.70	10.10	1172.39
112204	Access Floor	103.17	103.17	151.01	2.70	-3.20	-1.85	236.78
112206	Corridor	92.52	92.52	128.21	2.70	-3.20	-1.85	212.33
112208	Corridor	41.19	41.20	86.87	2.70	-3.20	-1.85	94.52
111821	Main Transport Route	130.35	128.70	498.95	12.70	0.00	6.35	981.71
111907	Valve Room	161.19	161.11	228.76	2.65	0.00	1.33	362.49
111936	Valve Room	71.44	71.44	131.53	2.65	0.00	1.33	160.91
111960	Pipe Channel (Air Removal System)	49.94	50.54	109.04	3.20	2.65	4.25	118.45
111977	Corridor	69.78	69.78	133.54	2.70	3.15	4.50	160.15
111980	Pipe Route	64.91	65.07	104.61	3.20	2.65	4.25	151.03

Compartment ID	Compartment Description	Floor Area [m^2]	Roof Area [m^2]	Wall Area [m^2]	Compartment Height [m]	Floor Elevation [m]	Centre Elevation [m]	Net Compartment Volume [m^3]
111993	Corridor	72.00	72.00	131.20	2.65	6.35	7.68	162.19
111994	Recirculation Cooling Unit	171.99	171.99	206.22	2.65	6.35	7.68	387.41
112210	Recirculation Cooling Unit	31.34	31.34	73.54	2.70	9.50	10.85	71.91
112019	Steam Generator Maintenance Hall	1788.93	1779.83	3118.10	23.70	12.70	24.55	16346.85
112002	Valves	20.69	20.69	73.95	2.70	9.50	10.85	52.76
112265	Pressure Relief System (PRS) Shaft	10.33	10.34	182.55	15.60	12.20	20.00	113.41
112268	Stack	5.41	5.41	328.45	44.40	36.40	48.20	204.24

Table 5: Junction characteristics for module 1

Opening Number	From	To	Area [m^2]	Height of Junction [m]	Length of Junction [m]	Type
0	111805	111606	40.8	0.30	3.42	Opening
1	111606	111742	0.6	-4.45	1.5	Rupture Panel
2	111742	111737	0.6	-8.30	0.75	Sealed
J2	111609	111737	0.5	-11.13	0.5	Opening
3	111742	112201	1.5	-7.90	2.3	Rupture Panel
4	112201	111648	82.6	-9.80	0.5	Opening
5	111648	111640	0.5	-11.38	0.4	Opening
6	112201	111773	8.5	-6.60	0.5	Opening
7	111773	111762	0.5	-5.03	0.4	Opening
8a	111773	112203	42.1	-3.45	0.5	Opening
8b	111773	112203	15.0	-3.45	0.5	Opening
9a	112203	112207	0.5	-1.85	0.3	Opening
9b	112203	112804	0.5	-1.85	0.3	Opening
10	112203	111848	8.4	-0.25	0.5	Opening
11	111848	111824	0.5	1.33	0.4	Opening
12a	111848	111966	31.0	2.90	0.5	Opening
12b	111848	111970	15.2	2.90	0.5	Opening
13	111966	111962	0.5	4.50	0.4	Opening
14a	111966	111988	6.0	6.10	0.5	Opening
14b	111970	111988	3.2	6.10	0.5	Opening
15	111988	111987	0.5	7.68	0.4	Opening
16a	111988	112209	23.0	9.25	0.5	Opening
16b	111988	111997	23.0	9.25	0.5	Opening
17	112009	112266	7.5	12.20	0.5	Rupture Panel
18	112266	112019	10.3	27.85	0.1	Opening
SO	112019	111821	40.2	11.10	3.7	Opening

Opening Number	From	To	Area [m^2]	Height of Junction [m]	Length of Junction [m]	Type
19A	112019	112268	1.2	31.70	2	Rupture Panel
19B	112019	112268	1.2	31.70	2	Rupture Panel
20	112268	Environment	5.9	60.00	0	Opening
21	111821	111729	0.5	28.23	0.35	Rupture Panel
22	111821	110581	0.5	-0.25	0.5	Rupture Panel
23	111821	111848	1.0	0.00	0.35	Rupture Panel

Table 6: Junction characteristics for module 2

Opening Number	From	To	Area [m^2]	Height of Junction [m]	Length of Junction [m]	Type
0	111809	111626	40.8	0.3	3.42	Opening
1	111626	111743	0.6	-4.45	1.5	Rupture Panel
2	111743	111738	0.6	-8.3	0.75	Sealed
J1	111738	111609	0.5	-11.125	0.5	Opening
3	111743	112202	1.5	-7.9	2.3	Rupture Panel
4	112202	111654	82.6	-9.8	0.5	Opening
5	111654	111624	0.5	-11.375	0.4	Opening
6	112202	111777	8.5	-6.6	0.5	Opening
7	111777	111768	0.5	-5.025	0.4	Opening
8a	111777	112206	42.1	-3.45	0.5	Opening
8b	111777	112204	15.0	-3.45	0.5	Opening
9	112204	112208	0.5	-1.85	0.3	Opening
10	112206	111907	8.4	-0.25	0.5	Opening
11	111907	111936	0.5	1.325	0.4	Opening
12a	111907	111980	31.0	2.9	0.5	Opening
12b	111907	111977	15.2	2.9	0.5	Opening
13	111977	111960	0.5	4.5	0.4	Opening
14a	111980	111994	3.2	6.1	0.5	Opening
14b	111977	111994	6.0	6.1	0.5	Opening
15	111994	111993	0.5	7.675	0.4	Opening
16a	111994	112002	23.0	9.25	0.5	Opening
16b	111994	112210	23.0	9.25	0.5	Opening
17	112002	112265	7.5	12.2	0.5	Rupture Panel
18	112265	112019	10.3	27.85	0.1	Opening

9. APPENDIX C

9.1 ASTEC MAIN INPUT FILE

```
(version_=GETENV("version_astec"))
(computer=GETENV(computer))
(name="NGNP")


(Wall = 0.5)
(Forward = 4.)
(Backward = 4.)
(Heat = "FRC+COD+FOC+WGR")
(Sat = 40.)
(Temp = 25.)
(Pressure = 101325.)
(mode = HECU)


CALL visu_plot.dat


STRU SAVE
  FILE "NGNP.bin"
  FREQ 20.
  STOP "crash.bin"
END



STRU SEQUENCE
  NAME (WORD(name))
  LOOK (name//"_"//computer//".quicklook")
  TINI    0.
  TIMA    18500.0
  TFP     0.
  STRU MACR
    DTFI 0.1
    MINI 0.1
    SR1 MAXI 0.0 0.1 800.0 0.1 801.0 10.0 TERM
    STRU CRIT
        PATH "BASE : CONTAINM 1: ZONE 1: THER 1"
        VARI PRES
        EVOL 10.
        TYPE ABSOLUTE
    END
  END
END


STRU PHYSICAL_OPTIONS
    SC1 FP 'Ag0'   'Ag0d'
           'Cs7'   'Cs7d'
           'Sr0'   'Sr0d'
           'Se1'
           'Te1'
           'Xe1'
    TERM
END
```

```
STRU SYSTEMS
    STRU FILTER
      TYPE    USER
      NAME    HEPA
      EFAERO  0.90D0
   END
END

CALL sourceterm.dat


STRU CALC_OPT
  SC1 MODULIST 'CPA' 'IODE' TERM
  STRU CPA
    DPLS   1.D4
    DPRS   1.D4
    IPLD   0
    IPLS   1000
    IPRI   3
    IPRS   10000
    ITST   3
    MDBL   50
    NORS   0
    PSTY   'TIC   '
    PTFM SECONDS


    STRU OUTPUT
      TYPE 'LISTING'
      FILE (name//"_cpa_"//computer//".lst")
      STAT 'U'
    END
    STRU OUTPUT
      TYPE 'PLOT_DAT'
      FILE (name//"_cpa_"//computer//".pd")
      STAT 'U'
    END
    STRU OUTPUT
      TYPE 'TIC'
      FILE (name//"_cpa_"//computer//".cur")
      STAT 'U'
      SR1 FREQ 0. 100. TERM
    END

      SC1 FP_LIST      'Ag0'   'Ag0d'
                  'Cs7'   'Cs7d'
                  'Sr0'   'Sr0d'
                  'Se1'
                  'Te1'
                  'Xe1'
      TERM

      SC1 FP_ASSO      ' '     'DUST'
                  ' '     'DUST'
                  ' '     'DUST'
                  'ASHES'
                  'ASHES'
                  'ASHES'
      TERM


    STRU ACTM
      NAME THY
```

```
    STRU MODU
      NAME   JUNCTION
      ICLI   0
    END

    STRU MODU
    NAME EQUIL._MOD
    CLIM  1.D-4
    CLIT  1.D-2
    EPSR  1.D-3
    ZFLM  0.2
    END
    STRU MODU
      NAME    NONEQUIL
      CLIF    1.00E-04
      CLIM    1.00E-04
      CLIT    1.00E-02
      EPSR    1.00E-03
    END
    STRU MODU
      NAME  HECU
      EPSR  0.1
      CLIT  0.1
    END
    STRU MODU
    NAME HEAT_TRANS

    STMP FIRST_LAYER_TEMP
    END
    STRU INTR
      STRU ROUT
        NAME FTRIX/FEBE
        ECKS 1.D-3
        HMAX 30.
        IFTR 3
        OFKT 0
        OFTX 0
        OIMP 0
        OUT  0
      END
    END
    STRU GP_I
      GRP  "ZONE_MODEL"  INTR "FEBE_IMP"
      GRP  "JUNCTION"    INTR "FEBE_IMP"
      GRP  "STRUCTURE"   INTR "FEBE_IMP"
    END
  END

  STRU ACTM
    NAME  AFP
    IMOU  100
    ISCA  -1
    KCOM  3
    KEYM  1
    NCOL  101
    NM    24
    NROW  45
    QMAX  1.E-2
    QMIN  1.E-9

    STRU MODU
      NAME  AEROSOLS
```

```
        ACCO  0.4
        ACTR  0.1
        CHI   1.0
        CLIM  1.D-20
        COLE  -1.
        DENS  1750.0
        DIBG  5.D-8
        DIED  5.D-4
        DYNA  0
        EPSA  1.D-3
        GAMM  1.
        HMAE  10.
        HMAX  20.
        IFCO  2
        IPRT  0
        LAEA  1
        LDIF  1
        LIMP  0
        LMTH  1
        LPCO  0
        LSLB  0
        LSLI  0
        LWSH  0
        NSTE  1
        PLOW  0.5D5
        PUPP  4.D5
        STIC  1.
        SURT  5.86D-2
       TKGO  3.D-3
        TLOW  280.
        TUPP  750.
        TURB  0.02
        WTMO  2.35D1
      END

     STRU MODU
      NAME FIPHOST
      CLIM  1.D-20
      ECKS  1.D-3
      EPSR  1.D-4
      FHPR  0
      HMIN  1.D-12
      OUTF  0
      OUTI  0
      END
    END
  END

  STRU IODE
     IOPT 2
    STRU CALC
      VMIN 1.D-3
    END
    STRU OUTPUT
      FILE (name//"_iod_"//computer//".lst")
      TYPE 'LISTING'
      SR1 FREQ 0.D0 1.D2 TERM
    END
    STRU OUTPUT
      FILE (name//"_iod_"//computer//".cur")
      TYPE 'TIC'
      SR1 FREQ 0.D0 100.D0 TERM
```

```
    END

    STRU CALC

      DTMA 0.1

    END
    STRU PHYS
      STRU PDRY   DRAT 1.E-3    DESO 1.E-5    END
      STRU PWET   DRAT 1.E-3    DESO 1.E-5    END
      STRU KC
        REFE LIQUID
        CH3I 1.0E-05
        I2   1.0E-05
      END
      STRU KC
        REFE GAS
        CH3I 5.0E-03
        I2   5.0E-03
      END
    END
  END
END


STRU CONTAINMENT

    STRU AERO
      STRU COMP
         NAME DUST
         ADPW 0.0
         CAER 0.0
         MOLW 12.0
         SOLU 0.0
      END

      STRU COMP
         NAME ASHES
         ADPW 0.0
         CAER 0.0
         MOLW 100.0
         SOLU 0.0
      END
    END


  STRU COMP
    NAME WATER
    PHAS FLUID
    MLMA 18.016
    CP   FUNCTION
    DL   FUNCTION
    ETA  FUNCTION
  END


  STRU COMP
    NAME N2
    PHAS GAS
    MLMA 28.01
    CDIF 2.0E-5
    CSTD 0.0
    CDIS 0.0
```

```
  CP   FUNCTION
  DL   FUNCTION
  ETA  FUNCTION
END


STRU COMP
  NAME STEAM
  PHAS GAS
  MLMA 18.016
  CDIF 0.58E-4
  CSTD 0.
  CDIS 0.
  CP   FUNCTION
  DL   FUNCTION
  ETA  FUNCTION
END


STRU COMP
   NAME H2
   PHAS GAS
   MLMA 2.016
   CDIF 6.11E-5
   CSTD 0.0
   CDIS 0.0
   CP FUNCTION
   DL FUNCTION
   ETA FUNCTION
END


STRU COMP
  NAME O2
  PHAS GAS
  MLMA 32.00
  CDIF 2.0E-5
  CSTD 0.0
  CDIS 0.0
  CP   FUNCTION
  DL   FUNCTION
  ETA  FUNCTION
END


STRU COMP
  NAME CO
  PHAS GAS
  MLMA 28.01
  CDIF 2.0E-5
  CSTD 0.0
  CDIS 0.0
  CP FUNCTION
  DL FUNCTION
  ETA FUNCTION
END

STRU COMP
  NAME CO2
  PHAS GAS
  MLMA 44.01
  CDIF 2.0E-5
  CSTD 0.0
```

```
    CDIS 0.0
    CP FUNCTION
    DL FUNCTION
    ETA FUNCTION
  END

  STRU COMP
    NAME HE
    PHAS GAS
    MLMA 4.00300E+00
    CDIF 1.00000E-04
    CSTD 0.00000E+00
    CDIS 0.00000E+00
    CP   FUNCTION
    DL   FUNCTION
    ETA  FUNCTION
  END


    STRU MATE
        NAME GROUND
        ARR PROGRESS
        CP 1150.0
        DL 1.74
        EMI 0.9
        RHO 2420.0
        MESH 3
        FAC 4.0
    END


    STRU MATE
        NAME CONCRETE
        ARR PROGRESS
        CP 1150.0
        DL 1.74
        EMI 0.9
        RHO 2420.0
        MESH 15
        FAC 2.0
    END

    STRU MATE
        NAME STEEL
        ARR PROGRESS
        CP 502.42
        DL 16.28
        EMI 1.0
        MESH 3
        RHO 7769.7
        FAC 0.5
    END

  CALL zones.dat
  CALL walls.dat
  CALL junctions.dat
END
```